Mean Stress Effect in Stress-Life for Hard Steels

by

Diogo Gaia da Silva

A thesis
presented to the University of Waterloo
in fulfilment of the
thesis requirement for the degree of
Master of Applied Science
in
Mechanical and Mechatronics Engineering

Waterloo, Ontario, Canada, 2017

AUTHOR'S DECLARATION

This thesis consists of material all of which I authored or co-authored: see Statement of Contributions included in the thesis. This is a true copy of the thesis, including any required final revisions, as accepted by my examiners.

I understand that my thesis may be made electronically available to the public.

STATEMENT OF CONTRIBUTIONS

I would like to acknowledge the names of my supervisors who contributed to the research presented in this dissertation:

- Professor Timothy Topper
- Professor Grzegorz Glinka

ABSTRACT

The work in this thesis examines the effect of mean stress on the fatigue behaviour of very hard (Rockwell C 60) steels (AISI 8822, 8620, 9310, and cold-worked pre-stressing wire). In the mean stress tests, the minimum stress in the fatigue cycle was varied from test to test over a range from -1200 MPa to a value approaching the true fracture stress of each material. The results are not adequately explained by current theories for the effect of mean stress on fatigue behaviour in the region of compressive mean stresses. All current theories suggest that the maximum stress at the fatigue limit decreases with decreasing minimum stress. The results of this study shows that instead of continuing to decrease with decreasing minimum stress the maximum stress at the fatigue limit remains constant indicating an insensitivity to the minimum stress in the fatigue cycle for minimum stresses below the value in a fully reversed fatigue test. The theory proposed by the author corrects this error by maintaining the maximum stress at the fatigue limit constant with decreasing minimum stress in the region of negative mean stresses. The results are of interest to designers of components in which high negative residual stresses are introduced into materials hardened by, for example, carburizing, nitriding, or induction hardening to improve the fatigue strength of components. The present work allows considerably higher design stresses for operating stresses in the negative mean stress region than previous theories permit.

ACKNOWLEDGEMENTS

First and foremost, I offer my most sincere and deepest gratitude to my MASc supervisor, Professor Emeritus Dr. Timothy Topper. Throughout my stay at the University of Waterloo, he guided me and taught me everything, from how to run fatigue tests in the laboratory, through helping me understand Metal Fatigue concepts, to how to adapt to the cold Winters in Canada. He provided encouragement, sound advice, great mentoring, and great company. With his endless patience and energy, he was always accessible and willing to help. One simply could not wish for a better or friendlier supervisor.

I would also like to thank my co-supervisor, Dr. Grzegorz Glinka, who has showed his support in a number of ways and without whom I wouldn't be here. I had the honour to attend his class and he sets an example of a world-class researcher for his passion on knowledge.

My warm thanks to my committee members, Professors Dr. Scott Walbridge, and Dr. Giovanni Cascante for reviewing my thesis, evaluating my research, and for their insightful feedback.

I am grateful to the technical staff at the University of Waterloo for their expertise and support throughout my graduate studies, namely, Richard Morrison, Douglas Hirst, Rob Sluban, and Rick Forgett.

Thanks to my friends and colleagues, Alex Marie, Andrew McLean, Antonio Miranda, Eric Chandler, Gregory Wentworth, Hisham Elhuni, Lauren Huston, Rakesh Ranjan, Rayed Alyousef, Shawna Wey, Stewart Russel, Taha Younes, and Zachary Matthews.

Moreover, I would like to thank the administrative staff at the Department of Civil and Environmental Engineering and the Department of Mechanical and Mechatronics Engineering for all the support.

DEDICATION

To My Mom, and Dad

TABLE OF CONTENTS

LIST OF FIGURES

LIST OF TABLES

LIST OF ABBREVIATIONS

GNP: Gross national product

BCC: Body-centered cubic

BCT: Body-centered tetragonal

FCC: Face-centered cubic

HRC: Rockwell C hardness

NOMENCLATURE

$b =$ exponent constant for a stress-life curve

$F_d =$ draw force

$\sigma_a =$ stress amplitude

$\sigma_{ar} =$ stress amplitude for $\sigma_m = 0$; equivalent completely reversed stress amplitude

$\sigma_{max} =$ maximum stress

$\sigma_{min} =$ minimum stress

$\sigma_u =$ ultimate tensile strength

$\Delta\sigma =$ stress range; $\Delta\sigma = 2\sigma_a$

$R =$ stress ratio; $R = \sigma_{min/}\, \sigma_{max}$

$\sigma_f' =$ intercept constant at 1/2 cycle for a stress-life curve

$\tilde{\sigma}_{fB} =$ true fracture strength, corrected

$\sigma_y =$ yield limit

$M_s =$ temperature at which martensite starts to form

$N_f =$ fatigue life, cycles to failure

$\gamma =$ fitting constant for the Walker method

CHAPTER 1

INTRODUCTION

The Eschede derailment was the worst high-speed-rail disaster so far. The German Inter-City Express derailed in June 1998, killing 101 people and leaving around 100 injured [1]. The train featured an innovative wheel design that used a rubber damping ring between the rail-contacting steel tyre and the steel wheel body to minimize vibration. Investigations following the accident showed that it was caused by fatigue failure of a steel tyre. Accidents like this are an example of the cost, both financial and in human lives, caused by mechanical failures.

A study of the economic impact of fractures of materials in the United States was published in 1983 by a division of the U.S. Department of Commerce, the National Institute of Standards and Technology [2]. The total annual cost was estimated in $119 billion in 1982 U.S. dollars, corresponding to 4% of the gross national product (GNP). A similar study of fracture costs in Europe also yielded an overall cost of 4% of the GNP, and similar results are likely to apply to all industrial nations according to Milne [3].

These reports considered the costs associated with fracture for repair, maintenance, inspection, recalls, litigation, insurance, etc. The U.S. study also included the cost of designing components beyond the minimum requirements for resisting yielding failure of the material, since designing against fracture due to fatigue requires the use of more raw material. According to the report, one-third of the $119 billion annual cost could be eliminated by better use of then-current technology, and another third could be eliminated through research and development. Hence, the use of inaccurate models for the design of machines, vehicles, and structures can have a severe economic impact by reducing the excess use of raw materials and the number of unexpected failures and their associated costs.

1.1 Fatigue

Mechanical components are frequently subjected to repeated loads, and the associated cyclic stresses can result in microscopic damage to the material, even at stresses well below a given material's ultimate static strength. With continued cycling, this microscopic damage can accumulate and develop into a crack, which may lead to the failure of the component. The process of accumulating damage and failure due to cyclic loading is called *fatigue*.

Fatigue is an important mechanical failure mechanism because most machines and structures work under dynamic loads that induce relevant variable stresses through their operational lives.

An estimated 80% of the fracture costs previously discussed involve situations where cyclic loading and fatigue are at least a contributing factor. This represents 3% of the GNP of the United States. These costs arise from the occurrence or prevention of fatigue failure for road vehicles, rail vehicles, aircraft, bridges, cranes, power plant equipment, offshore oil well structures, and a variety of miscellaneous machinery and equipment including everyday household items, toys, and sports equipment. For example, wind turbines used in power generation, are subjected to cyclic loads due to rotation and wind turbulence, making fatigue a critical aspect of the design of the blade and other moving parts.

1.2 Mean Stress

Engineering applications where stress or strain limits vary asymmetrically about zero are commonly encountered, i.e. the upper and lower limits of a loading cycle are not equidistant from the x-axis (Figure 2.1). This results in a non-zero mean stress. Some examples are pressure vessels, gear teeth and springs. Residual stresses can also induce a mean stress in a component subjected to fully reversed loading. The residual stresses may be induced by manufacturing processes such as welding, grinding, extrusion, carburizing, etc.

Compressive mean stresses are usually beneficial to the fatigue life of a component, while tensile mean stresses can greatly decrease its fatigue life. Therefore, it is important to quantify the effect of mean stresses on fatigue life.

The mean stress effect has been studied for over a century, but even though there are several methods available for evaluating it, there is no consensus as to which method is best. Inaccurate models are frequently used, resulting in unpredicted failures or the use of excess raw material due to the use of generous safety factors prescribed to compensate for the inaccuracy of the design methods.

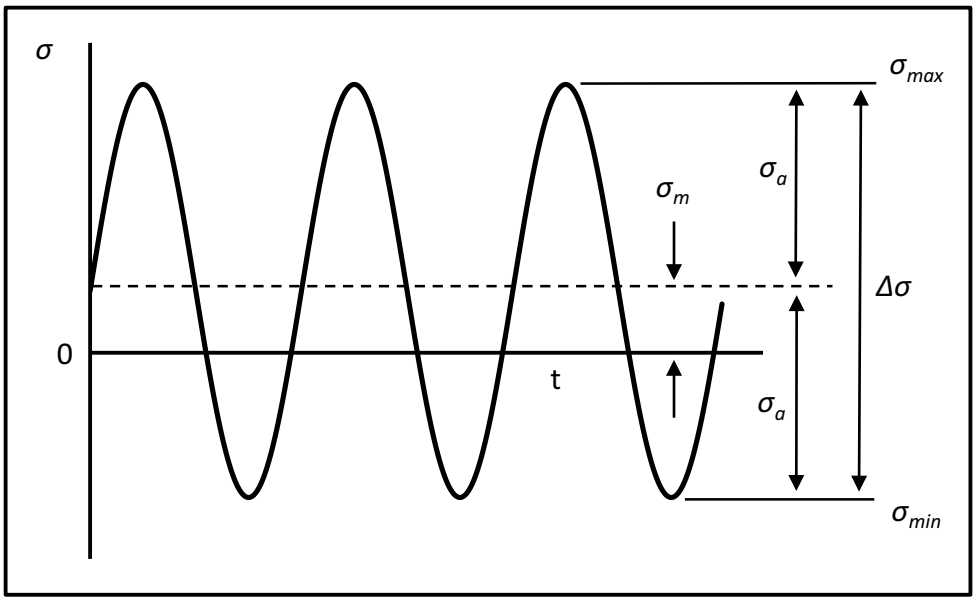

Figure 1.1: Constant amplitude cyclic loading and definition of stress variables.

1.3 Material hardening

A variety of heat treatments are available to modify a steel's microstructure, and subsequently, change its mechanical properties. Process annealing, is used to eliminate the effects of cold work; spheroidizing, is used to improve machinability; quenching, is used to harden most steels; and tempering is, used to increase the toughness.

In this thesis, we are interested in the hardening of steel. Reasons for hardening a steel include, achieving the high hardness and strength levels required by structural components subjected to high operating stresses. Also, tools such as dies, knives, cutting devices, and forming devices need a hardened structure to resist wear and deformation.

Hardening of a steel involves a change in its crystal structure, from the body-centered cubic (BCC), present at room temperature, to face-centered cubic (FCC) by heating it completely into the austenite region, followed by quenching to cause carbon to be trapped in the crystal structure. This can be accomplished by immersing the heated component into water, oil, or salt, depending on the desired cooling rate. The FCC structure of austenite, present at high temperatures, can hold more carbon in solution than the BCC of Ferrite. When rapidly cooled (quenched), the iron matrix can't return to its equilibrium BCC structure due to trapped carbon atoms. This results in a phase called martensite with a distorted crystal structure called body-centered tetragonal (BCT).

Steel is defined as an alloy of carbon and iron, with a carbon content ranging within 2 sufficient carbon content, usually 0.40%.

1.4 Residual Stresses

During the cooling of a heat-treated steel part, there are two processes responsible for the dimensional changes that ultimately result in residual stresses and distortions. One is the volume expansion resulting from the transformation of the more compact, FCC structure of austenite, into the more open-crystal structure of martensite. This transformation is associated with a volume expansion of the order of 1–3%. The other is the thermal contraction associated with cooling in the absence of a phase transformation. The former is the dominant factor in heat treatments involving cooling starting in the austenite phase, while the latter is the dominant one in subcritical heat treatments. The cooling rate varies depending on the section size and position in a part, leading to volume changes that occur in different locations at different times, resulting in residual stresses and distortions.

When a steel part is quenched from the austenite phase field, the surface layers cool down faster than the interior. Consequently, the austenite transformation with the following volume expansion occurs there first. This initially results in a compressive stress at the surface, which at elevated temperatures, is relaxed due to the low yield strength of the material. However, at a later point in the cooling process, when the interior transforms, its expansion is restrained by the hardened surface layer. This, places the surface in tension and the interior in compression. These tensile stresses can be reduced by using a steel of lower hardenability so that the interior does not go through a martensitic transformation, but instead transforms to bainite at a higher temperature than the martensitic transformation.

The reverse is true for subcritically heat treated parts, i.e., heat treatments that occur below the austenite transformation temperature. The surface cools and contracts first, and the still hot and ductile interior accommodates readily. However, when the interior eventually cools, its contraction is opposed by the higher strength surface. The restraint on the contraction places the interior in tension while the surface is, in turn, placed in compression by the contracting interior. In general, the resultant compressive stress in the surface layers is beneficial to fatigue performance, except when followed by machining, which may cause distortion due to the non-uniform removal of material from the surface.

The different cooling rates throughout a steel component may produce stresses that causes distortion is high enough to induce non-uniform yielding or plastic deformation. Even in the case where no yielding occurs, stresses of up to yield point magnitude may be present on reaching room temperature, and such residual stresses will be superimposed on the applied stresses in service unless a stress relief treatment is performed, such as

tempering. Surface compressive stresses are desirable, because they reduce the tensile stress peaks due to the loads applied in service. Residual tensile stresses, however, increase the stress peaks due to the applied loads which lowers the fatigue resistance.

1.5 Selective Hardening

Through-hardened steels are brittle at hardnesses over about 55 HRC (Rockwell C hardness). To prevent that as well as the distortion associated with the volume change resulting from the phase transformation in the heat treatment processes. Some more sophisticated processes are available to treat only the surface of the material, called *surface heat treatment*. They allow us to produce a part that is hard and strong at the surface, giving improved wear and fatigue resistance, while retaining a ductile, tough core that provides good impact failure resistance. Also, selective hardening is usually cheaper than through-hardening and distortion is minimized since a smaller volume of material is transformed.

Two mechanisms may be involved: (1) hardening by the diffusion of hardening elements into the surface of an "nonhardenable" steel, and (2) local austenitizing and quenching of a hardenable steel or iron.

An automobile axle and drive gear are examples of the application of these methods. Both parts require good fatigue resistance. The gear also should have a high hardness to avoid wear, and the axle should have a good overall strength to withstand bending and torsional loads.

1.5.1 Flame Hardening

Flame hardening is the process of selective hardening where the heat source for austenizing is a combustible gas flame. As mentioned previously, suitable materials with sufficient carbon content (0.40%) are necessary for selective hardening with the flame-hardening process to allow hardening. Quenching after heating to the austenitic transformation temperature is usually accomplished with a rapid water quench, because this process is normally performed on low-alloy or plain carbon steels with low hardenability (steels with high hardenability have a greater tendency to crack). Oxygen–acetylene, oxygen–manufactured gas, propane, or any other combination of fuel gases that will allow reasonable heating rate are used as fuel for the flame. The hardening temperatures are the same as those required for furnace hardening.

1.5.2 Induction Hardening

The mechanism and purpose of induction hardening are the same as for flame hardening. The primary difference is the heating source. In induction hardening heating is achieved by inducing an electric current flow in the component. A magnetic field surrounding a conductor is always created when there is a current flowing through the conductor. The reverse is also true, if a magnetic field is created around a conductor, an electric current is induced in the conductor. Therefore, if an electric conductor is place inside a wire coil, the magnetic field created by the coil will induce a current flow in the core component. Since the inner wire is a dead-end electric circuit the induced current cannot flow, resulting in the heating of the wire.

An alternating current in the coil, with frequencies ranging from 60 to millions of cycles per second, is used to obtain a current flow that changes rapidly in direction. Heating occurs from the outside inwards. The electrical resistance to the current flow causes fast heating of the core component. This heating is used to reach the austenizing temperature, and is following quenching is used to obtain hardening.

1.5.3 Carburizing

In cases where the steel has insufficient carbon content a diffusion treatment can be applied to add elements to the surface to allow for hardening. Diffusion is defined as the spontaneous movement of atoms or molecules from a region of high concentration to a region of low concentration that tends with time to make the composition uniform throughout the medium.

Carburizing is one of a series of heat-treatment processes that involve diffusion of alloying elements into a metal substrate that normally has a low concentration of that element. The purpose of carburization is to provide a hard surface on normally non-hardenable steels.

In carburization, a piece of low-carbon steel is placed in a carbon-saturated atmosphere at an elevated temperature, making the carbon diffuse into the steel, carburizing it. There are basically three processes used to provide a suitable carbon gradient to allow inward diffusion: pack, gas, and salt. In pack carburizing the part to be carburized is packed in a steel container so that it is completely surrounded by granules of charcoal. The charcoal is treated with an activating chemical such as barium carbonate ($BaCO_3$) that promotes the

formation of CO_2 gas. This gas in turn reacts with the excess carbon in the charcoal to produce carbon monoxide, CO. The carbon monoxide reacts with the low-carbon steel surface to form atomic carbon, which diffuses into the steel.

$$CO_2(g) + C \rightleftharpoons 2CO(g)$$

Gas carburizing can be done with any carbonaceous gas, but natural gas, propane, or generated gas atmospheres are most frequently used. The source of the diffusing species is carbon from CO that is produced from the starting gas CH_4, C_3H_2, and others. Most carburizing gases are flammable if not explosive, and controls are needed to keep carburizing gas at 1700°F (937°C) from contacting air (oxygen). The advantage of this process over pack carburizing is an improved ability to quench from the carburizing temperature.

Salt or liquid carburizing is performed in internally or externally heated molten salt pots. The carburizing salt usually contains cyanide compounds such as sodium cyanide, NaNC. The carbon from the cyanide provides the diffusing species. Because heating by liquid convection is faster than heating by gas convection, the cycle times for liquid carburizing are shorter than for gas or pack carburizing.

The carburizing process per se does not harden the steel. It only increases the carbon content to some predetermined depth below the surface to a sufficient level to allow subsequent quench hardening. There is no technical limit to the depth of hardening, but it is not common to carburize to depths beyond 0.050 in (1.27 mm).

Carburizing is carried out in the austenitic range and can lead to the development of a compressive residual stress at the surface during quenching for the following reason. Carbon is one of the elements that decreases the M_s Temperature (the temperature at which martensite starts to form in a given alloy) of a steel. The M_s temperature of the carburized surface layer, therefore, can be much lower than that of the interior because of the differential in carbon contents. On quenching, the interior, even though it is at a higher temperature than the surface, is the first to transform due to its higher M_s temperature. Later on, the surface transforms and tries to expand, but it is now restrained by the already transformed interior. As a result, the surface is left in a state of residual compression.

1.5.4 Nitriding

In this process, monatomic nitrogen is diffused into the surface of the steel being treated. The reaction of the nitrogen with the steel causes the formation of very hard iron and alloy

nitrogen compounds. The resulting nitride case can be harder than even the hardest tool steels or carburized steels. The outstanding advantage of this process over all the other hardening processes previously mentioned is that subcritical temperatures are used, and hardness is achieved without the oil, water, or air quench required of other heat-treating processes.

The source of the nitrogen for the diffusion process is most commonly ammonia. Parts to be nitride are placed in a retort racked to provide good gas circulation), and the retort is heated to the nitriding temperature, which is usually between 925^{o} and 1050^{o}F (500^{o} and 570^{o}C). Either nitrogen or ammonia is flowing during the heat-up cycle. At the nitriding temperature, the ammonia dissociates by the following reaction:

$$2NH_3 \rightarrow 2N + 3H_2 \uparrow$$

The nitrogen diffuses into the steel and the hydrogen is exhausted.

Nitriding is carried out at an elevated temperature below the eutectoid temperature for time periods of the order of 9–24 hours, and during the nitriding process any prior residual stresses are relaxed. Since the temperatures are lower than those in carburizing and no phased transformation is involved, problems with distortion are minimized, an important consideration when heat treating carefully machined parts such as crankshafts. The formation of nitrites leads to a beneficial compressive residual stress in the surface even after the usual slow cooling because of a lower coefficient of expansion of the nitrites.

1.5.5 Strain Hardening

During deformation of a metallic material, strengthening is obtained by increasing the number of dislocations. Before deformation, the dislocation density is about 10^6 cm of dislocation lines per cubic centimeter of metal.

When a stress greater than the yield limit is applied, dislocations begin to slip (Schimid's Law). Eventually, obstacles pin the ends of the dislocation line as a dislocation moves on its slip plane. As the stress continues to be applied, the dislocation bows in the centre as it attempts to continue moving. This may continue to a point where a loop is produced. When the dislocation loop touches itself, a new dislocation is created. The original dislocation is still pinned and this process can continue and create additional dislocation loops. This mechanism is called a Frank-Read source and is illustrate in Figure 1.2.

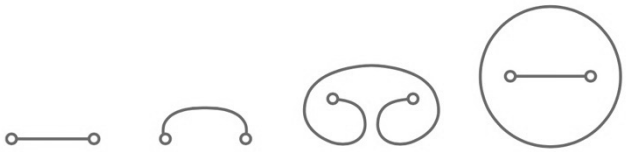

Figure 1.2: Dislocations looping on themselves and forming new dislocations.

The dislocation density may increase to about 10^{12} cm of dislocation line per cubic centimeter of metal during strain hardening. Dislocation motion is the cause for the plastic deformation in metallic materials. When there are too many dislocations, however, they disrupt their own motion. An analogy can be made with a room, when there are too many people in it, it is difficult for them to move around. As a result, metallic materials that have undergone cold working see an increase in strength at the expense of ductility.

During plastic deformation caused by cold or hot working, a microstructure consisting of elongated grains in the direction of the applied stress is often produced. The grains rotate and elongate, causing certain crystallographic planes and directions to become aligned with the direction of the applied stress. Thus, preferred orientations are created and cause anisotropic behaviour that means that the properties of a cold-worked component depend on the direction in which the property is measured.

A small portion of the applied stress is stored in the form of residual stresses within the structure as a tangled network of dislocations. Residual stresses generated by cold working may not always be desirable and can be relieved by a heat treatment known as a stress-relief anneal. In some instances, residual compressive stresses at the surface of a material are deliberately created to enhance its mechanical properties.

For example, the process of fabricating wires, also known as wire drawing, consists of pulling a rod through a die to produce a smaller cross-sectional area. For a given draw force F_d, a different stress is produced in the original and final wire. The stress on the original wire must exceed the yield limit of the material to cause deformation, while the stress on the final wire must remain below the yield limit to prevent failure. This can only be achieved if the wire strain hardens during drawing.

1.5.6 Shot peening

Shot peening consists of bombarding the surface of a component with shot (round metallic, glass, or ceramic particles) propelled at a high velocity causing plastic deformation;

therefore, introducing compressive residual stresses at the surface that increases the resistance of the metal surface to fatigue failure. The particles work as a ball-peen hammer.

Fatigue failures typically begin at the surface of a part

Shot peening is an inexpensive process that may be used to salvage components suffering from fatigue failures. Since this method does not alter the dimensions of the part, the functionality of the component is not compromised.

1.5.7 Others

There are a variety of other surface hardening processes that involve similar principles, or a combination of the treatments previously mentioned; Laser heat treatment, electron beam (EB) hardening, carbonitriding, cyaniding, ion implantation, etc.

1.6 Example

Consider a component that has been through quenched and tempered. It is made of steel, and its stress-life curve is shown in Figure 1.4. The component is subjected to a constant amplitude, fully reversed ($R = -1$), service load history with a peak stress of 500 MPa (Figure 1.3). According to the stress-life curve, the component will fail at 1,000 cycles.

Now suppose the same component was carburized instead of quenched and tempered. This process induced a compressive residual stress on the surface of 200 MPa. If the same load history is applied, the component will see a resultant cycle with peaks 300 and -700 MPa. Again, according to the stress-life curve, the new component will now fail at 30,000 cycles, 30 times longer. If the induced residual stress was 350 MPa instead, the component would be subjected to a resultant cycle with peak stress of 150 MPa. This stress is below the fatigue limit and therefor, the component would not fail.

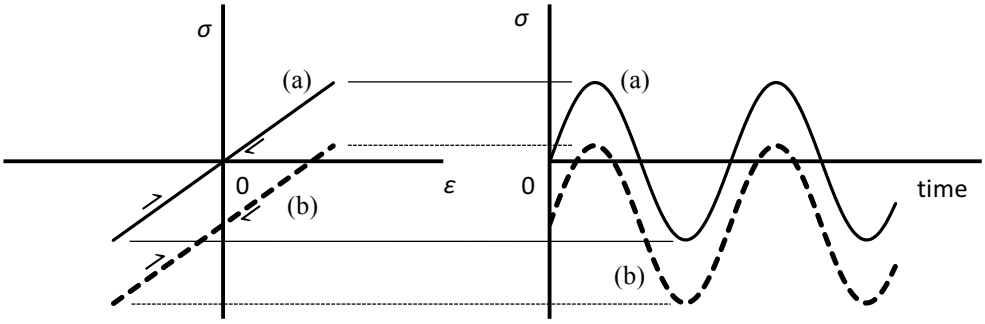

Figure 1.3: Example of a cyclic stress-strain diagram showing stress-strain loops for: (a) specimen free of residual stresses, (b) specimen with compressive residual stresses, and corresponding stress history

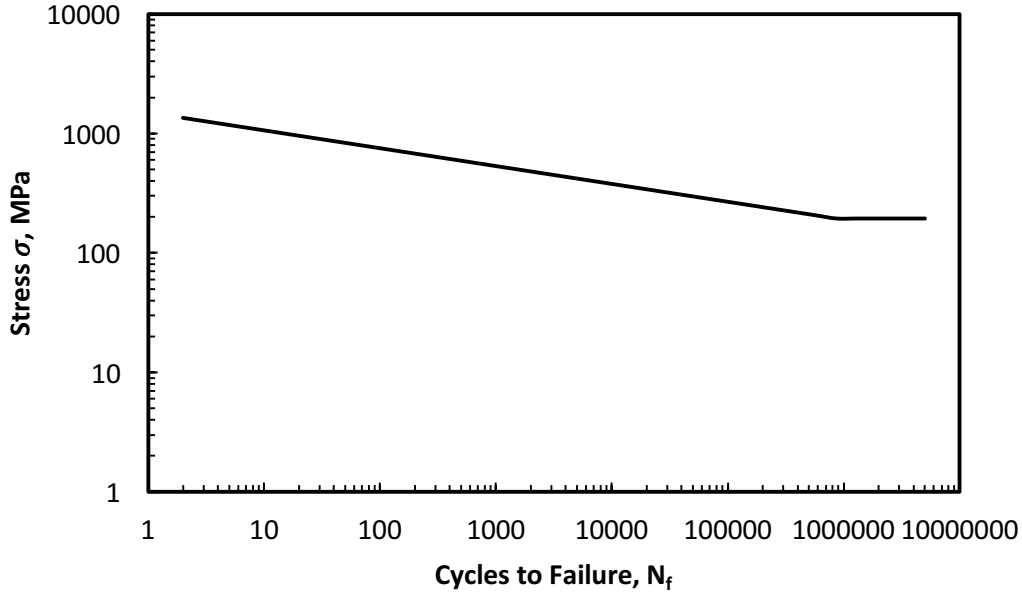

Figure 1.4: Example of a stress-life curve

1.7 Research Objectives

The importance of predicting the effect of mean stresses in fatigue arises from the fact that in real life applications many components are subjected to service loads that induce non-zero mean stresses and that in other applications the component has undergone a process that introduced residual stresses that consequently induce non-zero mean stresses even when the applied load cycle has no mean load. The effect of mean stress in the fatigue life of materials has been studied for over a century. However, despite all the work done, and the numerous methods proposed for calculating the allowable cyclic stresses and fatigue lives in the presence of mean stresses, there is no consensus on the suitability of the different

approaches. Moreover, recent technologies have allowed for the manufacturing of components with mechanical properties not achievable when most of these methods were developed. As a result, the existing approaches fail to predict the behaviour of such materials, as is the case for very hard steels (above 55 HRC).

The main objectives of this thesis are:

1. Provide a better understanding of the most used mean stress effect prediction methods;
2. Investigate the performance of these methods when applied to very hard steels;
3. Develop a better approach to account for mean stress effect in the fatigue life calculations of very hard steels.

1.8 Thesis Organization

Chapter 2 presents an in-depth background and literature review of topics and research studies. Chapter 3 presents the materials used in this study, as well as details of the experimental program. Test results are presented in Chapter 4, while Chapter 5 presents a detailed analysis and discussion of the experimental results, and comparison with a proposed method. Finally, Chapter 6 offers a closing summary, conclusions, and recommendations.

CHAPTER 2

BACKGROUND AND LITERATURE REVIEW

2.1 Introduction

Mechanical failures due to fatigue have been studied for more than 150 years. Starting in the 1850s, the work in Germany of August Wohler, motivated by railway axle failures, is of special importance. He developed design strategies for avoiding fatigue failures. Wöhler also demonstrated that fatigue was affected not only by cyclic stresses, but also by the accompanying steady (mean) stresses. More detailed studies following Wohler's lead included those of Gerber and Goodman who attempted to predict the effect of mean stresses on fatigue behaviour. The early work on fatigue and subsequent efforts up to the 1950s are reviewed in a paper by Mann [4].

Nomenclature used: σ_a is stress amplitude, σ_m is mean stress, $\Delta\sigma = 2\sigma_a$ is stress range, and $R = \sigma_{min}/\sigma_{max}$ is the stress ratio. The relationships given by Eq. (2.1) follow from the definitions illustrated in Figure Figure 2.1.

$$\sigma_a = \frac{\sigma_{max} - \sigma_{min}}{2} \quad \text{(a)}$$

$$\sigma_m = \frac{\sigma_{max} + \sigma_{min}}{2} \quad \text{(b)} \qquad (2.1)$$

$$\sigma_a = \frac{\sigma_{max}}{2}(1 - R) \quad \text{(c)}$$

$$\sigma_m = \frac{\sigma_{max}}{2}(1 + R) \quad \text{(d)}$$

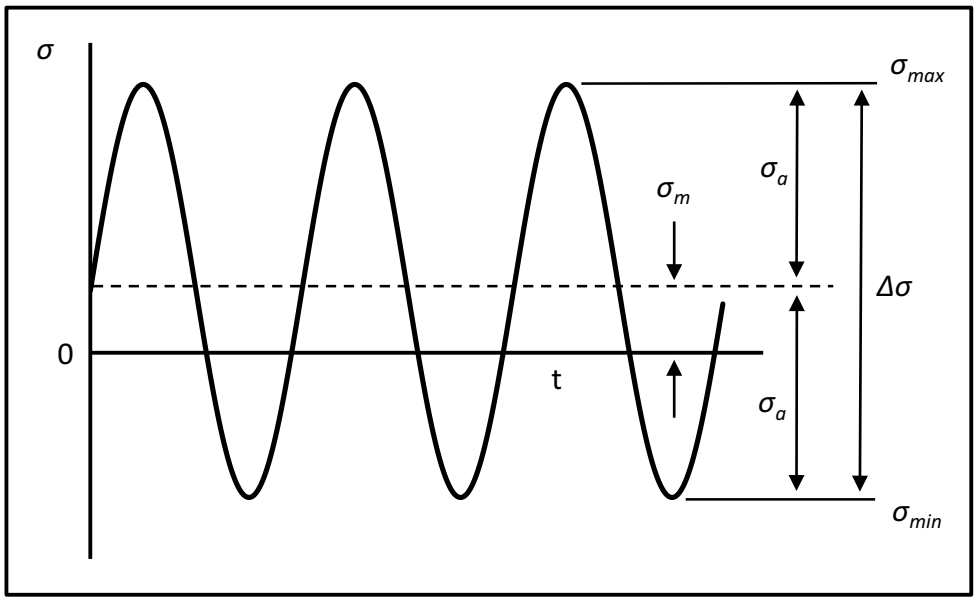

Figure 2.1: Constant amplitude cyclic loading and definition of stress variables.

2.2 Mean Stress Relationships

In the following mean stress rules σ_f and b are fitting constants. N_f is the number of cycles to failure, and σ_{ar} is the stress amplitude. The subscript r indicates the case where $\sigma_m = 0$, also called fully-reversed (R=-1)

To estimate the life N_f for non-zero mean stress cases, an equation $\sigma_{ar} = f(\sigma_a, \sigma_m)$ is needed.

The following relationship was developed by Smith [5] from a proposal made by Goodman, and it is called the *modified Goodman equation*. It uses the ultimate tensile strength σ_u, and for most ductile materials tends to be conservative, that is, the error in this method causes extra safety in life estimates.

$$\frac{\sigma_a}{\sigma_{ar}} + \frac{\sigma_m}{\sigma_u} = 1, \qquad \sigma_{ar} = \frac{\sigma_a}{1-\sigma_m/\sigma_u} \qquad \text{(a, b)} \qquad (2.2)$$

This method can be improved for ductile materials by replacing σ_u in Eq. (2.2) with either: (a) the corrected true fracture strength $\tilde{\sigma}_{fB}$ from a tension test or (b) the constant σ_f' from the unnotched axial S-N curve for $\sigma_m = 0$.

$$\frac{\sigma_a}{\sigma_{ar}} + \frac{\sigma_m}{\tilde{\sigma}_{fB}} = 1, \qquad \sigma_{ar} = \frac{\sigma_a}{1-\sigma_m/\tilde{\sigma}_{fB}} \qquad \text{(a, b)} \tag{2.3}$$

The constant σ_f' is the intercept for $N_f = 0.5$ (this interpret a tension test as a fatigue test of one half cycle).

$$\frac{\sigma_a}{\sigma_{ar}} + \frac{\sigma_m}{\sigma_f'} = 1, \qquad \sigma_{ar} = \frac{\sigma_a}{1-\sigma_m/\sigma_f'} \qquad \text{(a, b)} \tag{2.4}$$

These modifications of the Goodman relationship were proposed by J. Morrow in the first edition of the Society of Automotive Engineers' *Fatigue Design Handbook* (Graham, 1968) [6].

According to Landgraf [7], $\tilde{\sigma}_{fb} = \sigma_f'$ is a good estimate for steels, but not for aluminium alloys. Dowling [8] suggests that Eq. (2.3) with the true fracture strength is reasonably accurate in most cases, but the true fracture strength $\tilde{\sigma}_{fb}$ is usually not available and needs to be estimated. Eq. (2.4) with the fitting constant σ_f' is also reasonably accurate for steels, but non-conservative for aluminium alloys.

Smith-Watson-Topper (SWT) provides good results in most cases. For aluminium alloys it is more accurate than Morrow $\tilde{\sigma}_{fb}$. It has the advantage of simplicity since it does not rely on any material constant.

$$\begin{aligned}
&\sigma_{ar} = \sqrt{\sigma_{max}\sigma_a} && (\sigma_{max} > 0) \quad \text{(a)} \\
&\sigma_{ar} = \sigma_{max}\sqrt{\frac{1-R}{2}} && (\sigma_{max} > 0) \quad \text{(b)} \\
&\sigma_{ar} = \sigma_a\sqrt{\frac{2}{1-R}} && (\sigma_{max} > 0) \quad \text{(c)}
\end{aligned} \tag{2.5}$$

The Walker equation employs a material constant γ.

$$\begin{aligned}
&\sigma_{ar} = \sigma_{max}^{1-\gamma}\sigma_a^{\gamma} && (\sigma_{max} > 0) \quad \text{(a)} \\
&\sigma_{ar} = \sigma_{max}\left(\frac{1-R}{2}\right)^{\gamma} && (\sigma_{max} > 0) \quad \text{(b)}
\end{aligned} \tag{2.6}$$

$$\sigma_{ar} = \sigma_a \left(\frac{2}{1-R}\right)^{1-\gamma} \qquad (\sigma_{max} > 0) \qquad \text{(c)}$$

γ varies 0 to 1 theoretically. For metals, it's in the range 0.4-0.8. If $\gamma = 0.5$ the equation reduces to the SWT equation. The term $(1-\gamma)$ is a measure of a material's sensitivity to mean stress. $\gamma = 0.4$ is sensitive and $\gamma = 0.8$ is insensitive. When data is available for fitting the parameter γ, this method, according to Dowling [8], provides the best results but is seldom used because mean stress tests are needed to determine the constants.

The Gerber parabola is inaccurate and non-conservative for tensile mean stresses. And incorrectly predicts a harmful effect of compressive mean stress.

$$\frac{\sigma_a}{\sigma_{ar}} + \left(\frac{\sigma_m}{\sigma_u}\right)^2 = 1 \qquad (\sigma_m \geq 0) \qquad \text{(a)}$$

$$\sigma_{ar} = \frac{\sigma_a}{1-(\sigma_m/\sigma_u)^2} \qquad (\sigma_m \geq 0) \qquad \text{(b)} \qquad (2.7)$$

Soderberg uses the yield limit σ_y.

$$\frac{\sigma_a}{\sigma_{ar}} + \frac{\sigma_m}{\sigma_y} = 1 \qquad \text{(a)}$$

$$\sigma_{ar} = \frac{\sigma_a}{1-\sigma_m/\sigma_y}. \qquad \text{(b)} \qquad (2.8)$$

Results for this method are conservative according to Fatemi [9].

Figure Figure 2.2 illustrates the predictions of the various mean stress correction rules.

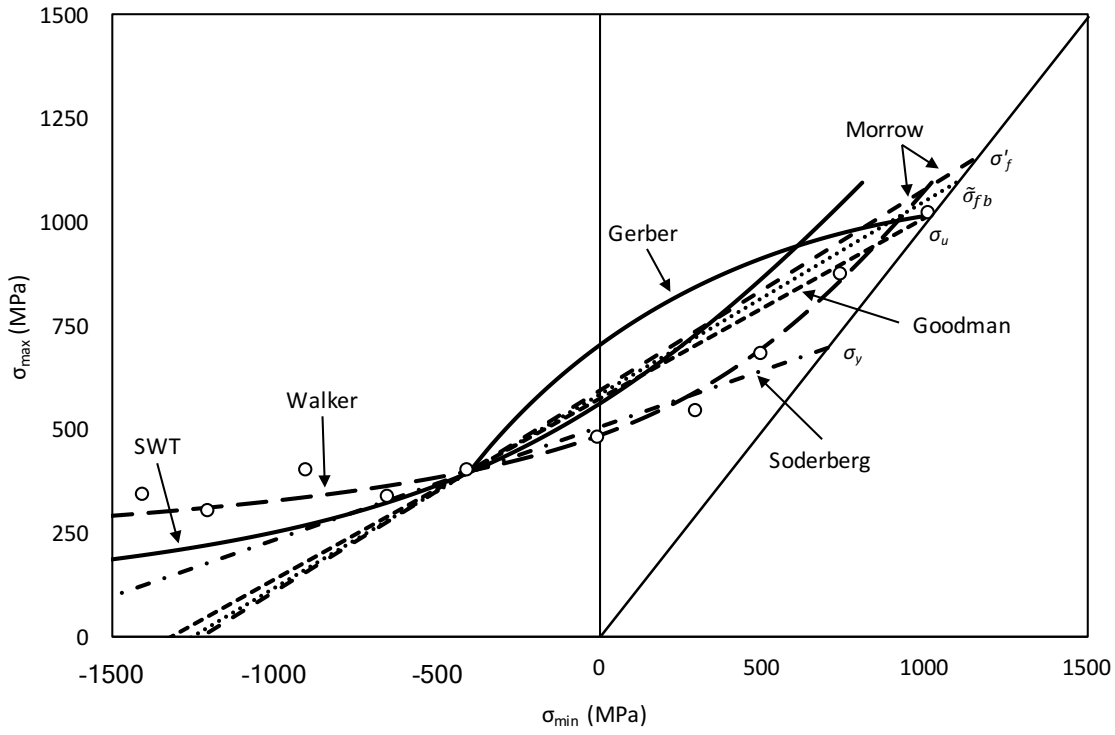

Figure 2.2: Max-min stress diagram comparing the predictions of the most common mean stress correction methods to a sample material data

CHAPTER 3

MATERIALS AND EXPERIMENTAL PROCEDURE

3.1 Test Equipment and Procedure

3.1.1 Monotonic Tensile Tests

Tension tests were carried out on AISI 9310 and AISI 8620 through carburized steels (data for other materials were obtained from internal reports). These tests provided information on the strength and ductility of the material under uniaxial tensile stresses as well as the engineering monotonic tensile stress-strain curves.

3.1.2 Fully Reversed Constant Amplitude Tests

All fatigue tests were carried out in a laboratory environment at approximately 25^{o}C using an MTS servo-controlled closed-loop electro-hydraulic testing machine. A process control computer, controlled by FLEX software [11] was used to output strain or load amplitudes. These tests were used to determine the cyclic properties of the studied steels and to generate the cyclic stress-strain and the total strain-life curves.

Axial, constant strain amplitude, fully reversed (R=-1), strain-controlled fatigue tests were performed on smooth specimens. The stress-strain limits for each specimen were recorded for the initial cycles of the test via peak reading voltmeters. Failure of a specimen was defined as a 50 percent drop in the tensile peak load from the peak load observed at one half the expected specimen life. The loading frequency varied from 0.05 Hz to 3 Hz. For fatigue lives greater than 100,000 reversals (once the stress-strain loops had stabilized) in constant amplitude tests, the specimens were tested in load control. For the load-controlled tests, failure was defined as the separation of the smooth specimen into two pieces. The test frequencies used in this case were between 30 and 120 Hz.

Prior to testing, the load train alignment (load cells, grips, specimen, and actuator) was checked. Then the smooth specimen was inserted and secured into the lower grip, and the hydraulic actuator was raised until the second end of the specimen was inserted and secured into the upper grip.

3.1.3 Mean Stress Tests

The mean stress tests were conducted for a series of specimens of each material at several minimum stress levels. In each series, the minimum stress was kept constant while the maximum stress was lowered for each specimen until the fatigue limit was reached. The minimum stress was varied from -1200 MPa to a tensile value approaching the true fracture stress of the material.

3.2 Materials

The materials used in this investigation are AISI 8822, AISI 9310 through carburized steel, AISI 8620 through carburized steel (simulated case), and the centre strand of a 7-strand pre-stressing wire.

3.3 Carburized steels

The material for this study was received in the form of 2" diameter bars. Smooth fatigue specimens, shown in Figure Figure 3.1, were machined from the metal bars and prepared in accordance to ASTM standard E606 - 04. The specimens were then polished in the gauge section using 240, 400, and 600 emery paper. Then they received a final polish in the loading direction using an extra fine Cratex™ wheel. Before testing, the specimens were carburized. Finally, a thin band of M-coat D acrylic coating was applied along the central gauge section. The purpose of the M-coat D application was to prevent scratching of the smooth surface by the knife-edges of the strain extensometer, thus reducing the incidence of knife-edge failures.

Figure 3.1: Uni-axial smooth cylindrical fatigue specimen

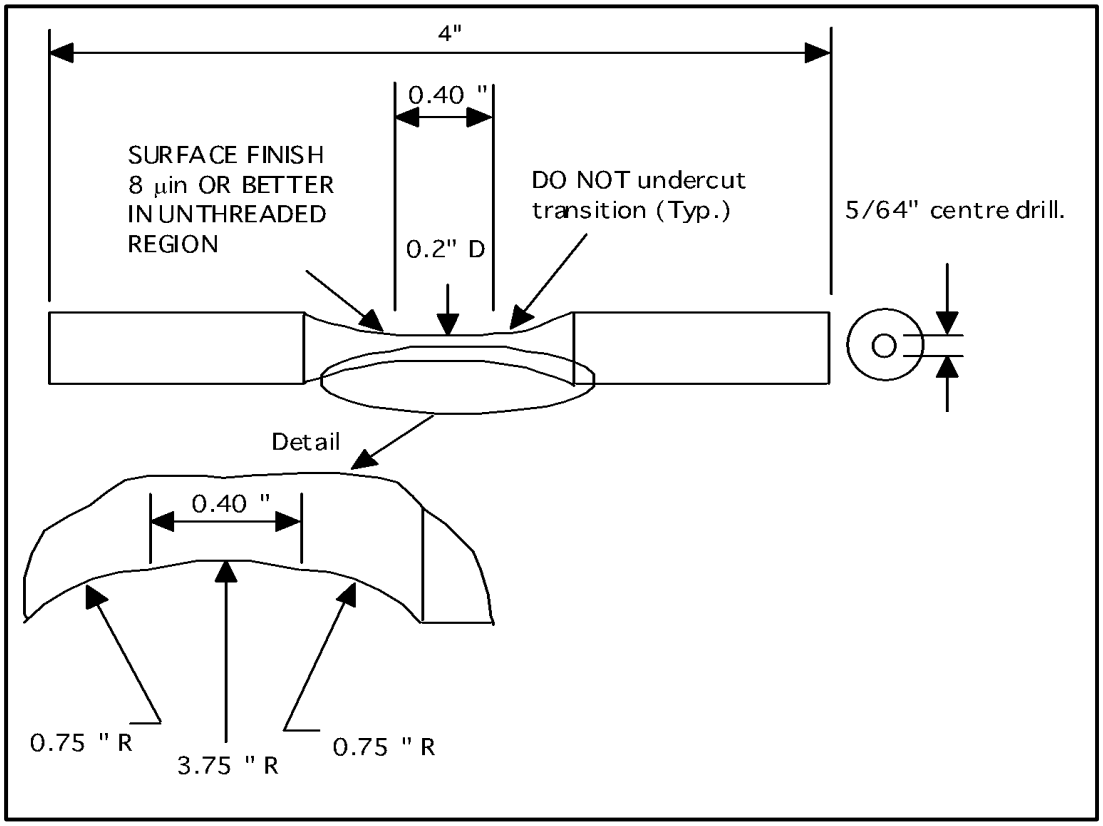

Figure 3.2: Uni-axial smooth cylindrical fatigue specimen drawing

3.3.1 AISI 8822

The chemical composition for AISI 8822 was obtained from El-Zeghayar [13] and is shown in Table 3.1. The mechanical properties, both monotonic and cyclic, were also obtained from El-Zeghayar [13] and is presented in Table 3.2.

Table 3.1: Chemical composition of AISI 8822 steel (percentage by weight)

Alloy	C	Mn	P	S	Si	Cu	Ni	Cr	Mo	Cb	Sn	Al	V	N
AISI 8822	0.22	0.86	0.013	0.025	0.17	-	0.43	0.54	0.39	0.24	0.01	0.028	0.004	-

Source: El-Zeghayar [13]

Table 3.2: Mechanical (monotonic and cyclic) properties of AISI 8822 steel

Mechanical Properties	Units	Magnitude
Elastic Modulus, E	GPa	209
Yield Strength, S_y	MPa	-
Ultimate Tensile Strength, S_u	MPa	1480
% Elongation	%	0.87
% Reduction of area	%	-
True Fracture Strain,	%	0.87
True Fracture Stress, σ_f	MPa	1480
Monotonic Tensile Strength Coefficient, K	MPa	-
Monotonic Tensile Strain Hardening Exponent, n	-	-
Hardness, Rockwell C (HRC)	-	60
Cyclic Yield Strength, (0.2% offset) = K' (0.002)n'	MPa	-
Cyclic Strength Coefficient, K'	MPa	-
Cyclic Strain Hardening Exponent, n'	-	-
Cyclic Elastic Modulus, E_c	GPa	-
Fatigue Strength Coefficient, σ'_f	MPa	2234
Fatigue Strength Exponent, b	-	-0.159
Fatigue Ductility Coefficient, ε'_f	-	0.0006
Fatigue Ductility Exponent, c	-	-0.295

Source: El-Zeghayar [13]

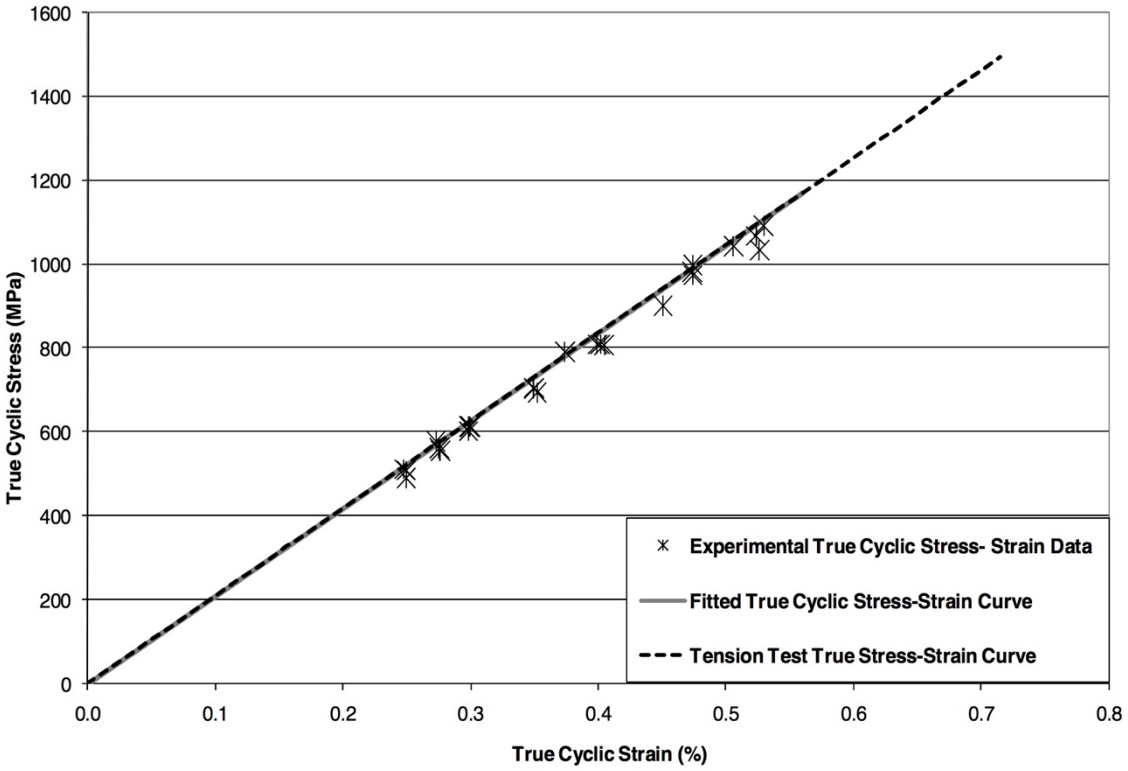

Figure 3.3: Monotonic and cyclic stress-strain curve for AISI 8822. Source: El-Zeghayar [13]

3.3.2 AISI 9310

The chemical analysis for AISI 9310 was performed by Gerdau and is shown in Table 3.3. The mechanical properties, both monotonic and cyclic, were obtained through tests performed as part of the experimental program for this thesis and are presented in Table 3.4.

Surface hardness tests taken as direct Rockwell indentation were performed on the grip section of 8 samples, 5 by the author and another 3 by Dana Co., and the results are shown in Table 3.5.

Micro-hardness tests were performed by Dana Co. on both the grip and gauge sections. The results are shown in Figures Figure 3.4 and Figure 3.5. Hardness reading were done using a 500g load reported in Vickers and then converted to HRC.

Figures Figure 3.6, and Figure 3.7 show the microstructure of the steel, where we can observe the characteristic structure of martensitic materials.

Table 3.3: Chemical composition of AISI 9310 steel (percentage by weight)

Alloy	C	Mn	P	S	Si	Ni	Cr	Mo	Cu	Sn	Al	V	B	Ca	N	As
AISI 9310	0.12	0.62	0.007	0.014	0.19	3.12	1.11	0.09	0.16	0.008	0.022	0.003	0.0002	0.0012	0.0066	0.004

Table 3.4: Mechanical (monotonic and cyclic) properties of AISI 9310 steel

Mechanical Properties	Units	Magnitude
Elastic Modulus, E	GPa	199
Yield Strength, S_y	MPa	764
Ultimate Tensile Strength, S_u	MPa	1019
% Elongation	%	0.94
% Reduction of area	%	0.37
True Fracture Strain,	%	0.94
True Fracture Stress, σ_f	MPa	1019
Monotonic Tensile Strength Coefficient, K	MPa	4312
Monotonic Tensile Strain Hardening Exponent, n	-	0.273
Hardness, Rockwell C (HRC)	-	58-60
Cyclic Yield Strength, (0.2% offset) = K' (0.002)n'	MPa	1959
Cyclic Strength Coefficient, K'	MPa	15793
Cyclic Strain Hardening Exponent, n'	-	0.336
Cyclic Elastic Modulus, E_c	GPa	199
Fatigue Strength Coefficient, σ'_f	MPa	4851
Fatigue Strength Exponent, b	-	-0.183
Fatigue Ductility Coefficient, ε'_f	-	0.083
Fatigue Ductility Exponent, c	-	-0.67

Table 3.5: Rockwell C hardness test results for AISI 9310

	Author						Dana Co.		
	Test 1	Test 2	Test 3	Test 4	Test 5		Test 1	Test 2	Test 3
9310	53	53	53	53	52.5		55	56	56

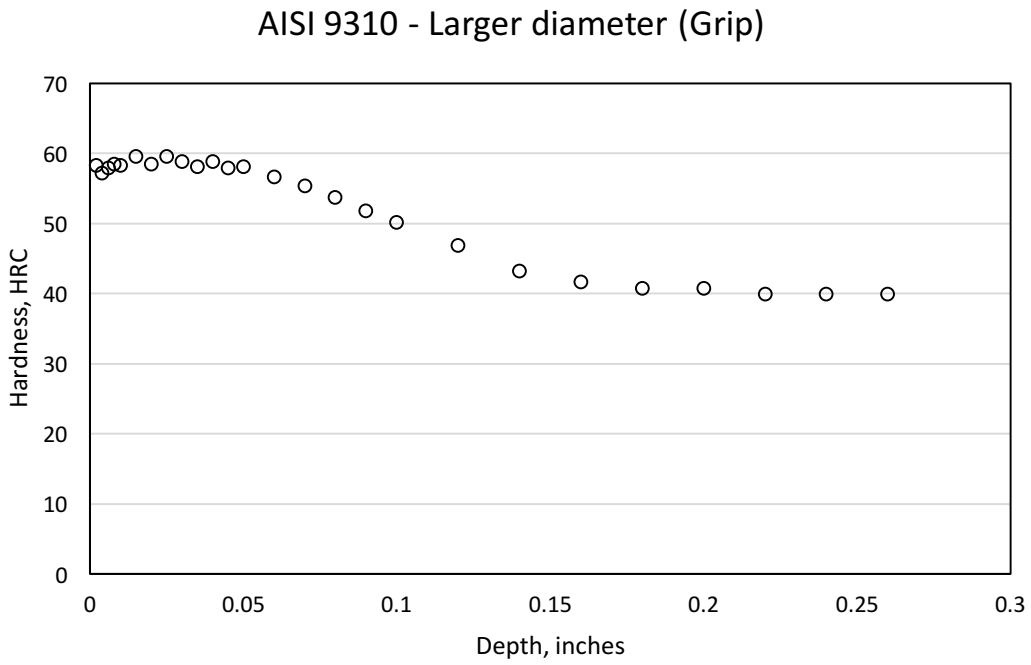

Figure 3.4: Hardness (HRC) versus distance from the surface at the grip section of a sample of AISI 9310

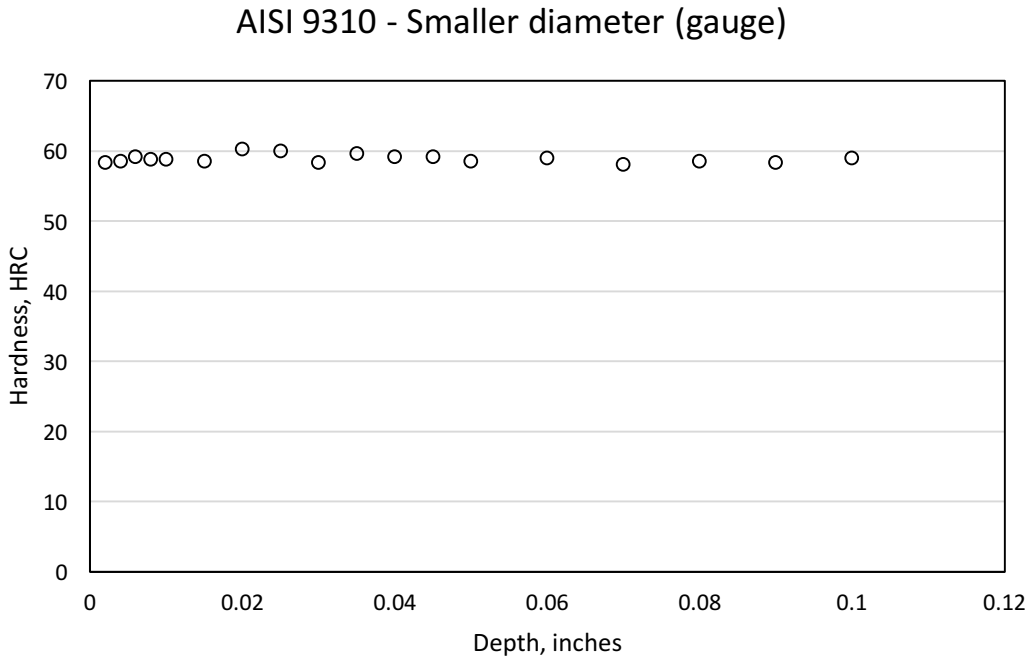

Figure 3.5: Hardness (HRC) versus distance from the surface at the gauge section of a sample of AISI 9310

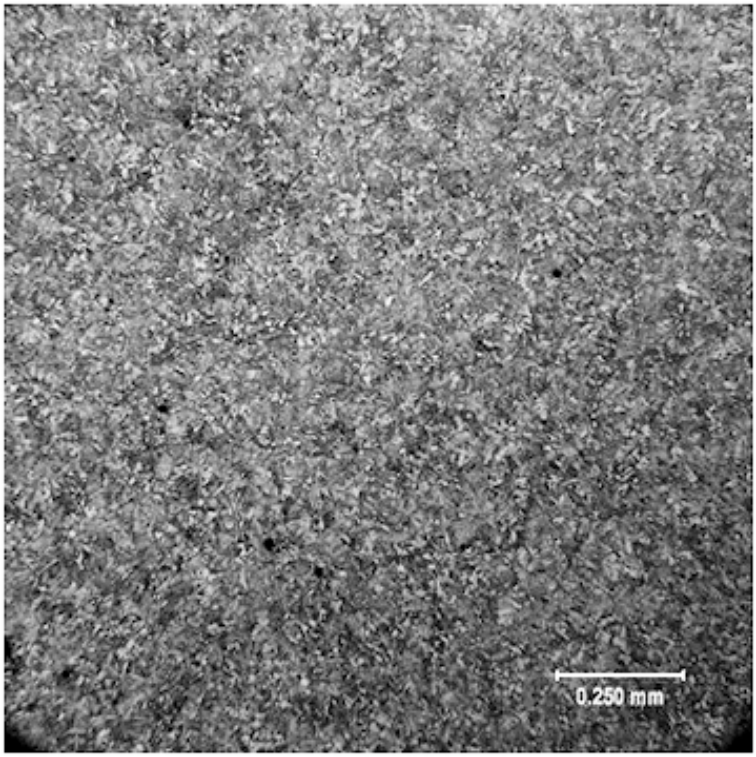

Figure 3.6: Microstructure of AISI 9310, low magnification.

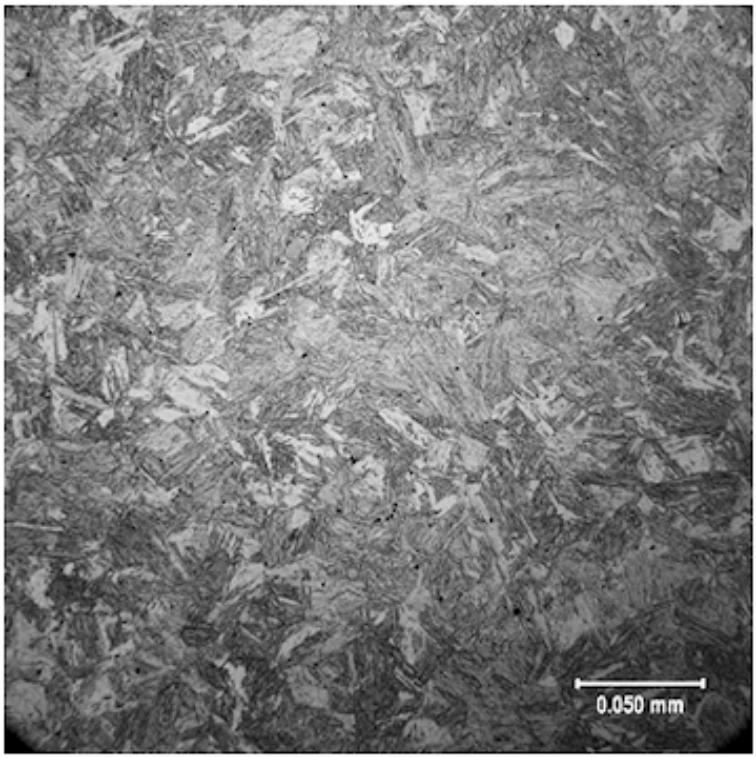

Figure 3.7: Microstructure of AISI 9310, high magnification.

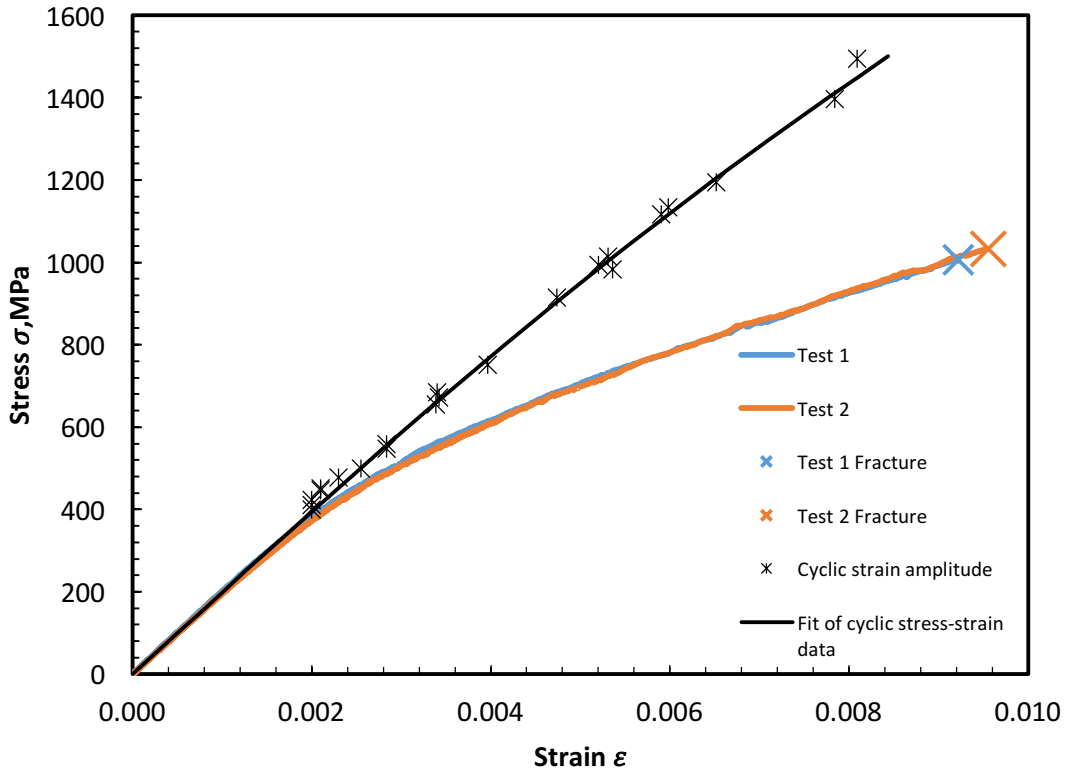

Figure 3.8: Monotonic and cyclic stress-strain curves for AISI 9310

3.3.3 AISI 8620

The chemical analysis for AISI 8620 was performed by Gerdau and is shown in Table 3.6. The mechanical properties, both monotonic and cyclic, were obtained through tests performed as part of the experimental program for this thesis and are presented in Table 3.7.

Surface hardness tests taken as direct Rockwell indentations were performed on the grip section of 8 samples, 5 by the author and another 3 by Dana Co., and the results are shown in Table 3.8.

Micro-hardness tests were performed by Dana Co. on both the grip and gauge sections. The results are shown in Figures Figure 3.9 and Figure 3.10. Hardness readings were obtained using a 500g load reported in Vickers and then converted to HRC.

Figures Figure 3.11, and Figure 3.12 show the microstructure of the steel, where we can observe the characteristic structure of martensitic materials.

Table 3.6: Chemical composition of AISI 8620 steel (percentage by weight)

Alloy	C	Mn	P	S	Si	Ni	Cr	Mo	Cu	Sn	Al	V	Nb

AISI 8620	0.22	0.85	0.013	0.009	0.25	0.50	0.57	0.21	0.21	0.009	0.024	0.002	0.003

Table 3.7: Mechanical (monotonic and cyclic) properties of AISI 8620 steel

Mechanical Properties	Units	Magnitude
Elastic Modulus, E	GPa	203
Yield Strength, S_y	MPa	690
Ultimate Tensile Strength, S_u	MPa	757
% Elongation	%	0.5
% Reduction of area	%	0.24
True Fracture Strain,	%	0.5
True Fracture Stress, σ_f	MPa	757
Monotonic Tensile Strength Coefficient, K	MPa	2710
Monotonic Tensile Strain Hardening Exponent, n	-	0.214
Hardness, Rockwell C (HRC)	-	60-63
Cyclic Yield Strength, (0.2% offset) = K' (0.002)n'	MPa	3590
Cyclic Strength Coefficient, K'	MPa	72987
Cyclic Strain Hardening Exponent, n'	-	0.485
Cyclic Elastic Modulus, E_c	GPa	203
Fatigue Strength Coefficient, σ'_f	MPa	2404
Fatigue Strength Exponent, b	-	-0.159
Fatigue Ductility Coefficient, ε'_f	-	0.0006
Fatigue Ductility Exponent, c	-	-0.295

Table 3.8: Rockwell C hardness test results for AISI 8620

	Author						Dana Co.		
	Test 1	Test 2	Test 3	Test 4	Test 5		Test 1	Test 2	Test 3
8620	56	56	57	56	56		59	60	60

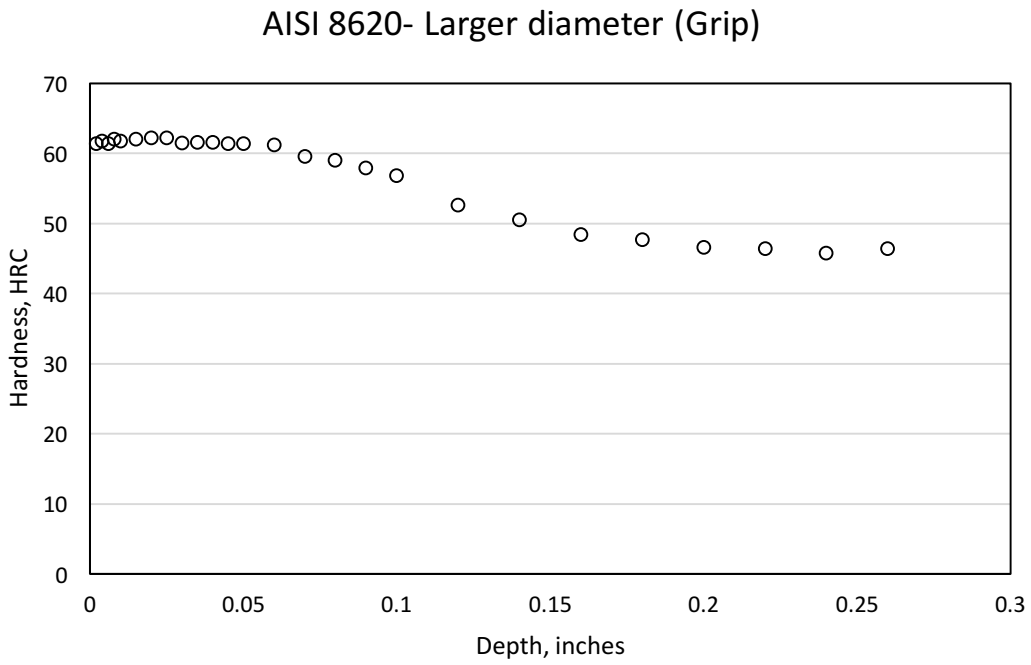

Figure 3.9: Hardness (HRC) versus distance from the surface at the grip section of a sample of AISI 8620

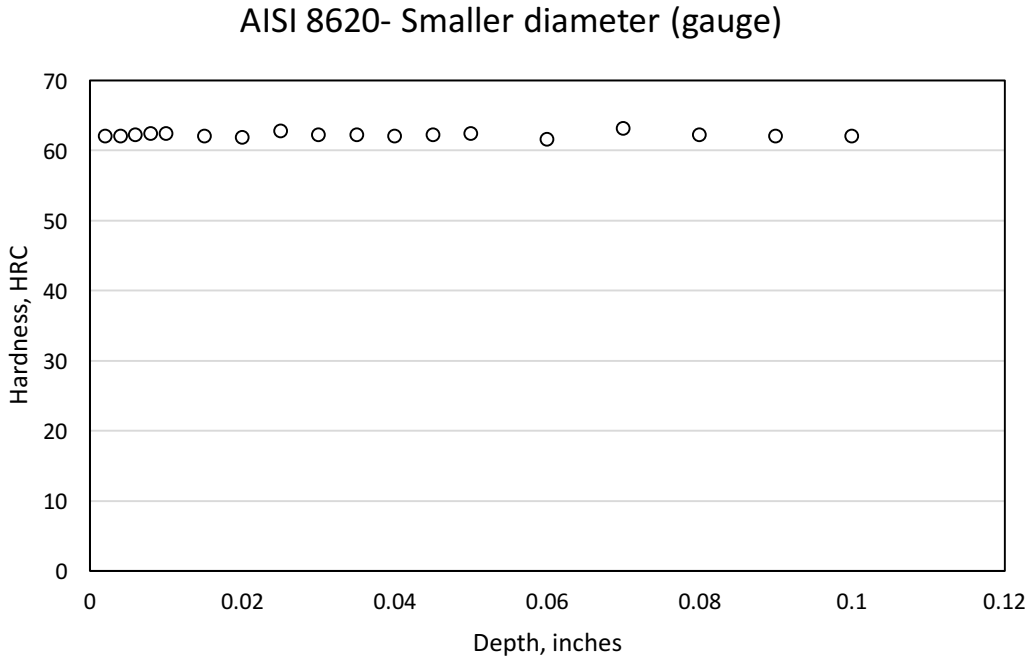

Figure 3.10: Hardness (HRC) versus distance from the surface at the gauge section of a sample of AISI 8620

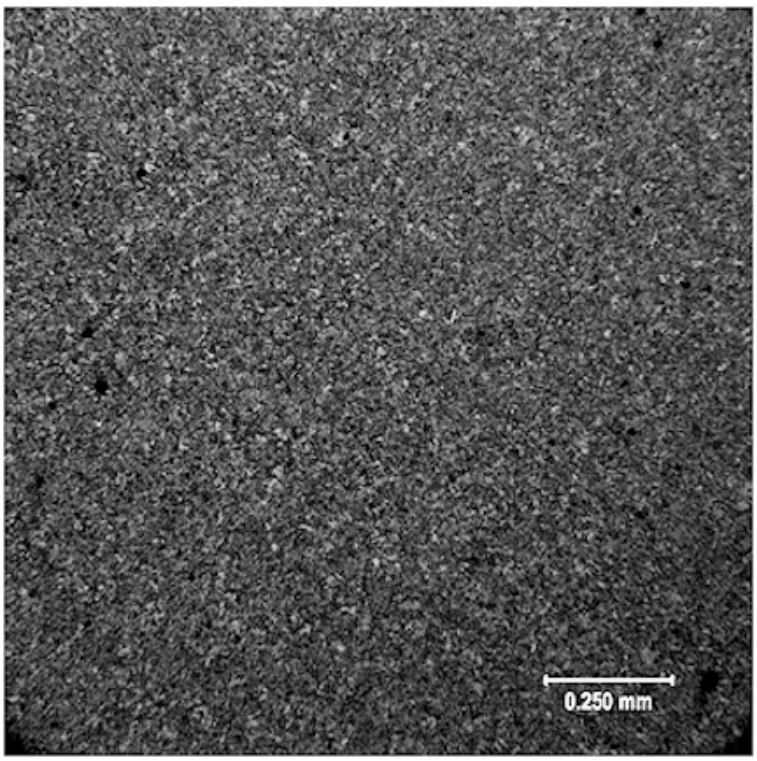

Figure 3.11: Microstructure of AISI 8620, low magnification.

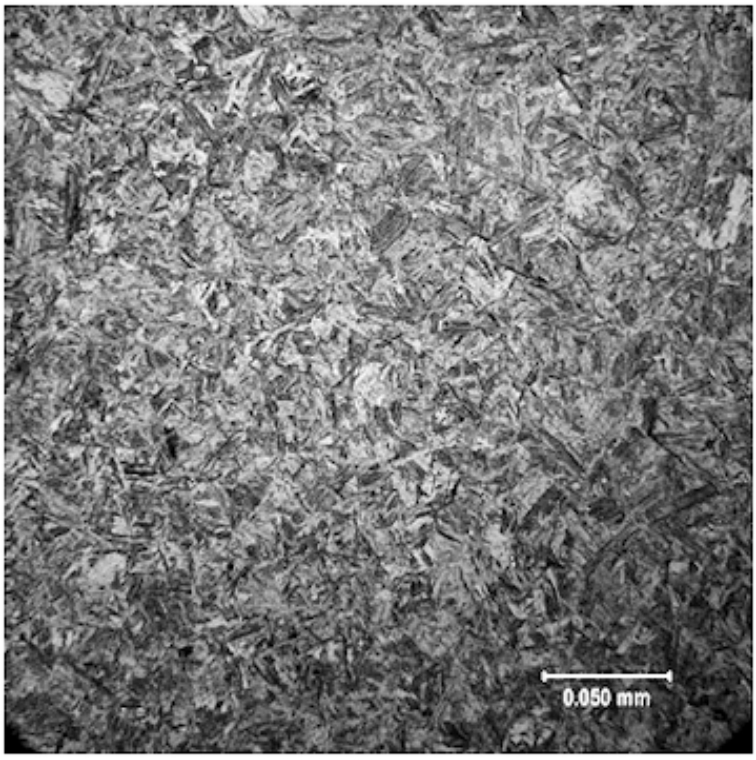

Figure 3.12: Microstructure of AISI 8620, high magnification.

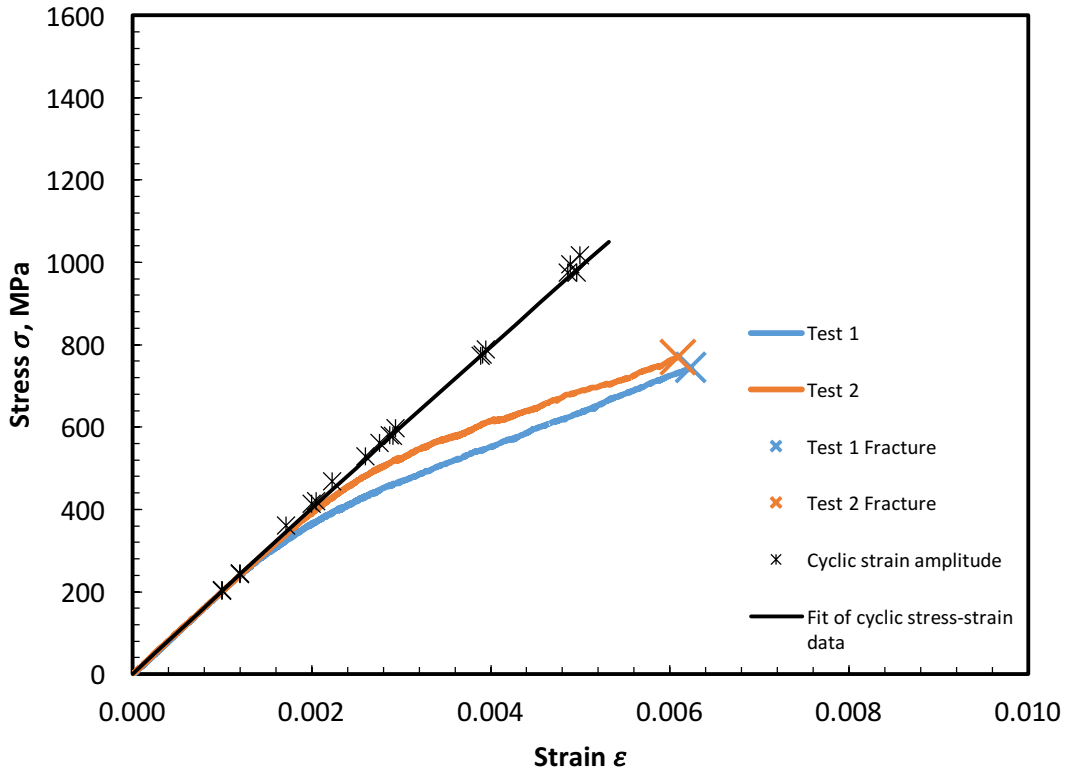

Figure 3.13: Monotonic and cyclic stress-strain curve for AISI 8620

3.3.4 Retained Austenite

It was observed for AISI 9310 and AISI 8620 that the cyclic stress-strain curve is above the monotonic curve, indicating that if the stress cycle was fully reversed in stress the specimen would see stresses above its ultimate strength.

Looking at the initial stress-strain loops of the strain controlled tests used in this investigation helps us to understand this behaviour. It was noted that these materials cyclic-harden, i.e., it requires a higher stress to impose the same deformation as cycling proceeds. Furthermore, under the strain control used in these tests the loops shift down into the compression region as observed in Figure 3.14. The stress-strain graphs (Figures Figure 3.8 and Figure 3.13) show the stress amplitudes of the fatigue tests, which are indeed greater than the ultimate stress of the tensile test, but since the loops were shifted, the maximum tensile stress achieved during a test never exceeded the ultimate tensile strength of the materials.

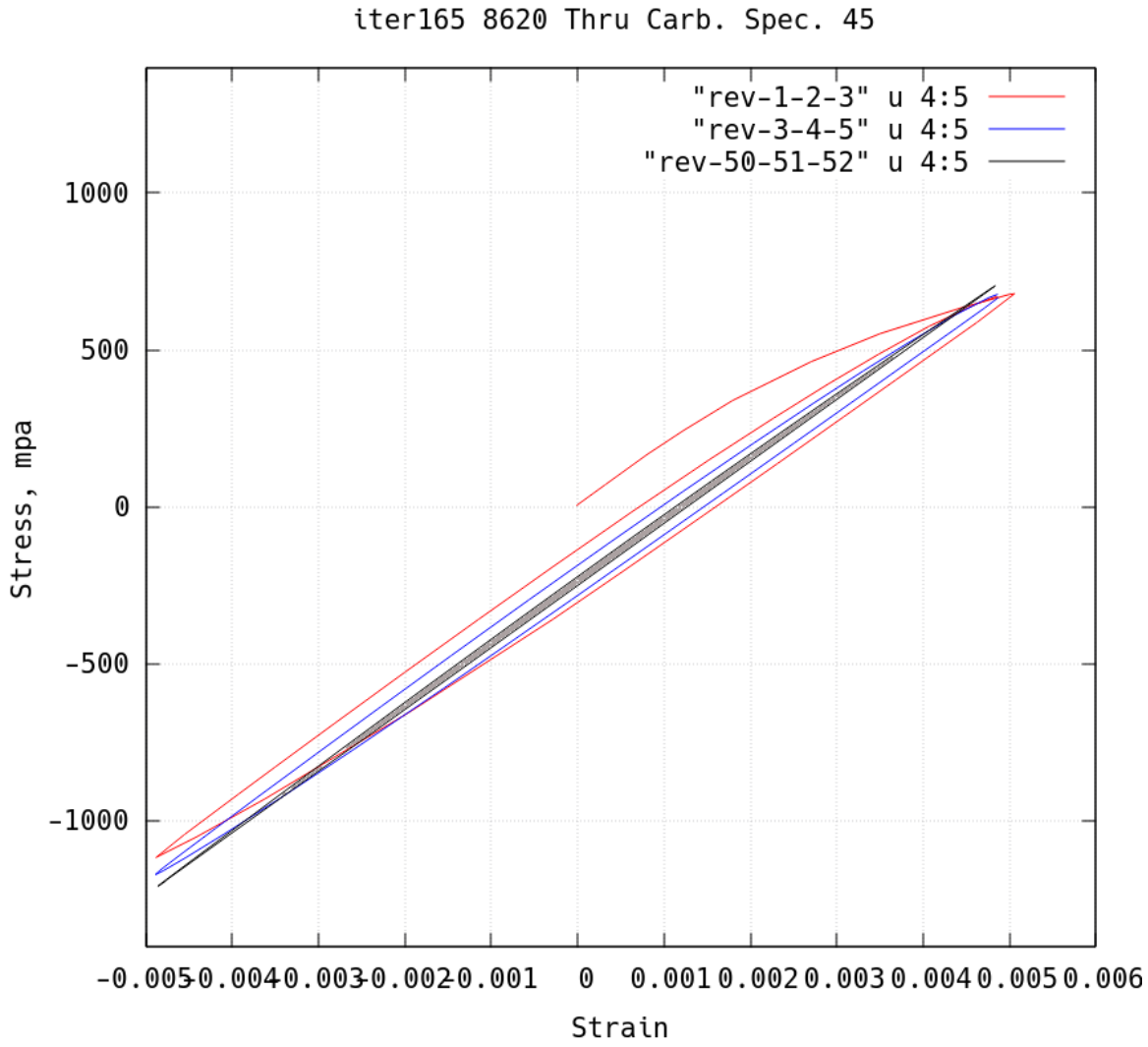

Figure 3.14: Stress-strain loops of AISI 8620 specimen 45 for the first, second, and 25th cycles.

It is also important to understand the cause of the shift of the stress-strain loops. According to a report from Dana Co., where the microstructure was determined, they observed retained austenite in the gauge section of the specimens of these materials. When deformed, this austenite transforms into martensite, which has a larger crystal form. The specimen then wants to expand to accommodate the larger structure, but since the test was strain controlled with an extensometer that enforces zero deflection, compressive residual stresses result.

The same report also indicates that these two materials show evident grain growth in both the grip and gauge sections, and present pits from the vacuum carburizing process.

3.4 Pre-stressing Wire Specimens

The 7-wire strands were unravelled and the centre wire was cut into 130 mm long samples. A ratio of diameter to free wire length between the grips of 2:1 was used to avoid buckling of the specimens due to fully reversed loading. Also, the free length was machined down gradually to a diameter of 2 mm to ensure failure in the free length zone, and prevent anchor failure by avoiding stress concentrations caused by a sudden change in diameter as shown in Figure 3.16.

Figure 3.15: 7-wire pre-stressing strands

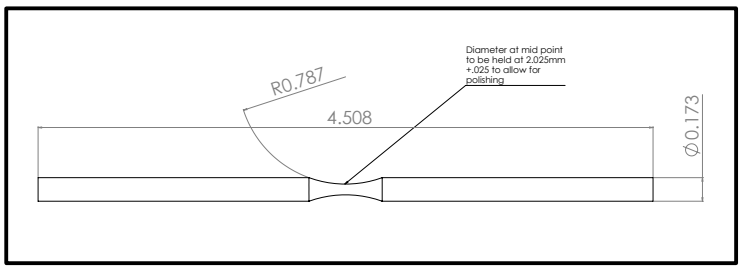

Figure 3.16: CAD drawing of strand specimen (units in inches)

Figure 3.17: Specimen machined from centre 7-wire strand

The mechanical properties, both monotonic and cyclic, were obtained from El-Menoufy [12] and are presented in Table 3.9. A tension test was done to determine the fracture stress and strain, yielding a true fracture stress of 940 MPa, and a true fracture strain of 42%.

Table 3.9: Mechanical (monotonic and cyclic) properties of cold-worked pre-stressing wires

Mechanical Properties	Units	Magnitude
Elastic Modulus, E	GPa	
Yield Strength, S_y	MPa	
Ultimate Tensile Strength, S_u	MPa	2150
Hardness, Rockwell C (HRC)	-	53
Cyclic Yield Strength, (0.2% offset) = K' (0.002)n'	MPa	1338.5
Cyclic Strength Coefficient, K'	MPa	2415.6
Cyclic Strain Hardening Exponent, n'	-	0.095
Cyclic Elastic Modulus, E_c	GPa	196
Fatigue Strength Coefficient, σ'_f	MPa	2319
Fatigue Strength Exponent, b	-	-0.061
Fatigue Ductility Coefficient, ε'_f	-	1.09
Fatigue Ductility Exponent, c	-	-0.707

Source: El Menoufy [12]

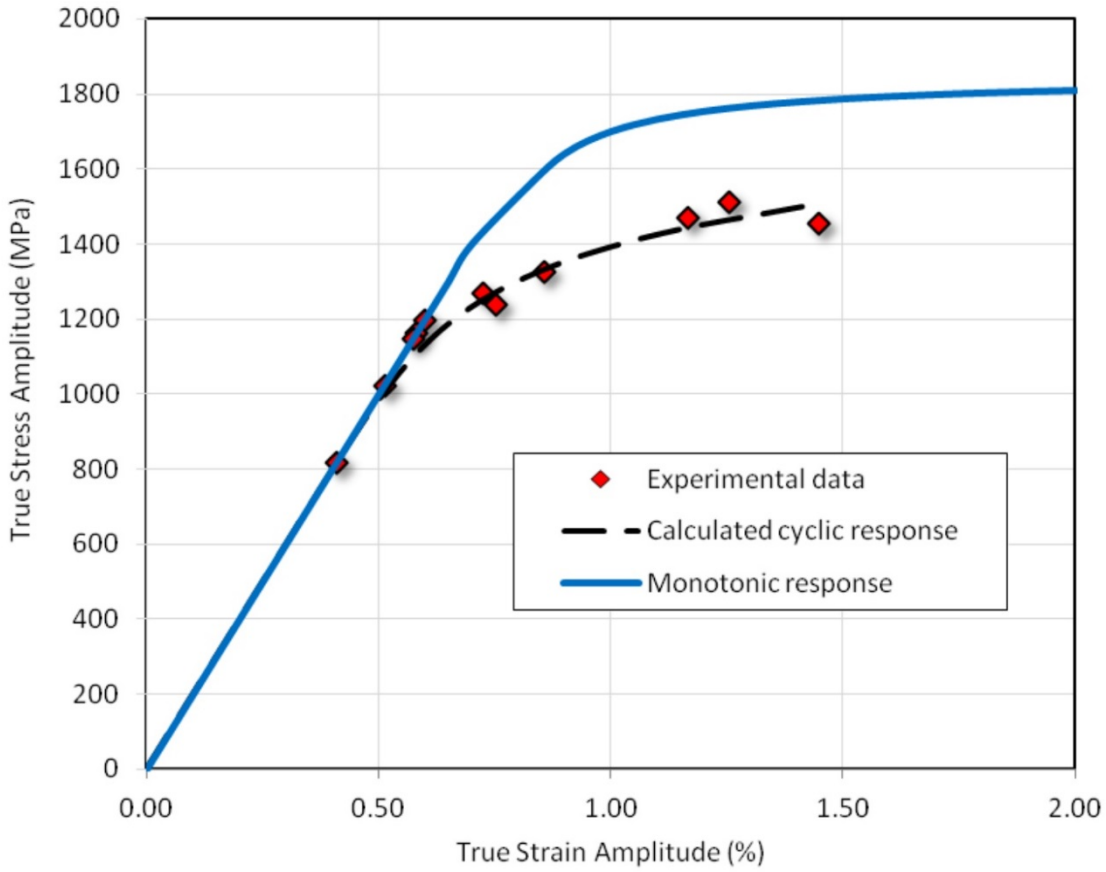

Figure 3.18: Monotonic and cyclic stress-strain curve for pre-stressing wire. Source: El Menoufy [12]

CHAPTER 4

EXPERIMENTAL RESULTS

4.1 Introduction

This chapter aims to present the experimental results of the research. The main goal is to visualize the data in a form that helps to identify the strengths and weaknesses of each mean stress correction model.

4.2 Results

Firstly, the stress-life plots containing the fully-reversed fatigue test results for each of the materials are presented in figures Figure 4.1, Figure 4.14, Figure 4.28, and Figure 4.42.

Figures Figure 4.2, Figure 4.15, Figure 4.29, and Figure 4.43 show the stress-life plots for the fatigue tests performed at different mean stresses. As expected, the results show a detrimental effect of positive mean stresses, with samples exhibiting lower stress amplitudes at given lives than the fully-reversed tests. The beneficial effect of compressive mean stresses is also observed, with samples withstanding higher stress amplitudes at the same lives than the fully-reversed tests.

Then, with the purpose of comparing the different methods, minimum stress versus maximum stress graphs were plotted. Each graph contains the fatigue limit results for each mean stress level along with the curve representing the predictions of one of the mean stress correction methods. Similar results for a life of 200,000 reversals were also included when data was available.

In order to correctly interpret this type of graph, note that if the curve is below the data point it means that the method predicts failure at a lower stress level than the results showed. That means that the method is conservative, i.e., it overestimates the effect of mean stress. Conversely, if the curve is above the data point, it means that the method underestimates the effect of mean stress, i.e., it is non-conservative.

The Morrow and Goodman curves fit the data well in the positive mean stress region for the carburized steels (Figures Figure 4.3Figure 4.16Figure 4.30), and all the data for the pre-stressing wire Figure 4.44.

For these hard steels the Morrow method is equivalent to the Goodman method because the ultimate stress is the same as the fracture stress for these materials, Figures Figure 4.4, Figure 4.17Figure 4.31). It can also be observed that the Modified Morrow method (dotted lines) does not fit the data properly. This is because the intercept constant σ_f' is affected by the material behaviour caused by retained austenite, as explained in chapter 3. For the pre-stressing wire material however, both methods are suitable as can be observed in Figure Figure 4.45. This is because this material presents a behaviour characteristic of ductile materials, with sensitivity to compressive mean stresses.

The Smith-Watson-Topper relationship presents a reasonably good fit for AISI 8822 (Figure Figure 4.5), but for AISI 9310 it is non-conservative in the tensile mean stress region and conservative in the compressive mean stress region as seen in Figure Figure 4.18. The same occurs for AISI 8620 (Figure Figure 4.32) and the pre-stressing wire (Figure Figure 4.46).

Using a value of 0.3 for the gamma (γ) exponent the Walker equation (Eq. (2.6)) was found to give a better fit all the data than the other traditional methods. This method is over conservative for AISI 8822 (Figure Figure 4.6), but offers the best fit out of all the traditional methods for AISI 9310 and AISI 8620 (Figures Figure 4.19 and Figure 4.33). It gives a good fit to the pre-stressing wire data in the tensile mean stress region, but is non-conservative in the compressive mean stress region (Figure Figure 4.47).

The Gerber method is only suited for the tensile mean stress region. It fits the data for AISI 8822 (Figure Figure 4.7) reasonably well, but is highly non-conservative for the other materials as observed in Figures Figure 4.20Figure 4.34Figure 4.48.

The AISI 8620 data in the positive mean stress region is described well by the Soderberg criterion (Figure Figure 4.35), but the method is highly inaccurate for the other materials (Figures Figure 4.21Figure 4.49). This method could not be used to fit the AISI 8822 data because the material does not have a yield limit.

4.3 Proposed Method

A new method is proposed after observing the experimental results for the carburized steels. The Goodman and Morrow methods seem to offer the best fit overall in the tensile mean stress region. However, these metals show insensitivity to compressive mean stresses. Therefore, it is suggested that one uses these criteria in the tensile region, while maintaining the maximum stress equal to the tensile peak of the fully-reversed result in the compressive

mean stress region. This takes advantage of the simplicity of Goodman and Morrow methods and their good fit to the data in the tensile mean stress region, while improving the accuracy for the compressive mean stress region. This proposed method fits the carburized steel data very well as can be seen in Figures Figure 4.8, Figure 4.22, and Figure 4.36. However, it does not fit the pre-stressing wire results in the compressive mean stress region for which the Goodman and Morrow criteria are better (Figure Figure 4.50).

Stress-life diagrams with equivalent stress amplitude versus fatigue life given by the various mean stress rules were plotted to compare the accuracy of the different mean stress rules at all fatigue lives. For each graph, the equivalent stress amplitude was calculated using one of the various methods. The closer the calculated results are to the fully-reversed data, the more accurate the mean stress correction method is. The results for the Goodman criterion can be seen in Figures Figure 4.9, Figure 4.23, Figure 4.37, and Figure 4.51. The results for the Morrow criterion can be seen in Figures Figure 4.10, Figure 4.24, Figure 4.38, and Figure 4.52. The results for the Smith-Watson-Topper criterion can be seen in Figures Figure 4.11, Figure 4.25, Figure 4.39, and Figure 4.53. The results for the Walker criterion can be seen in Figures Figure 4.12, Figure 4.26, Figure 4.40, and Figure 4.54. The results for the proposed criterion can be seen in Figures Figure 4.13, Figure 4.27, Figure 4.41, and Figure 4.55. These graphs confirm the analysis previously discussed. It is important to mention that the proposed method only changes the prediction for the compressive mean stress region, therefore the difference for this plot between the Goodman and the proposed method are observable only for the negative mean stress data points.

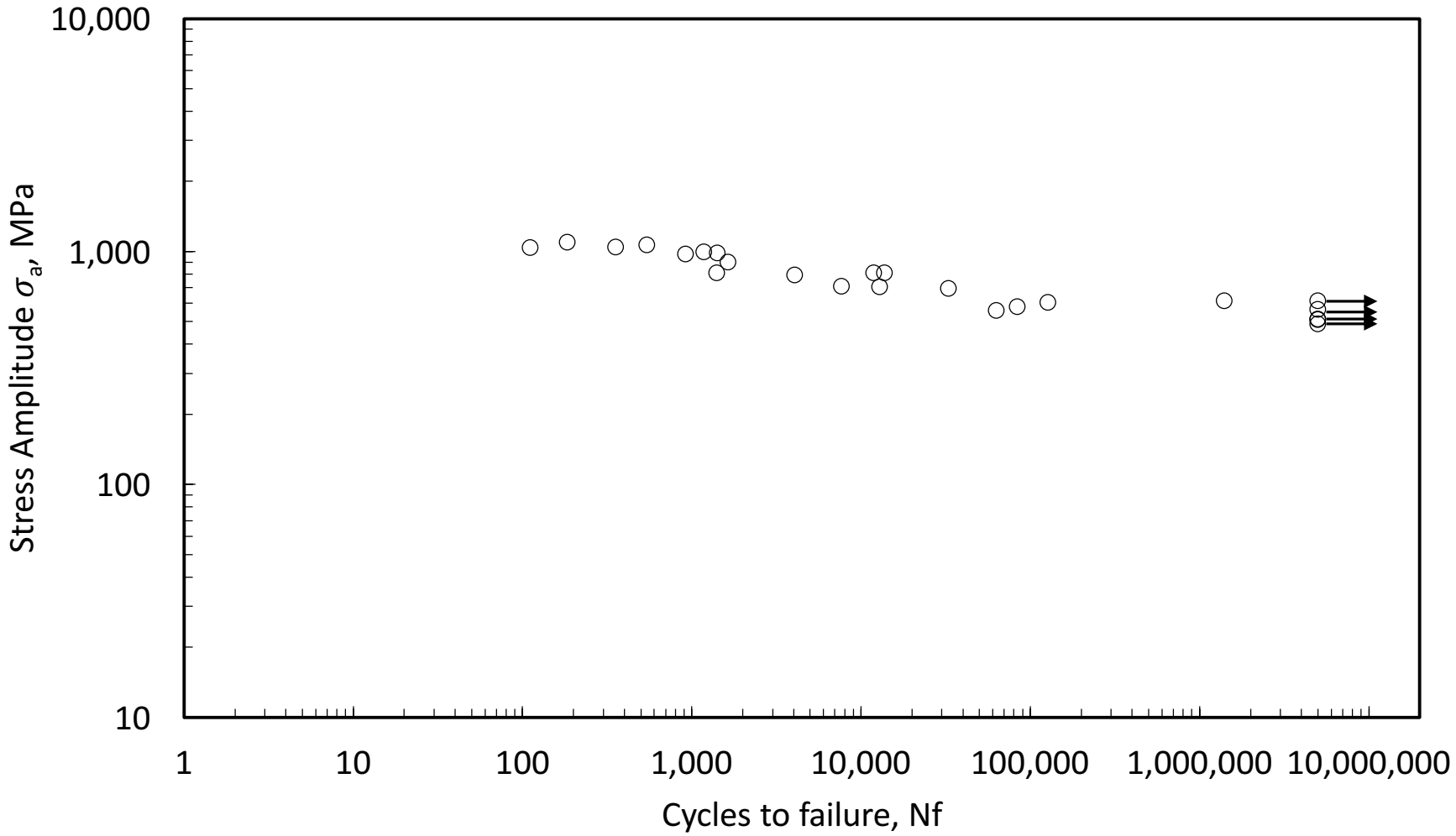

Figure 4.1: Stress-life fatigue curve for AISI 8822

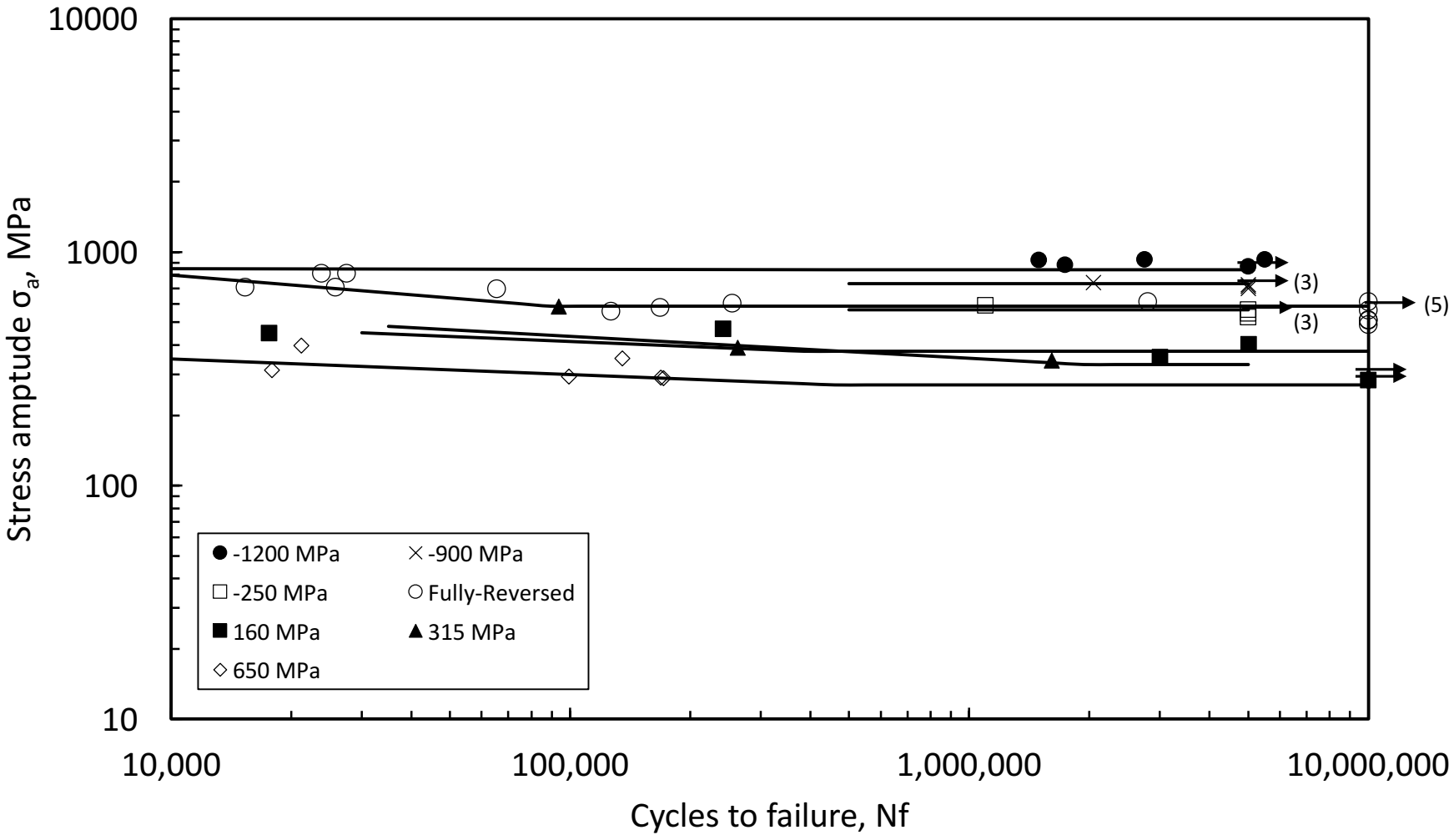

Figure 4.2: Fatigue life of AISI 8822 for different mean stresses

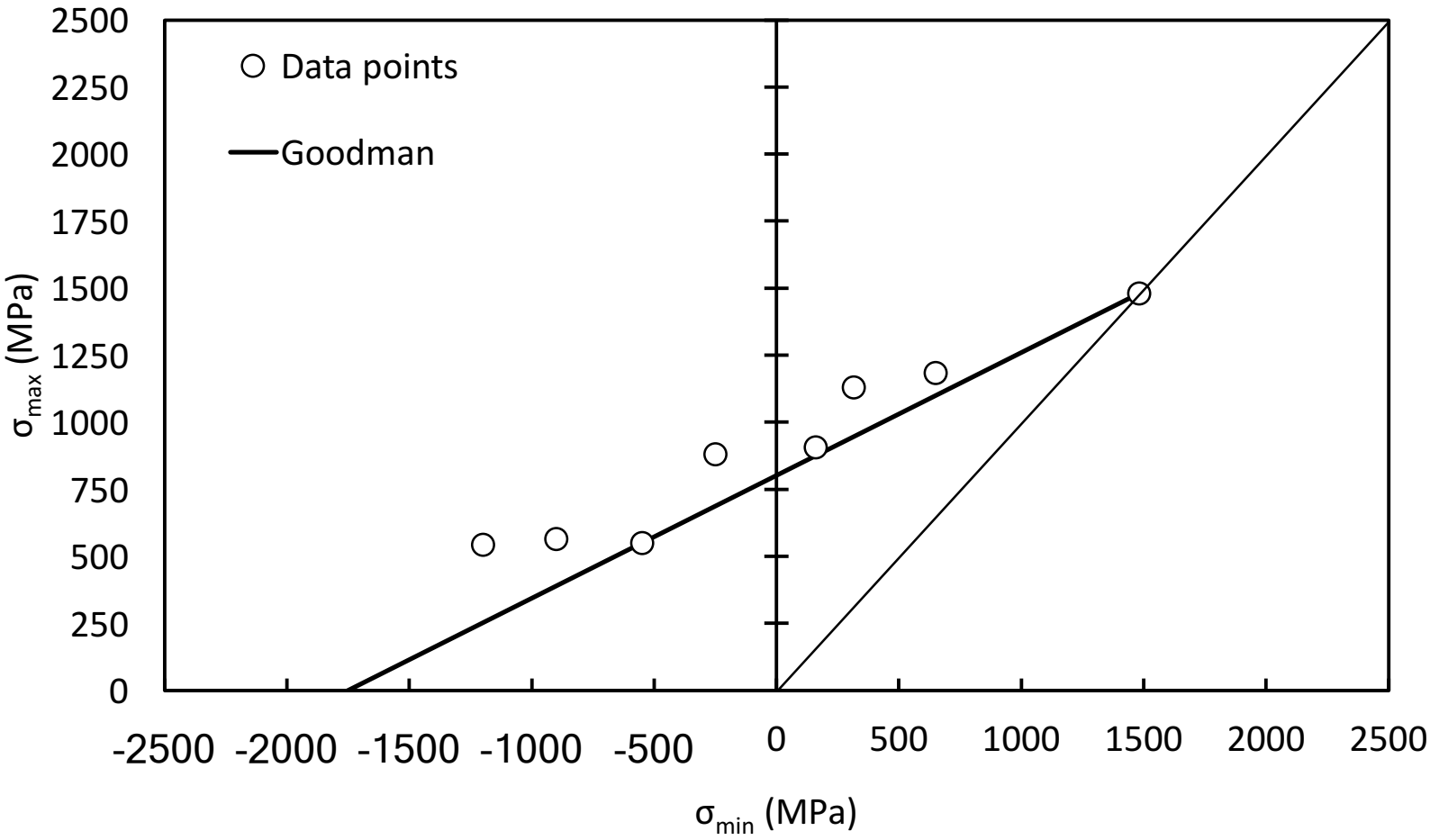

Figure 4.3: Max-min stress diagrams comparing the experimental data for AISI 8822 with the prediction of the Goodman mean stress correction model for the fatigue limit (10,000,000 reversals)

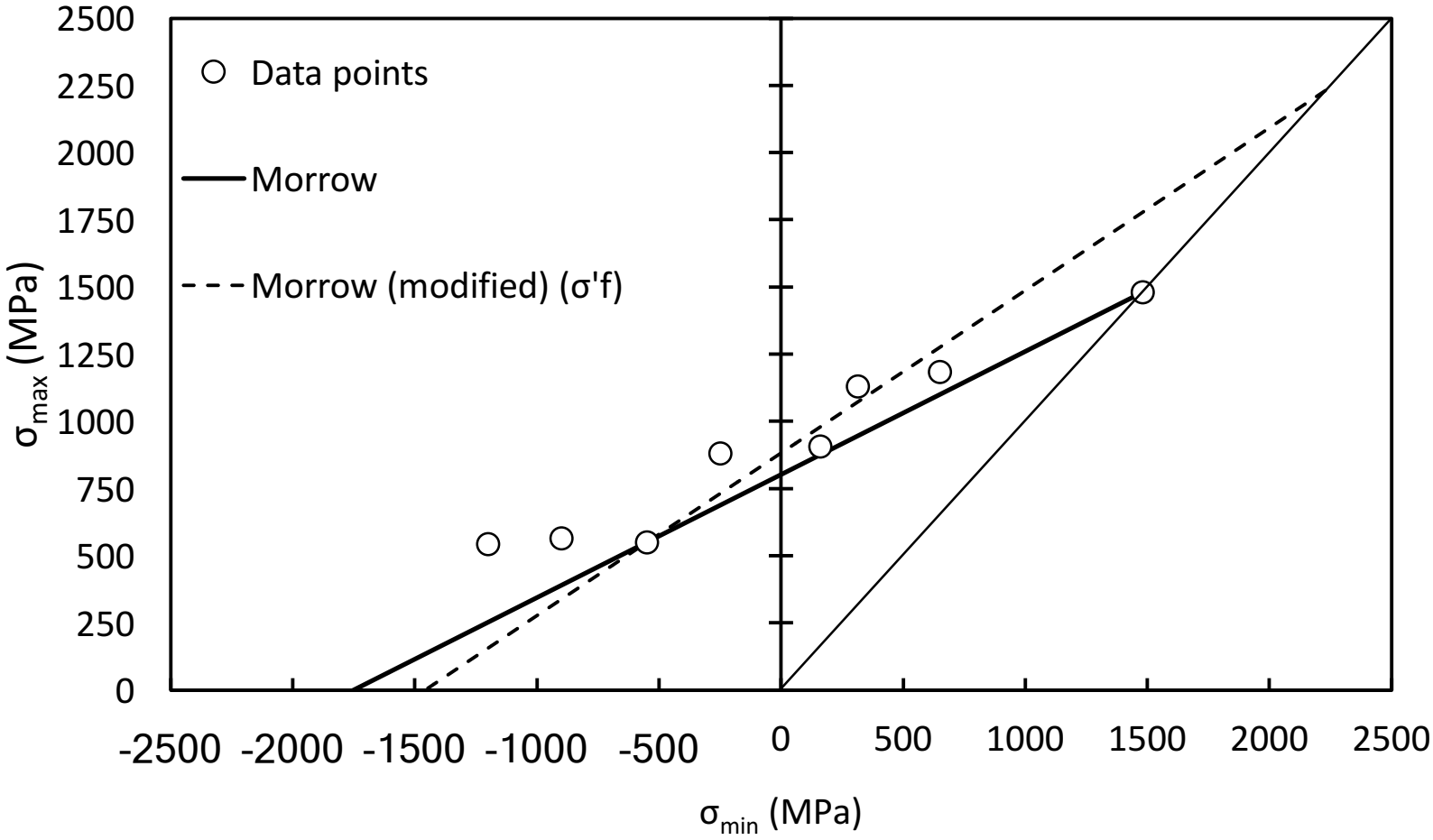

Figure 4.4: Max-min stress diagrams comparing the experimental data for AISI 8822 with the prediction of the Morrow and modified-Morrow mean stress correction models for the fatigue limit (10,000,000 reversals)

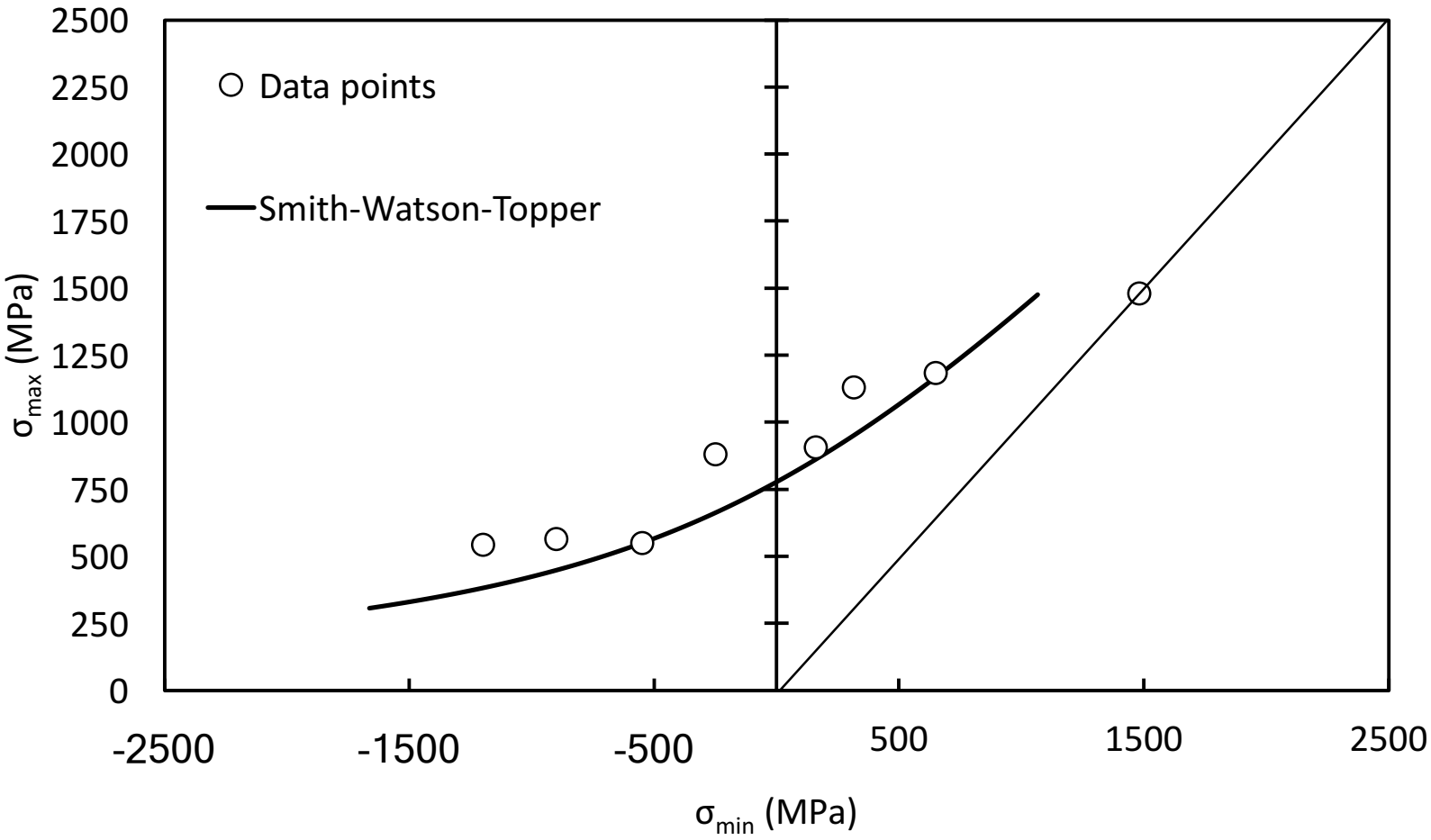

Figure 4.5: Max-min stress diagrams comparing the experimental data for AISI 8822 with the prediction of the Smith-Watson-Topper mean stress correction model for the fatigue limit (10,000,000 reversals)

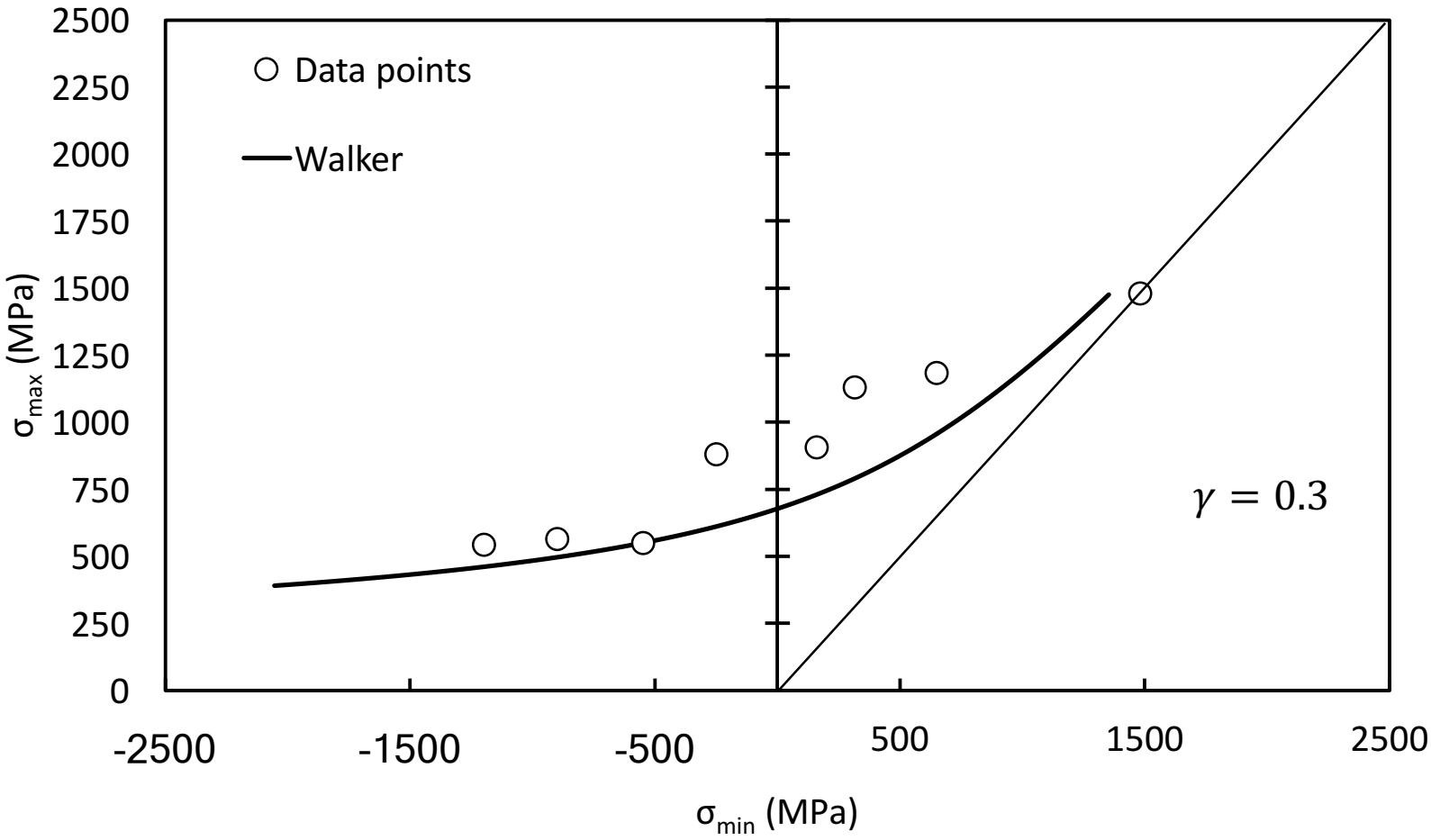

Figure 4.6: Max-min stress diagrams comparing the experimental data for AISI 8822 with the prediction of the Walker mean stress correction model for the fatigue limit (10,000,000 reversals)

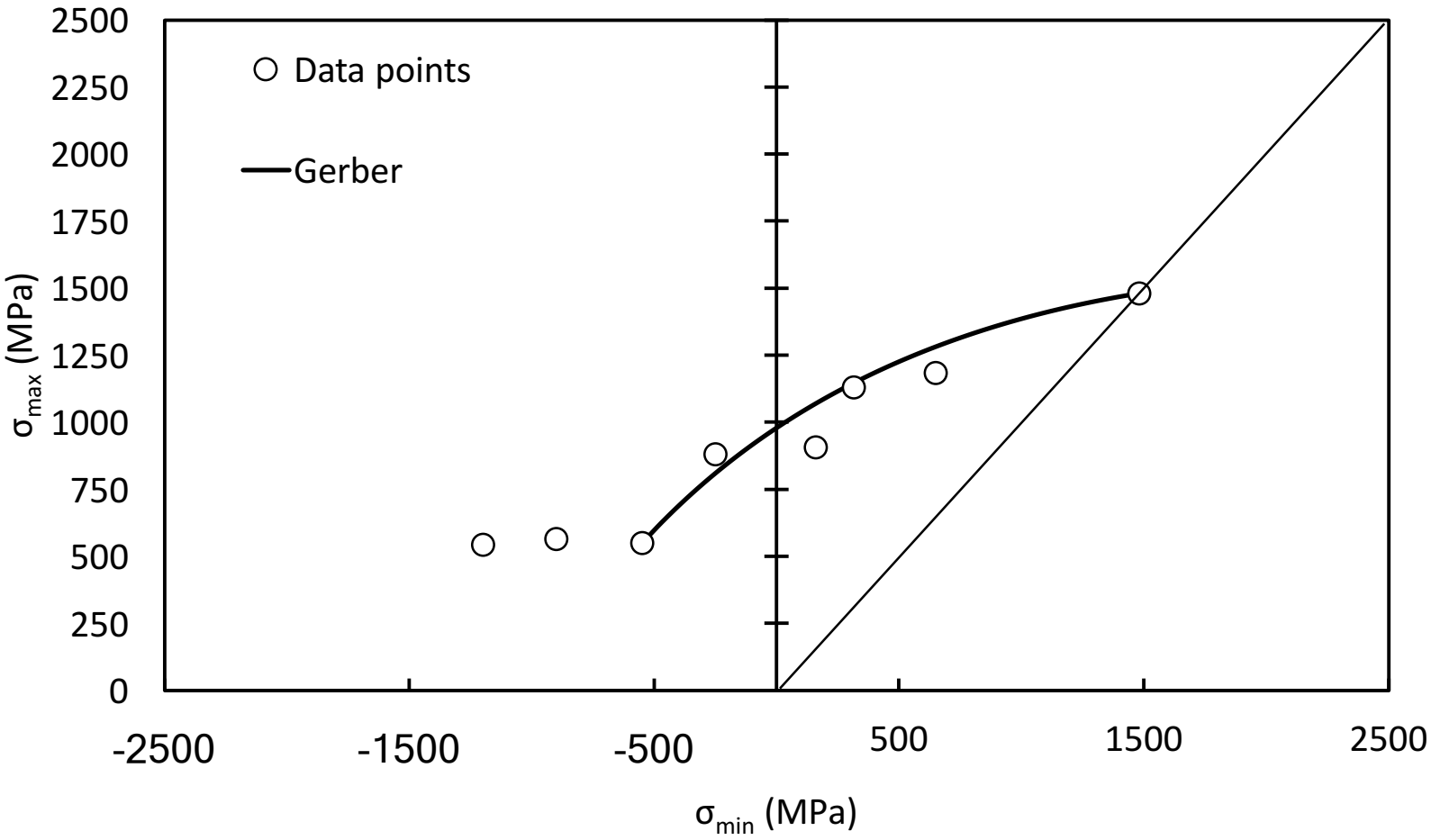

Figure 4.7: Max-min stress diagrams comparing the experimental data for AISI 8822 with the prediction of the Gerber mean stress correction model for the fatigue limit (10,000,000 reversals)

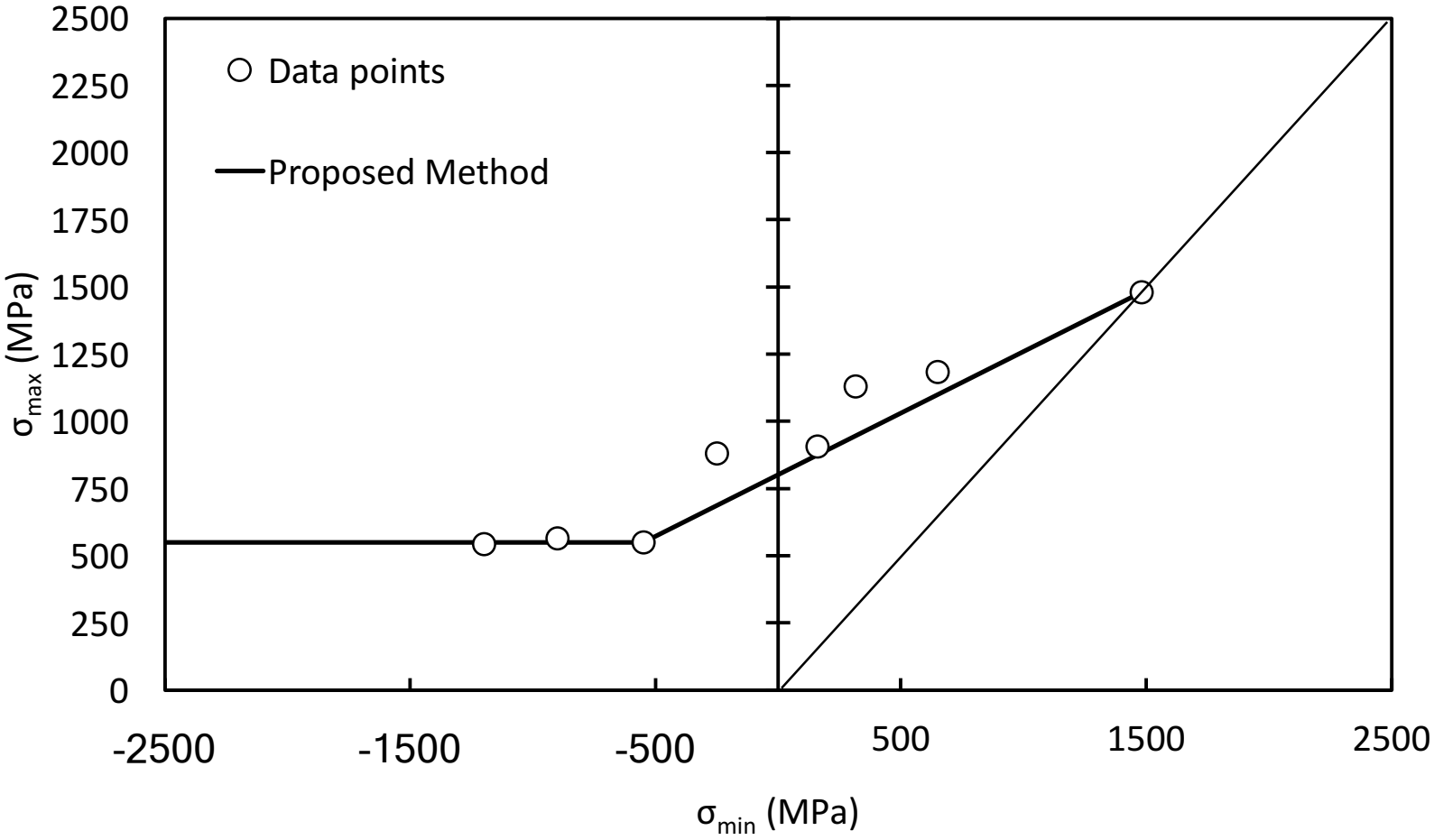

Figure 4.8: Max-min stress diagrams comparing the experimental data for AISI 8822 with the prediction of the proposed mean stress correction model for the fatigue limit (10,000,000 reversals)

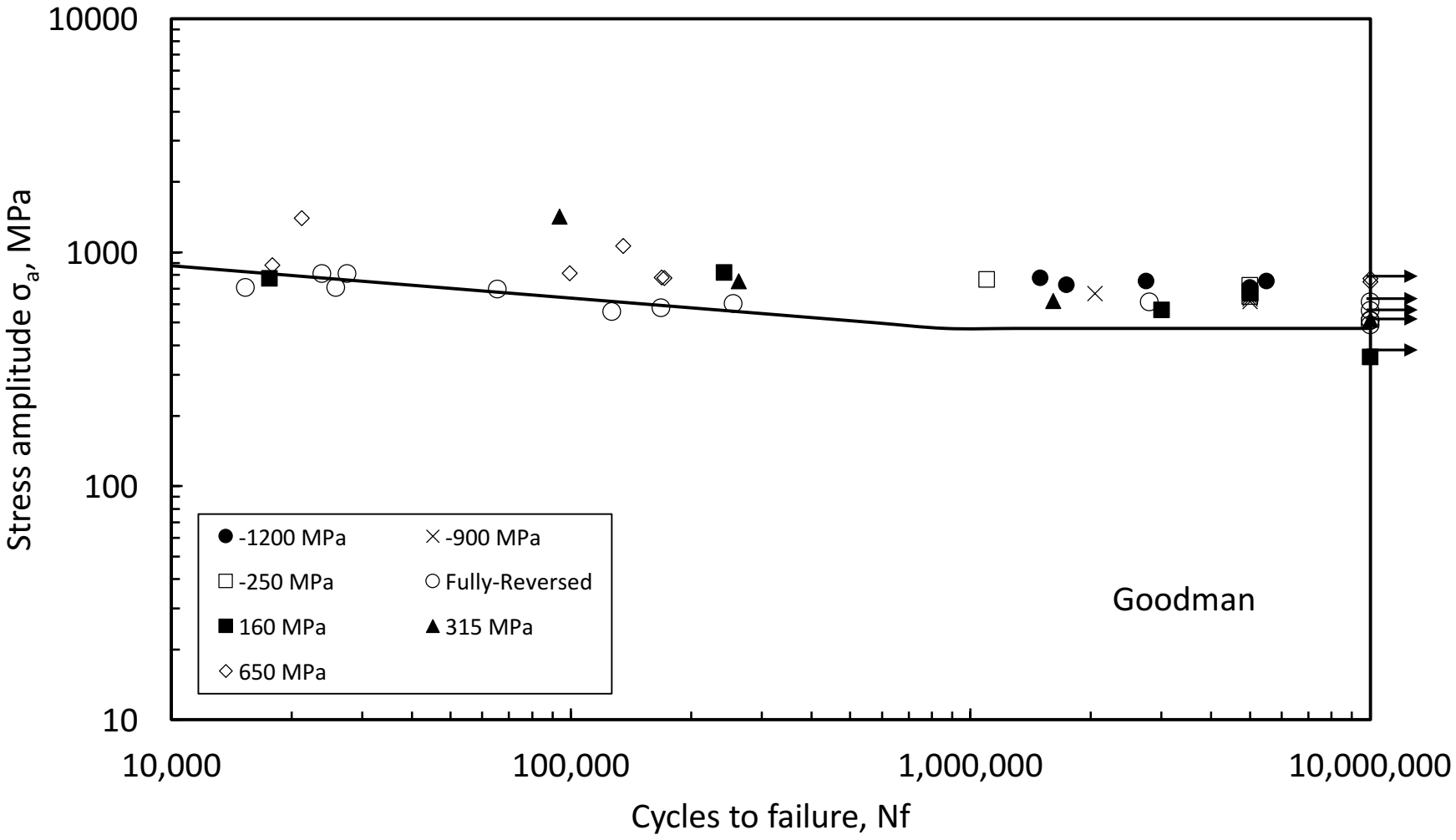

Figure 4.9: Stress-life diagram showing the equivalent stress amplitude for different mean stress levels as corrected by Goodman (AISI 8822)

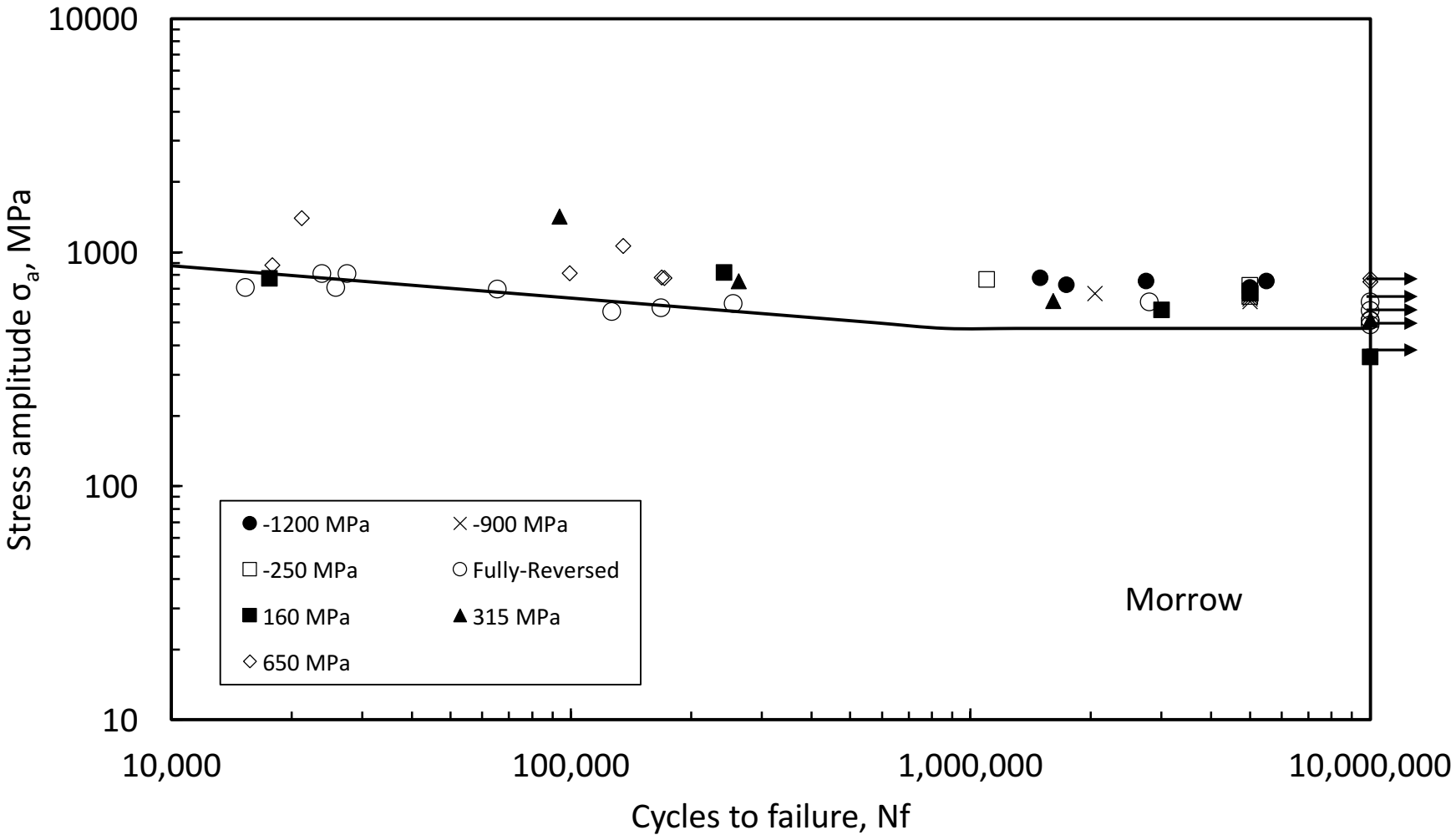

Figure 4.10: Stress-life diagram showing the equivalent stress amplitude for different mean stress levels as corrected by Morrow (AISI 8822)

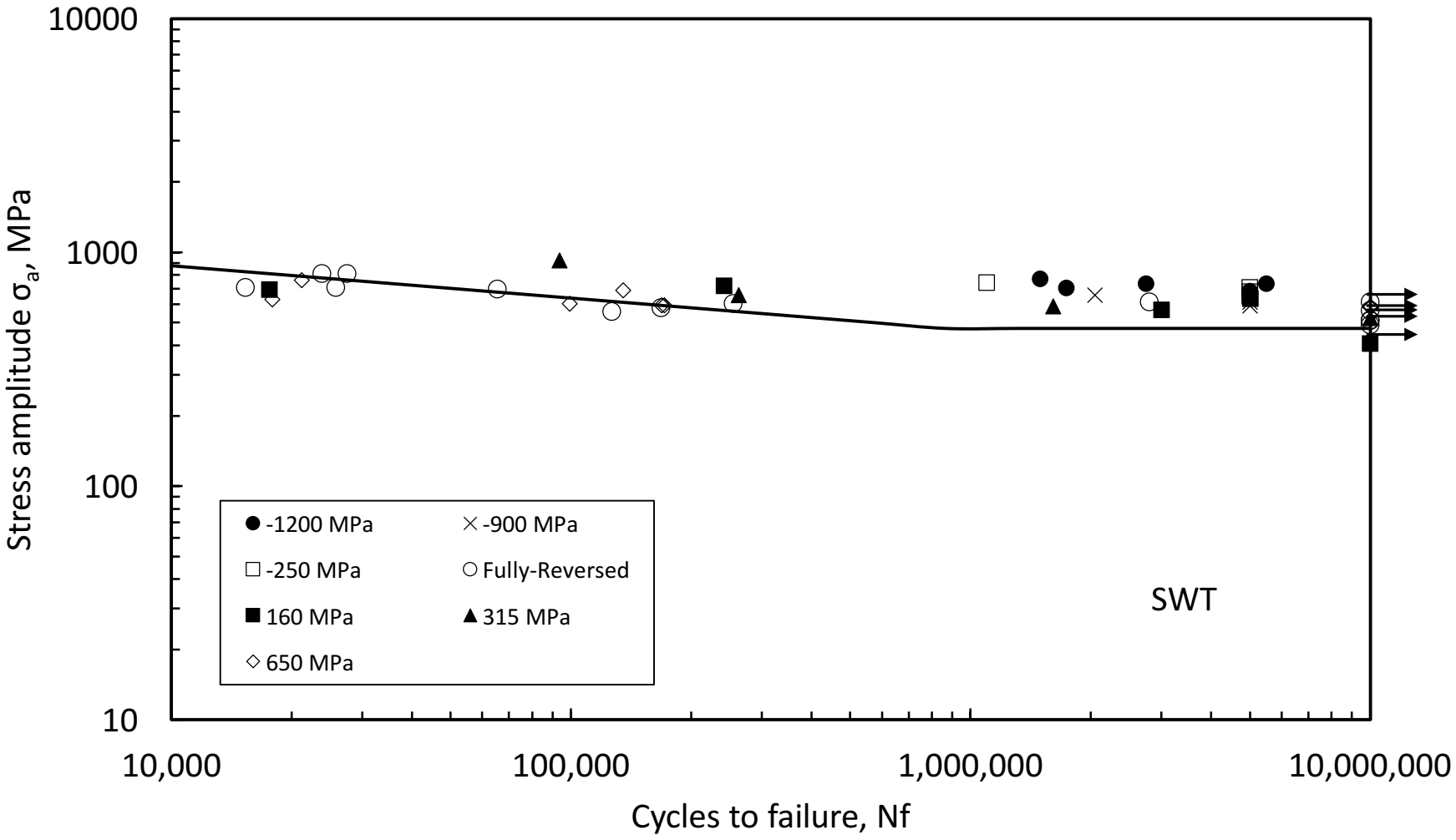

Figure 4.11: Stress-life diagram showing the equivalent stress amplitude for different mean stress levels as corrected by Smith-Watson-Topper (AISI 8822)

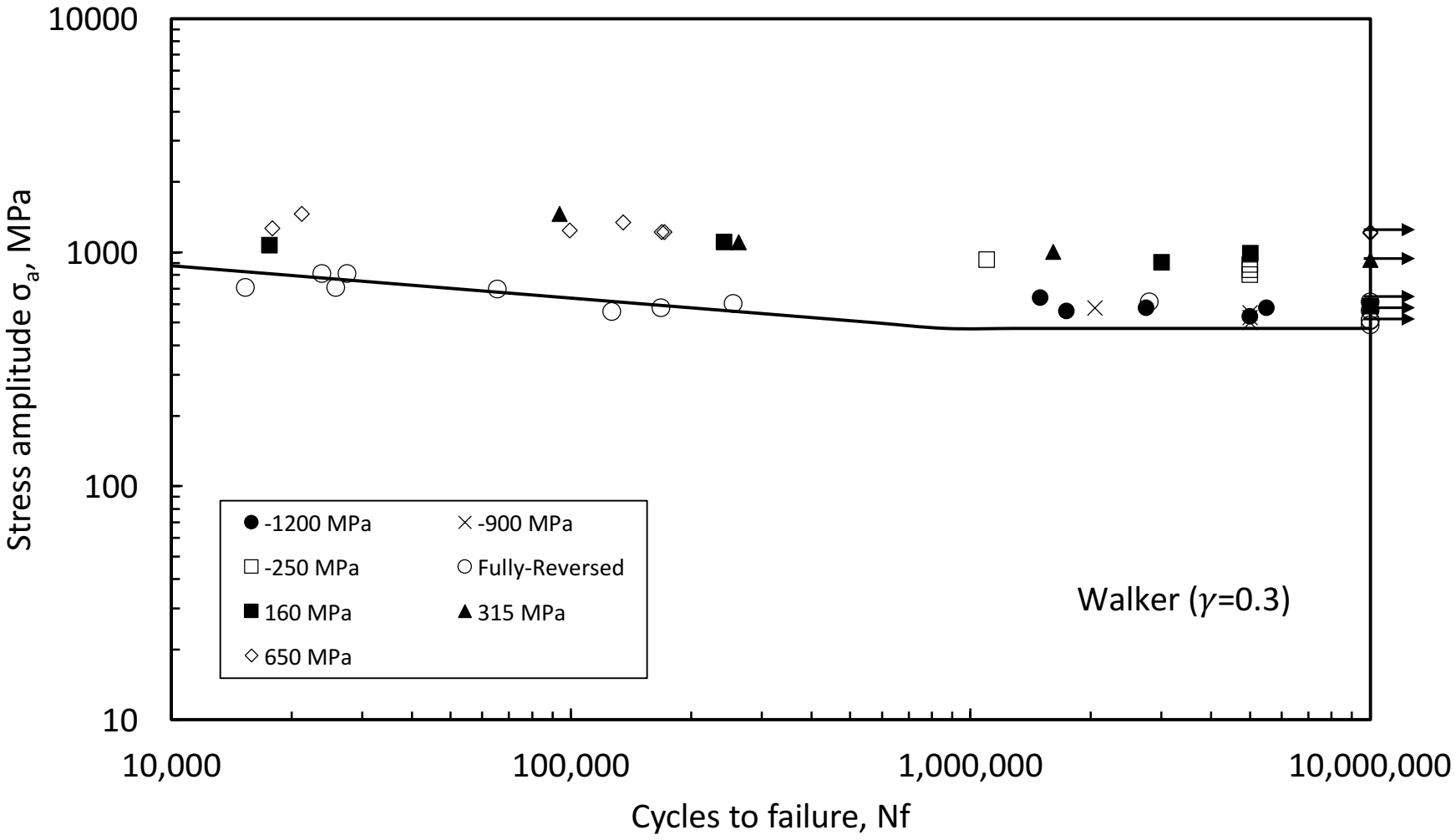

Figure 4.12: Stress-life diagram showing the equivalent stress amplitude for different mean stress levels as corrected by Walker (AISI 8822)

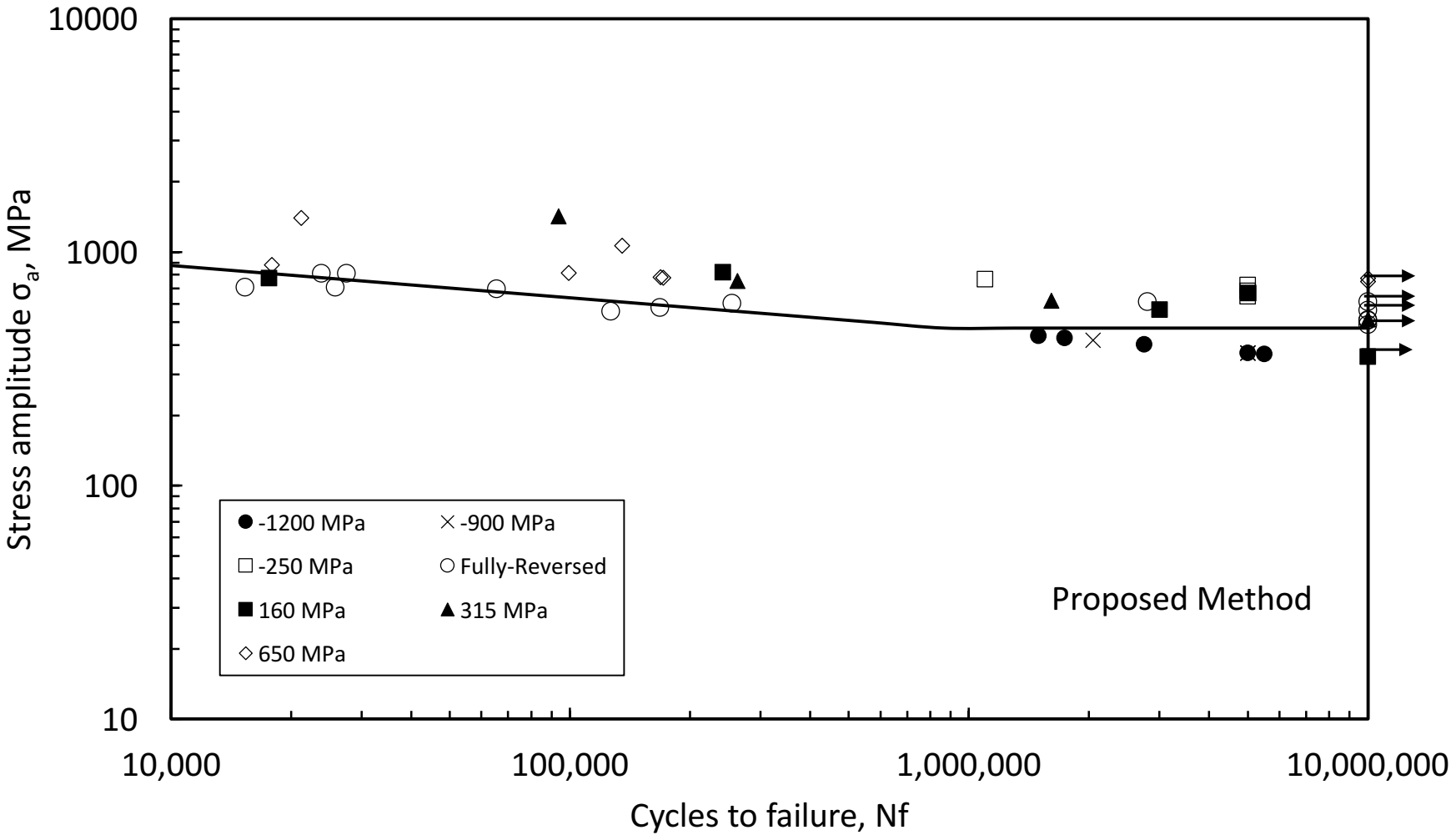

Figure 4.13: Stress-life diagram showing the equivalent stress amplitude for different mean stress levels as corrected by the proposed mean stress method (AISI 8822)

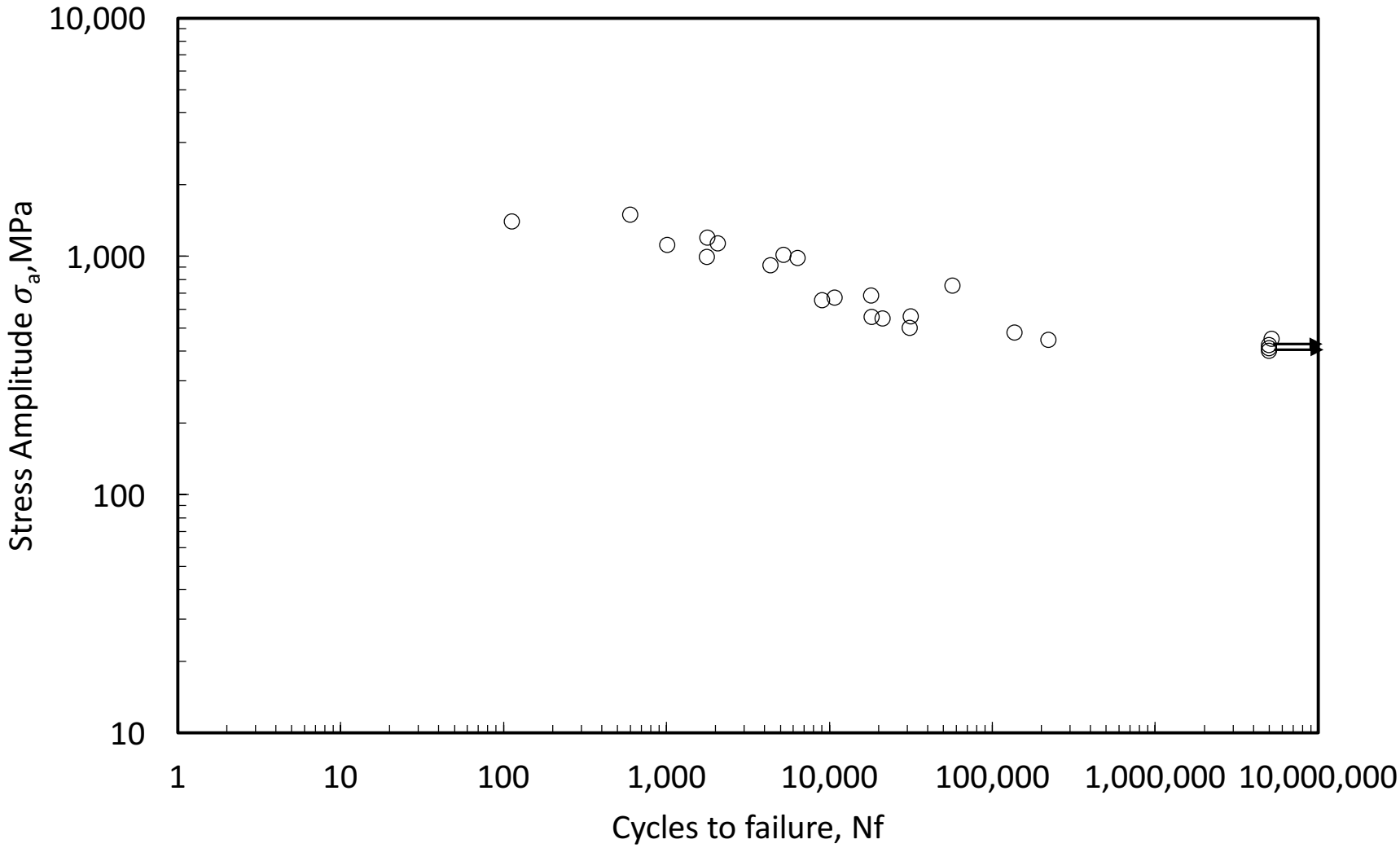

Figure 4.14: Stress-life fatigue curve for AISI 9310

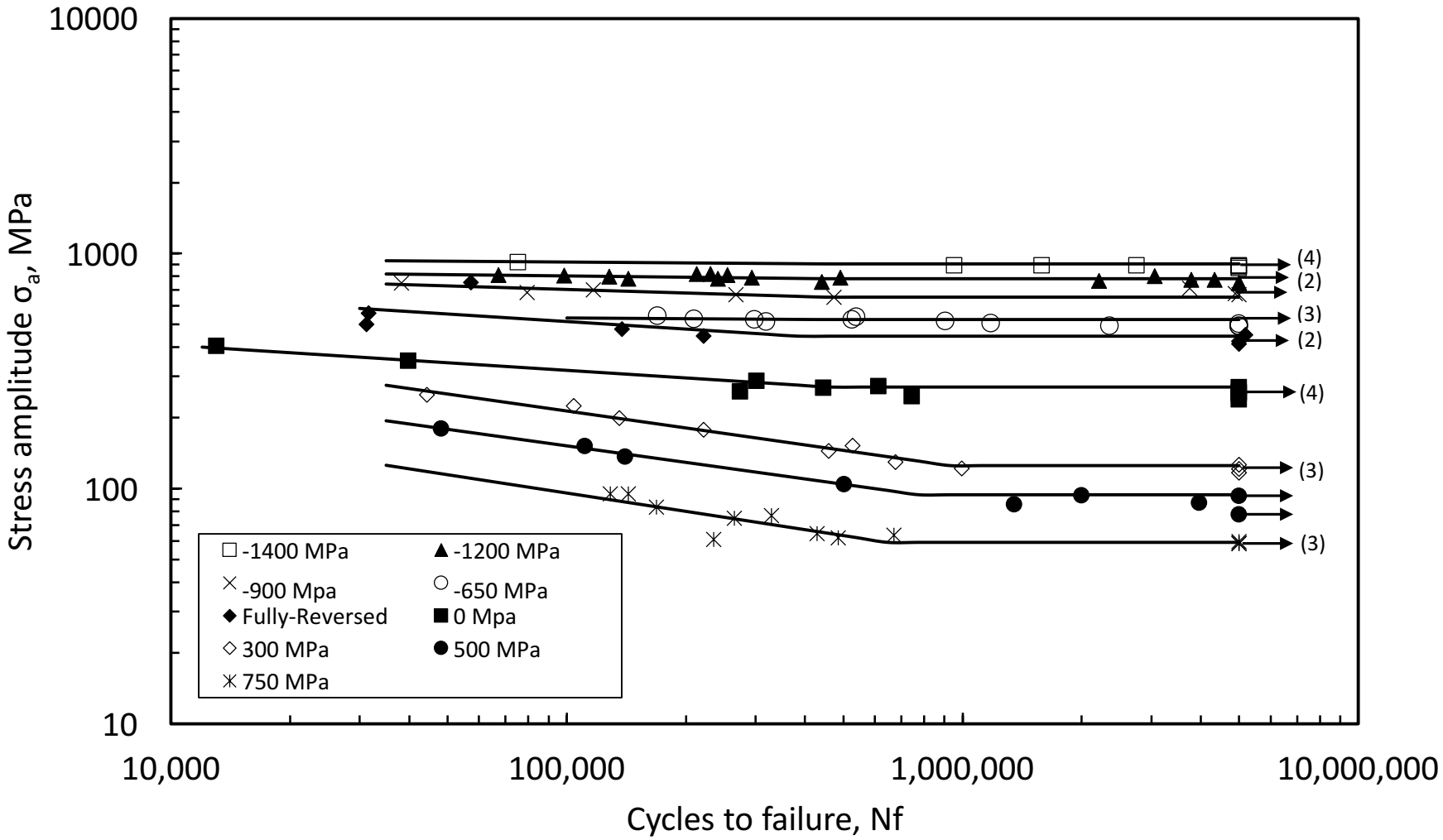

Figure 4.15: Fatigue life of AISI 9310 for different mean stresses

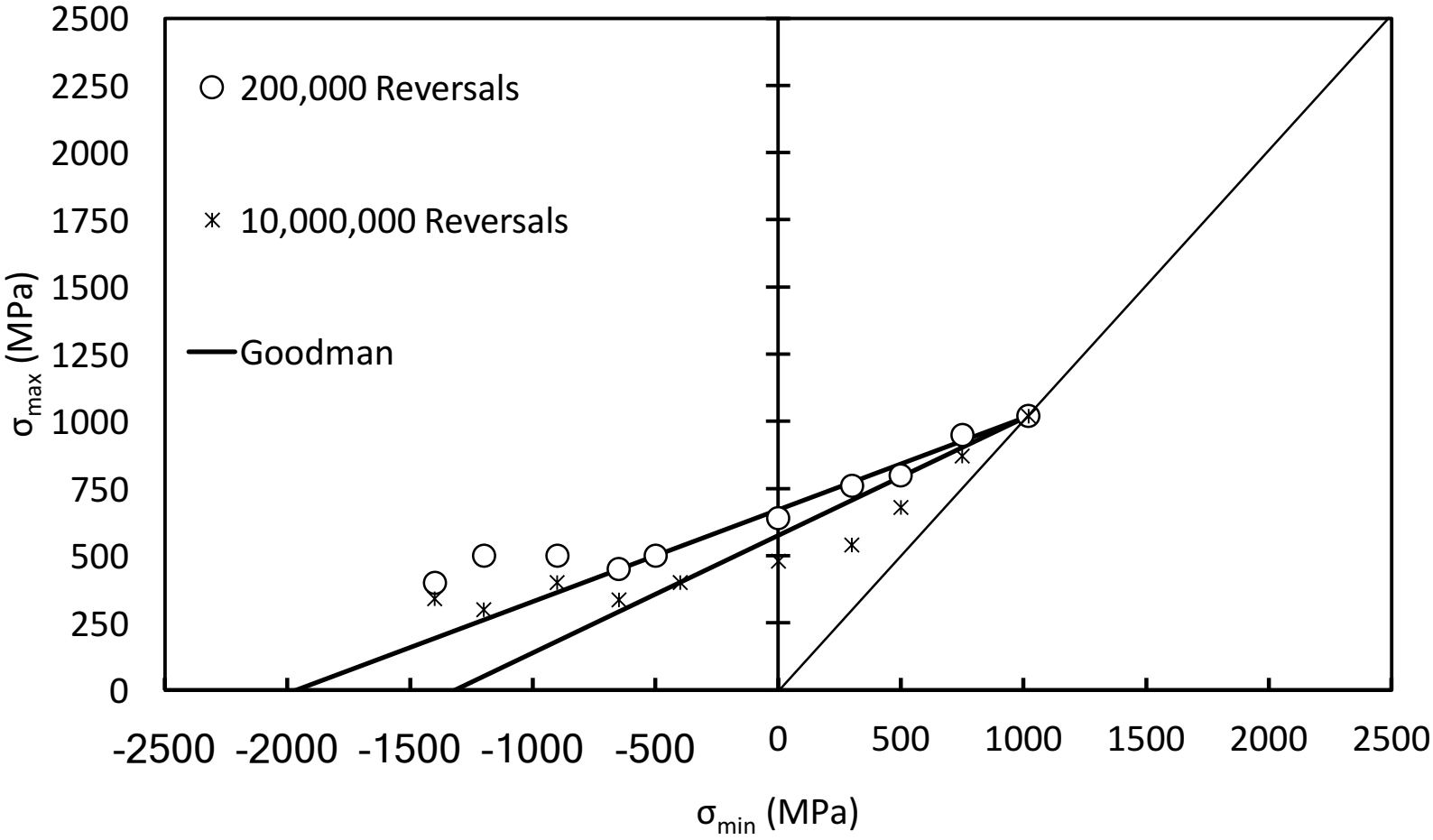

Figure 4.16: Max-min stress diagrams comparing the experimental data for AISI 9310 with the prediction of the Goodman mean stress correction model for 200,000 and 10,000,000 reversals

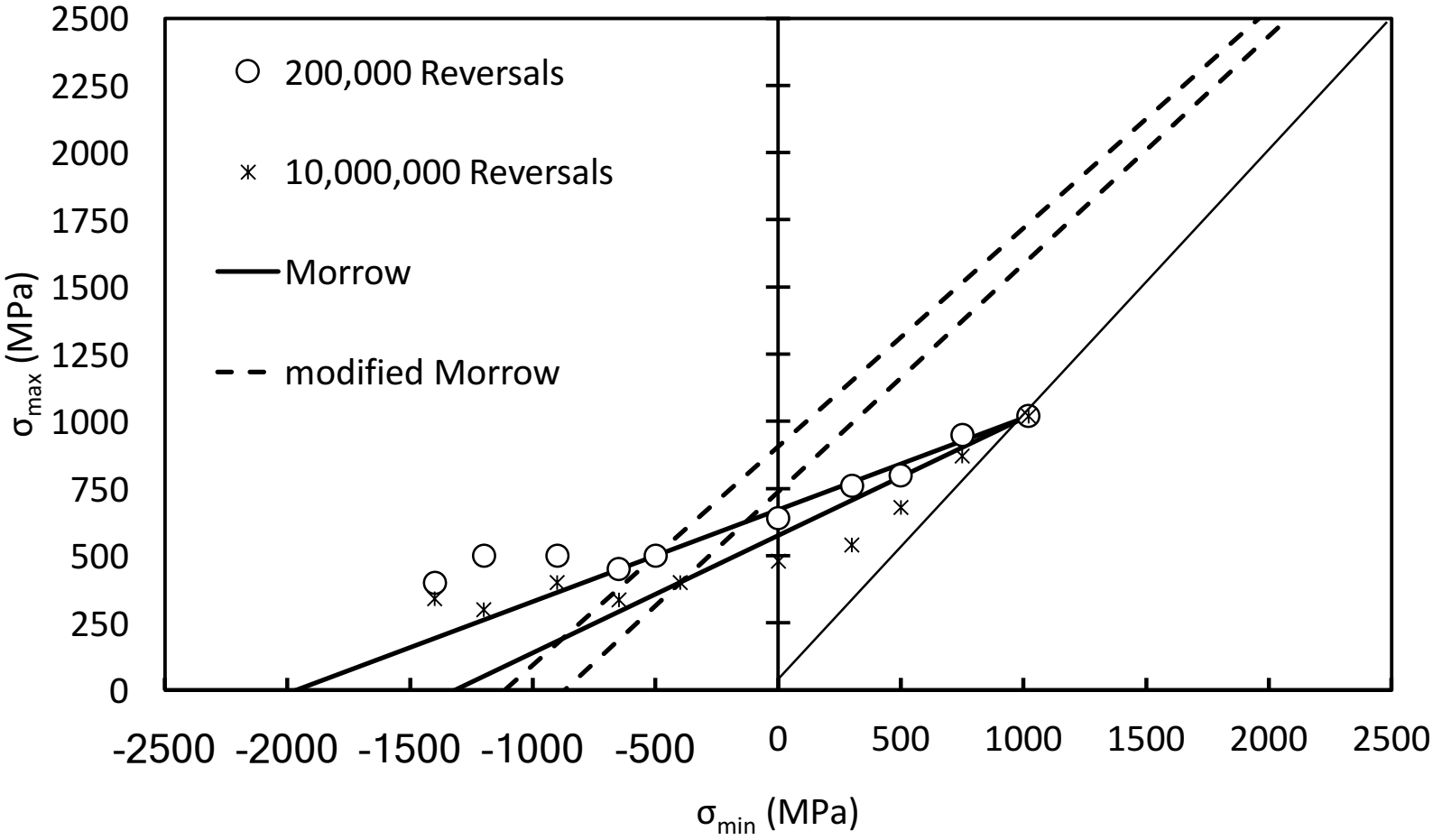

Figure 4.17: Max-min stress diagrams comparing the experimental data for AISI 9310 with the prediction of the Morrow and modified-Morrow mean stress correction models for 200,000 and 10,000,000 reversals

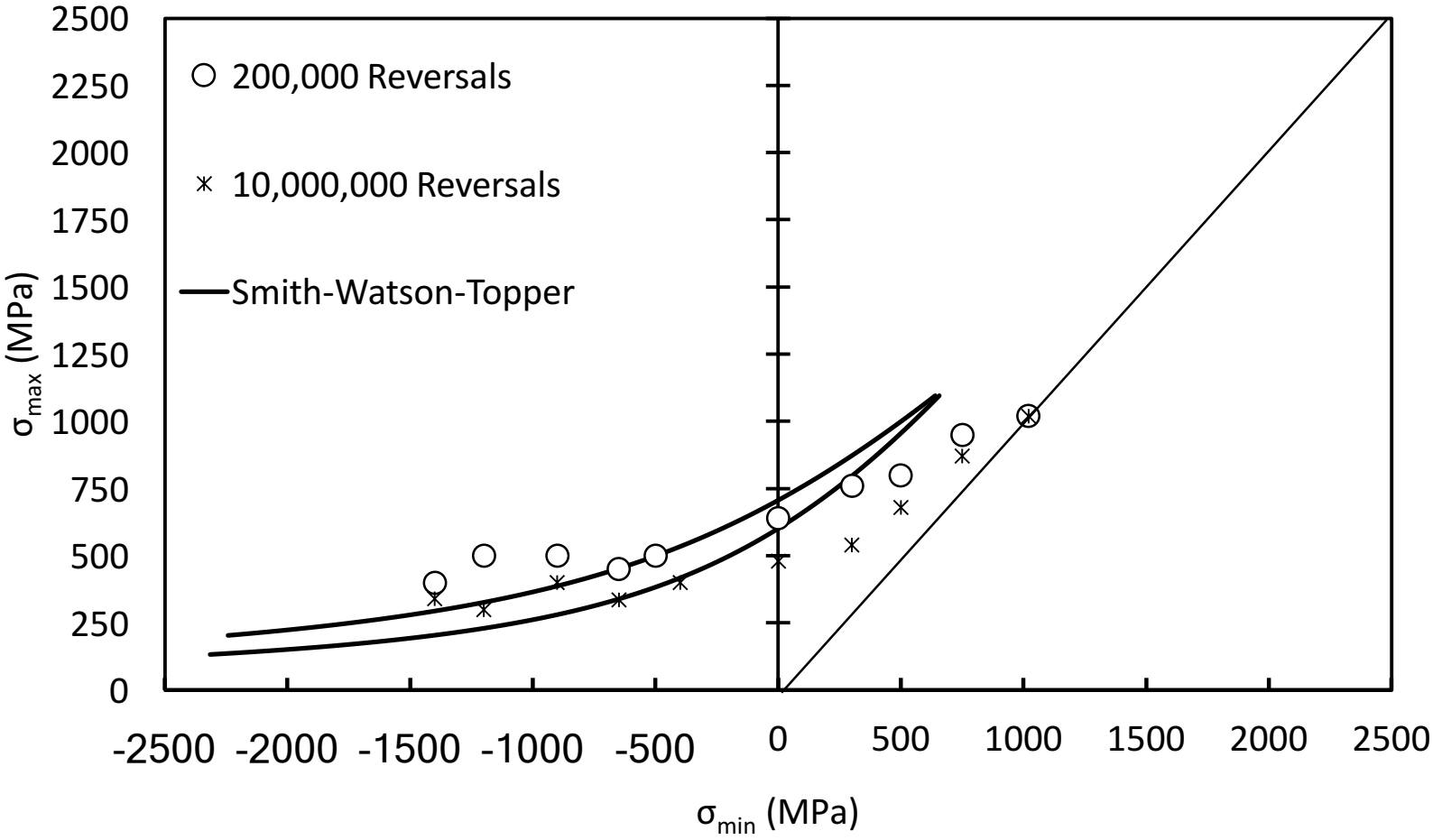

Figure 4.18: Max-min stress diagrams comparing the experimental data for AISI 9310 with the prediction of the Smith-Watson-Topper mean stress correction model for 200,000 and 10,000,000 reversals

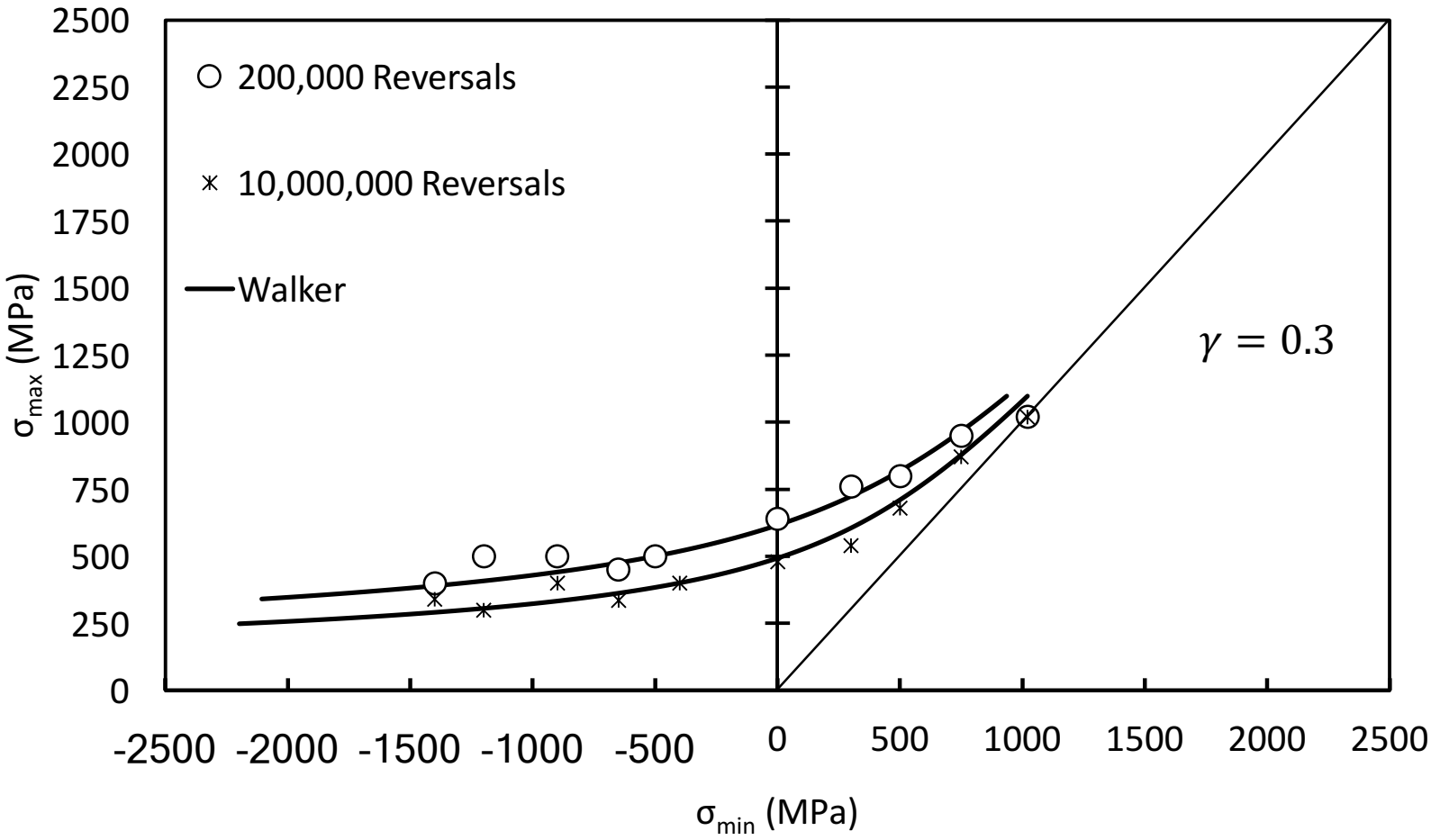

Figure 4.19: Max-min stress diagrams comparing the experimental data for AISI 9310 with the prediction of the Walker mean stress correction model for 200,000 and 10,000,000 reversals

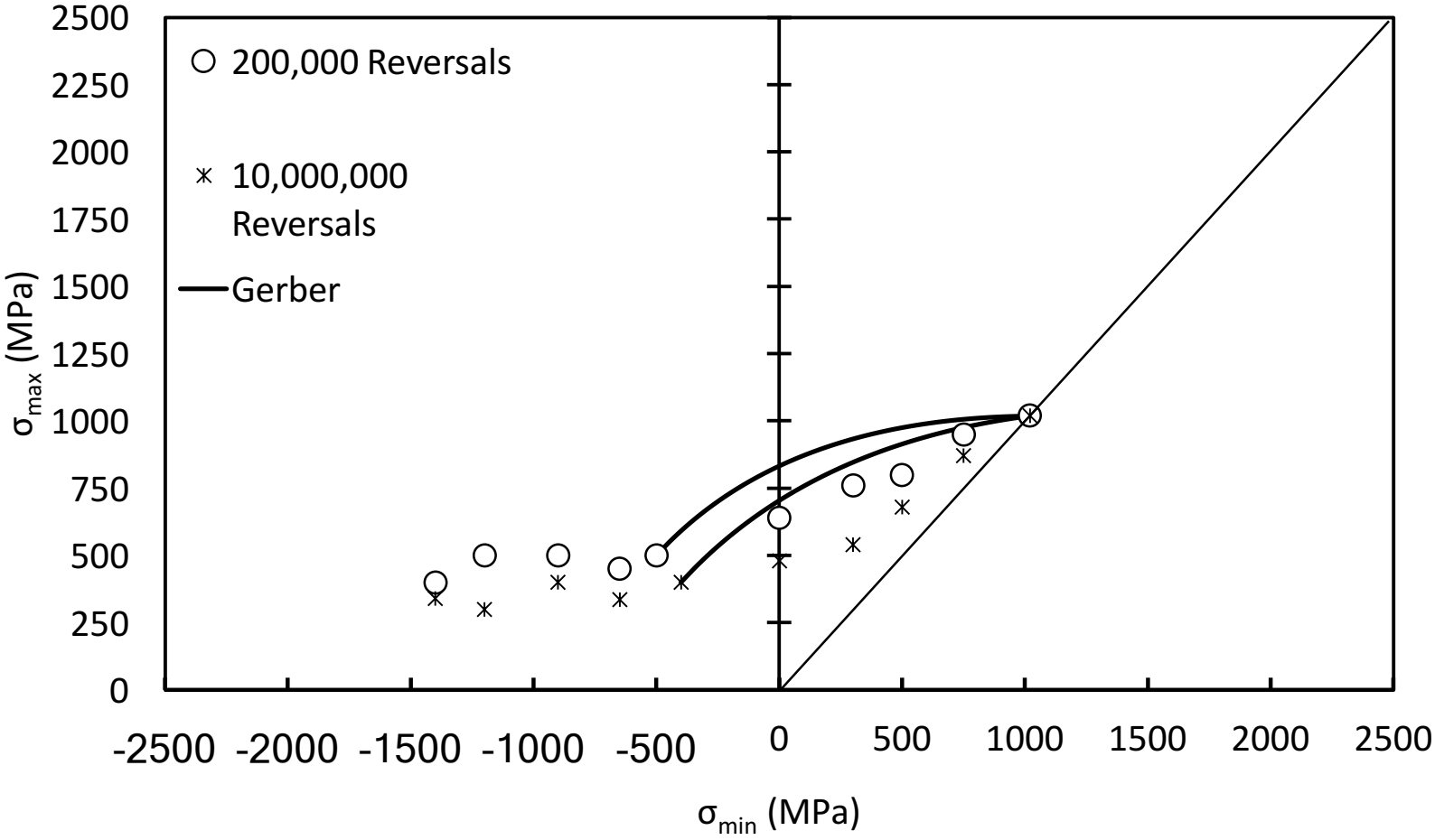

Figure 4.20: Max-min stress diagrams comparing the experimental data for AISI 9310 with the prediction of the Gerber mean stress correction model for 200,000 and 10,000,000 reversals

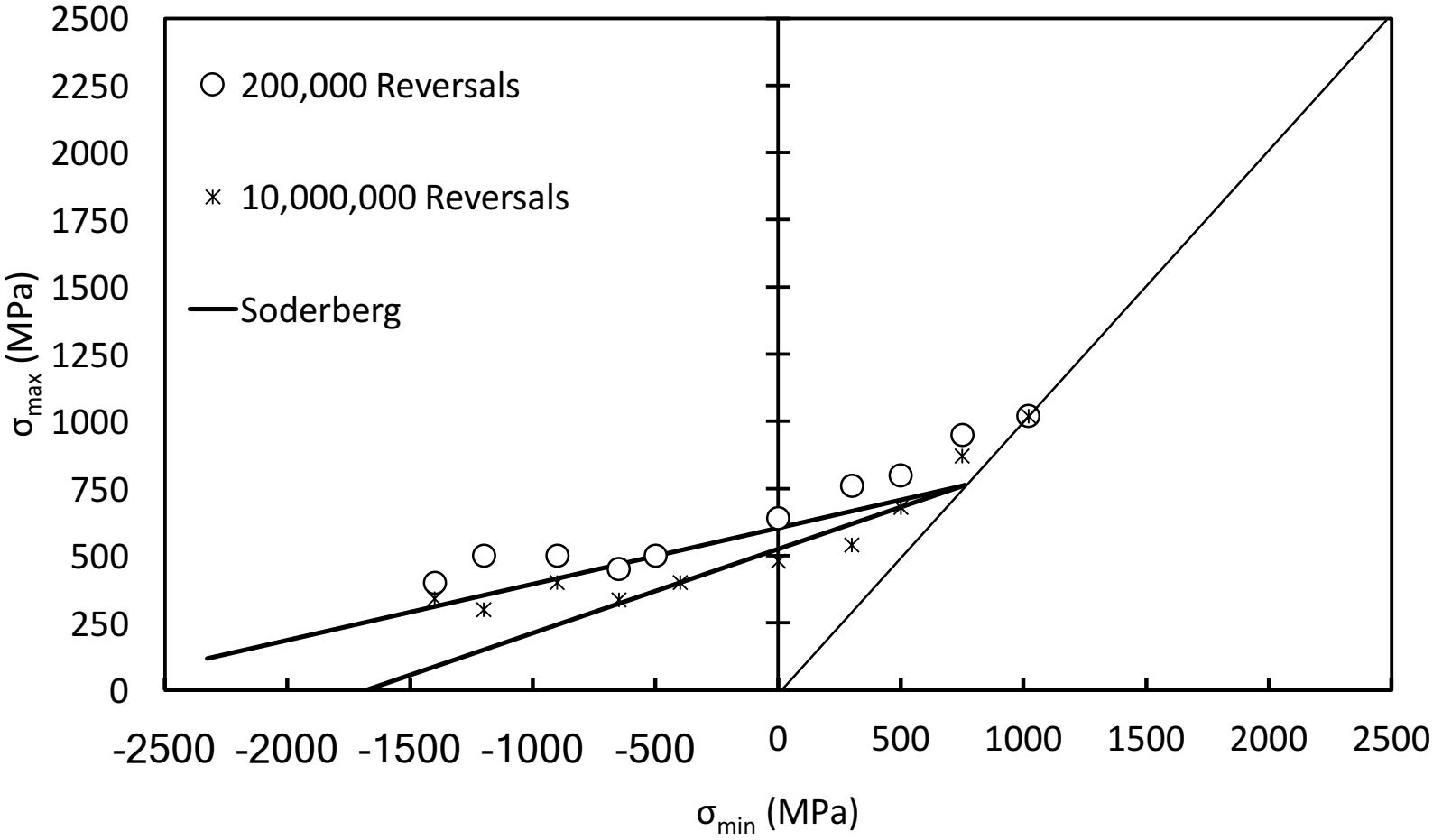

Figure 4.21: Max-min stress diagrams comparing the experimental data for AISI 9310 with the prediction of the Soderberg mean stress correction model for 200,000 and 10,000,000 reversals

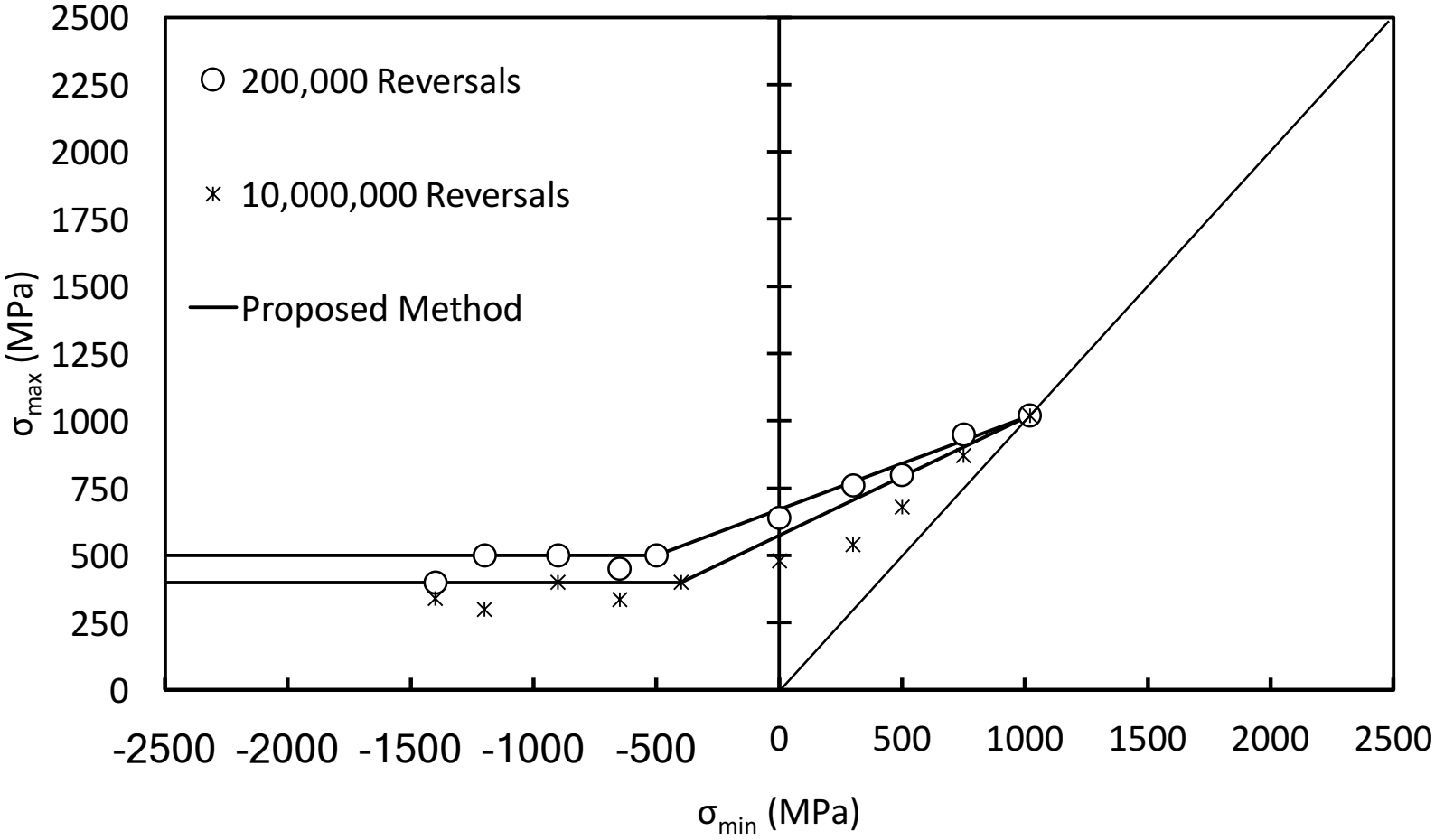

Figure 4.22: Max-min stress diagrams comparing the experimental data for AISI 9310 with the prediction of the proposed mean stress correction model for 200,000 and 10,000,000 reversals

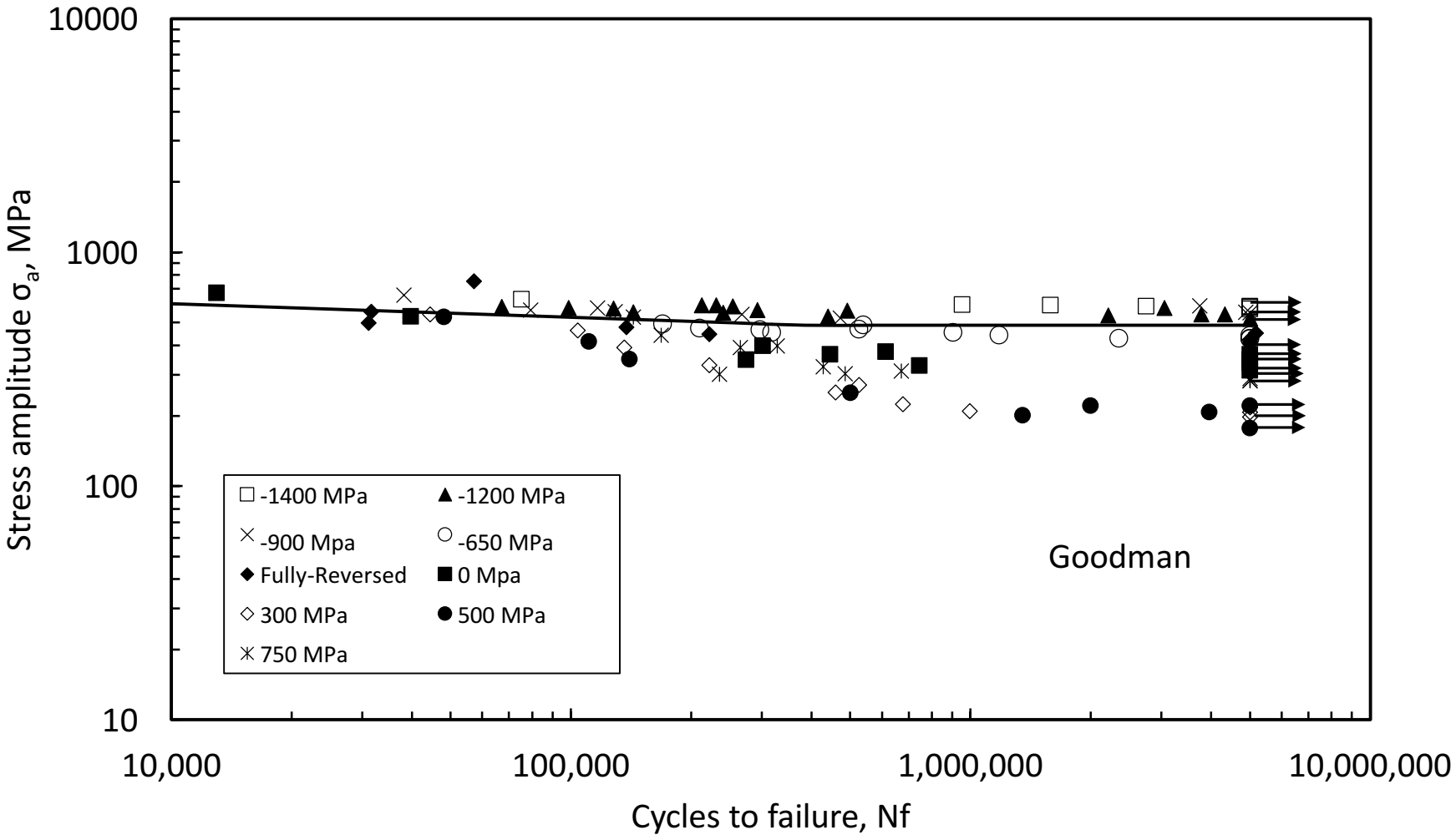

Figure 4.23: Stress-life diagram showing the equivalent stress amplitude for different mean stress levels as corrected by Goodman (AISI 9310)

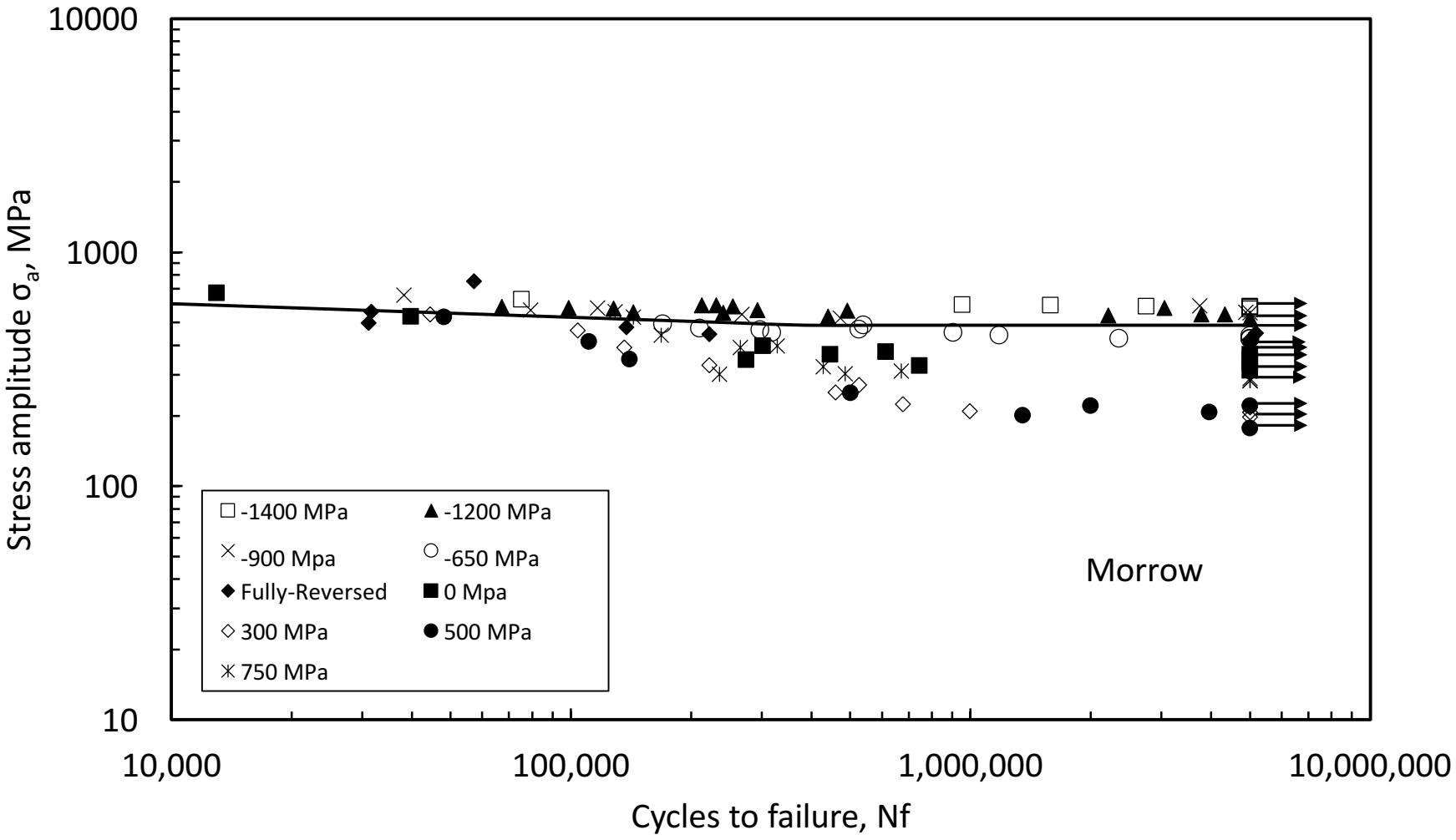

Figure 4.24: Stress-life diagram showing the equivalent stress amplitude for different mean stress levels as corrected by Morrow (AISI 9310)

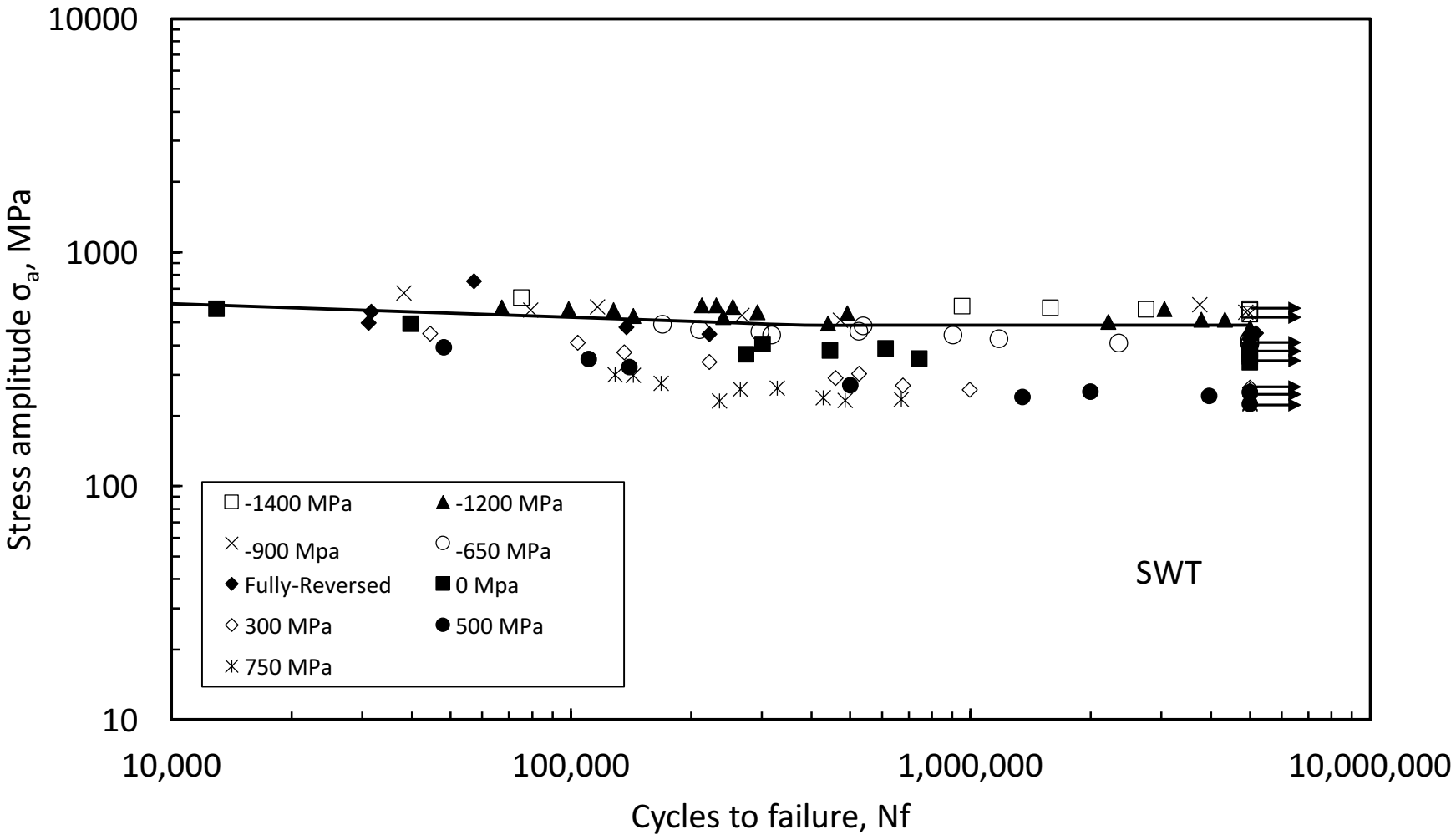

Figure 4.25: Stress-life diagram showing the equivalent stress amplitude for different mean stress levels as corrected by Smith-Watson-Topper (AISI 9310)

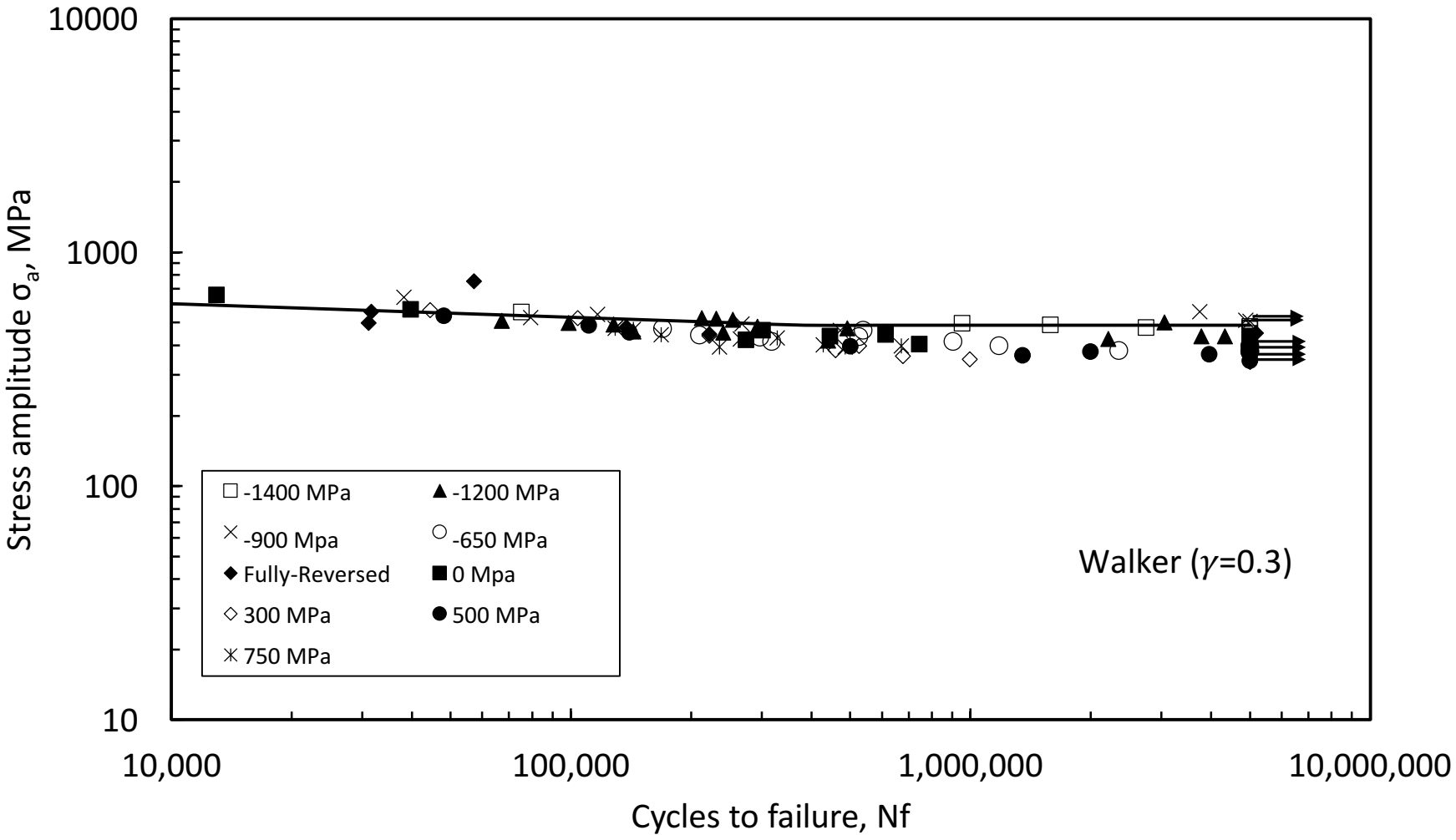

Figure 4.26: Stress-life diagram showing the equivalent stress amplitude for different mean stress levels as corrected by Walker (AISI 9310)

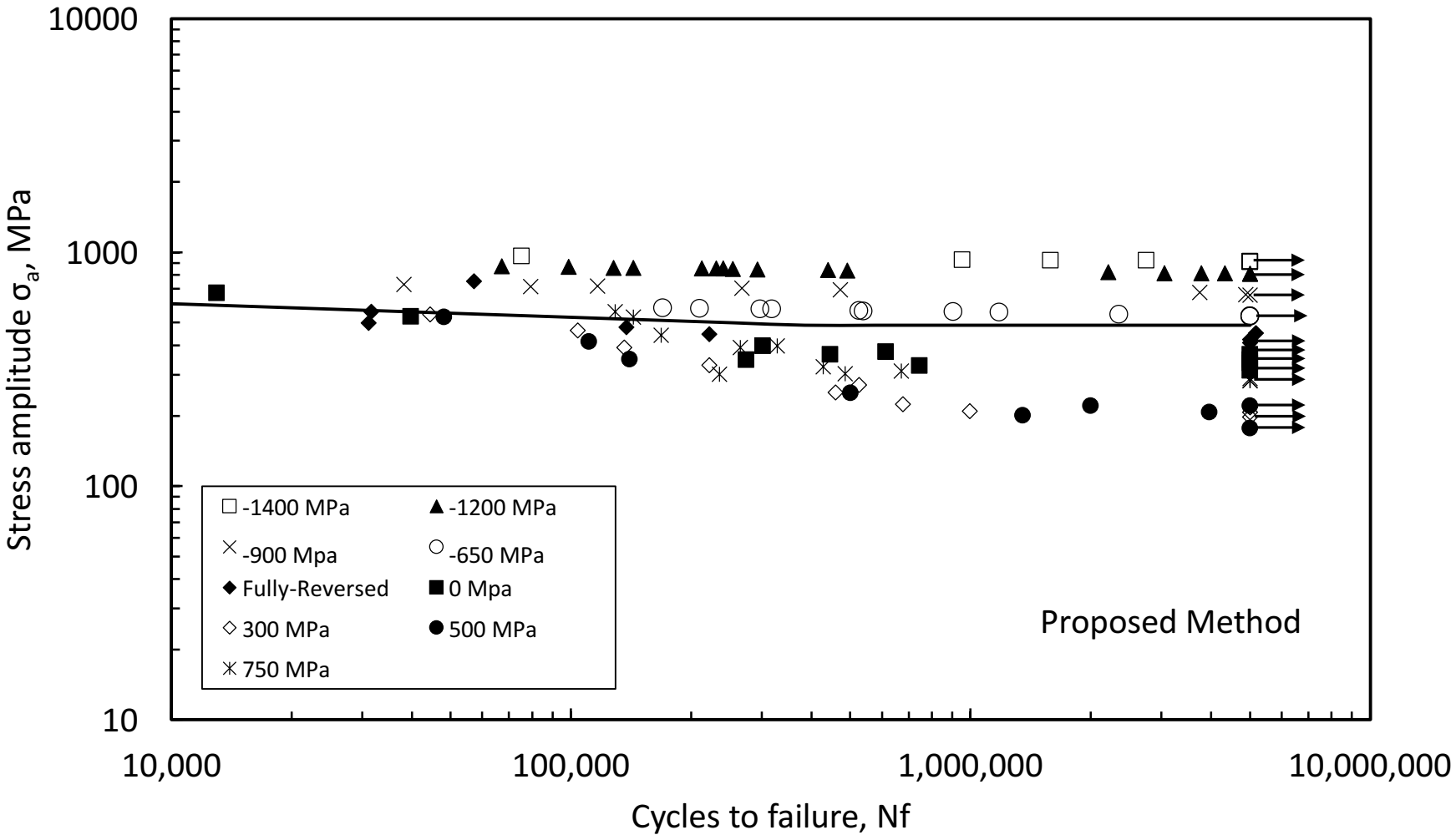

Figure 4.27: Stress-life diagram showing the equivalent stress amplitude for different mean stress levels as corrected by the proposed mean stress method (AISI 9310)

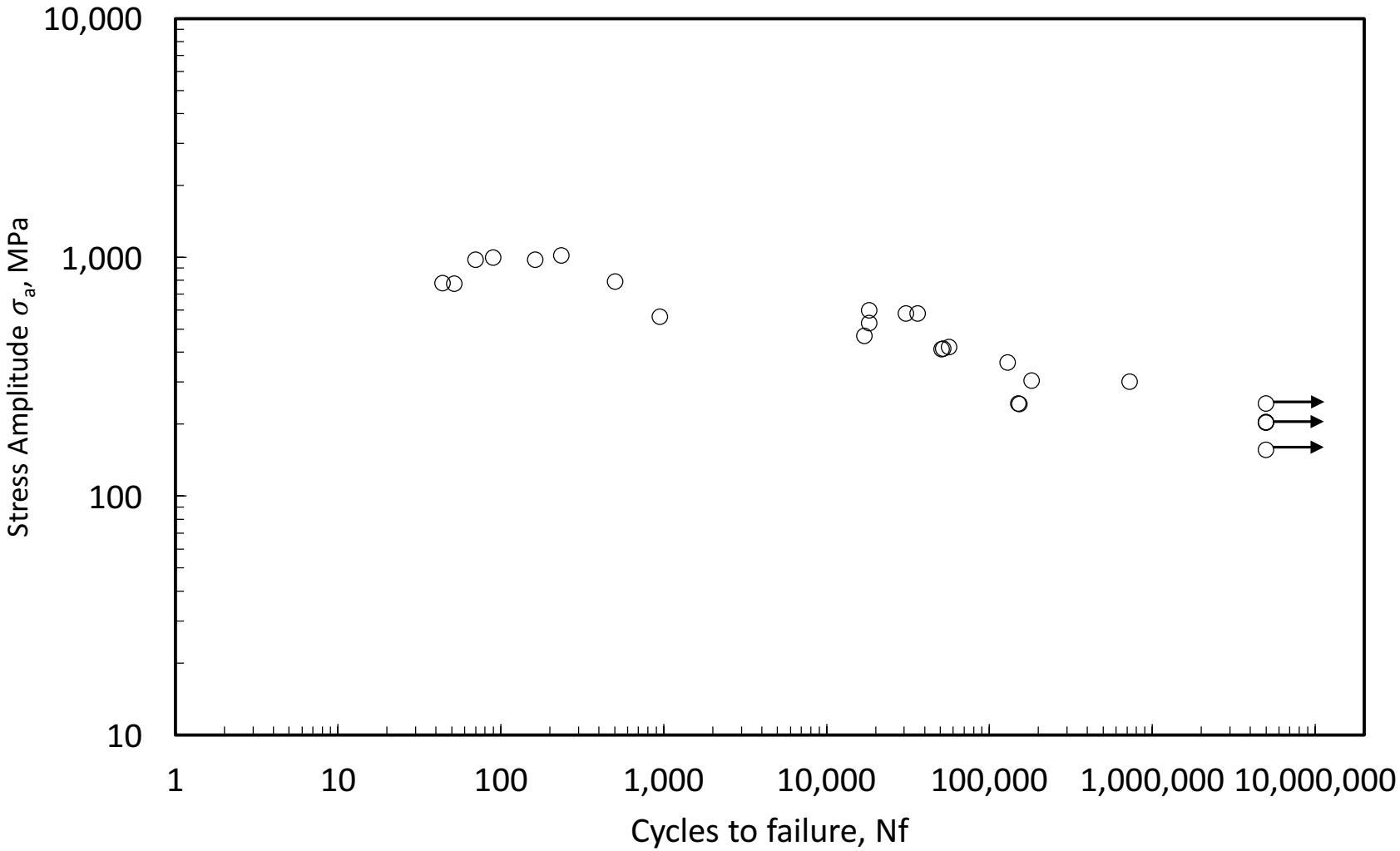

Figure 4.28: Stress-life fatigue curve for AISI 8620

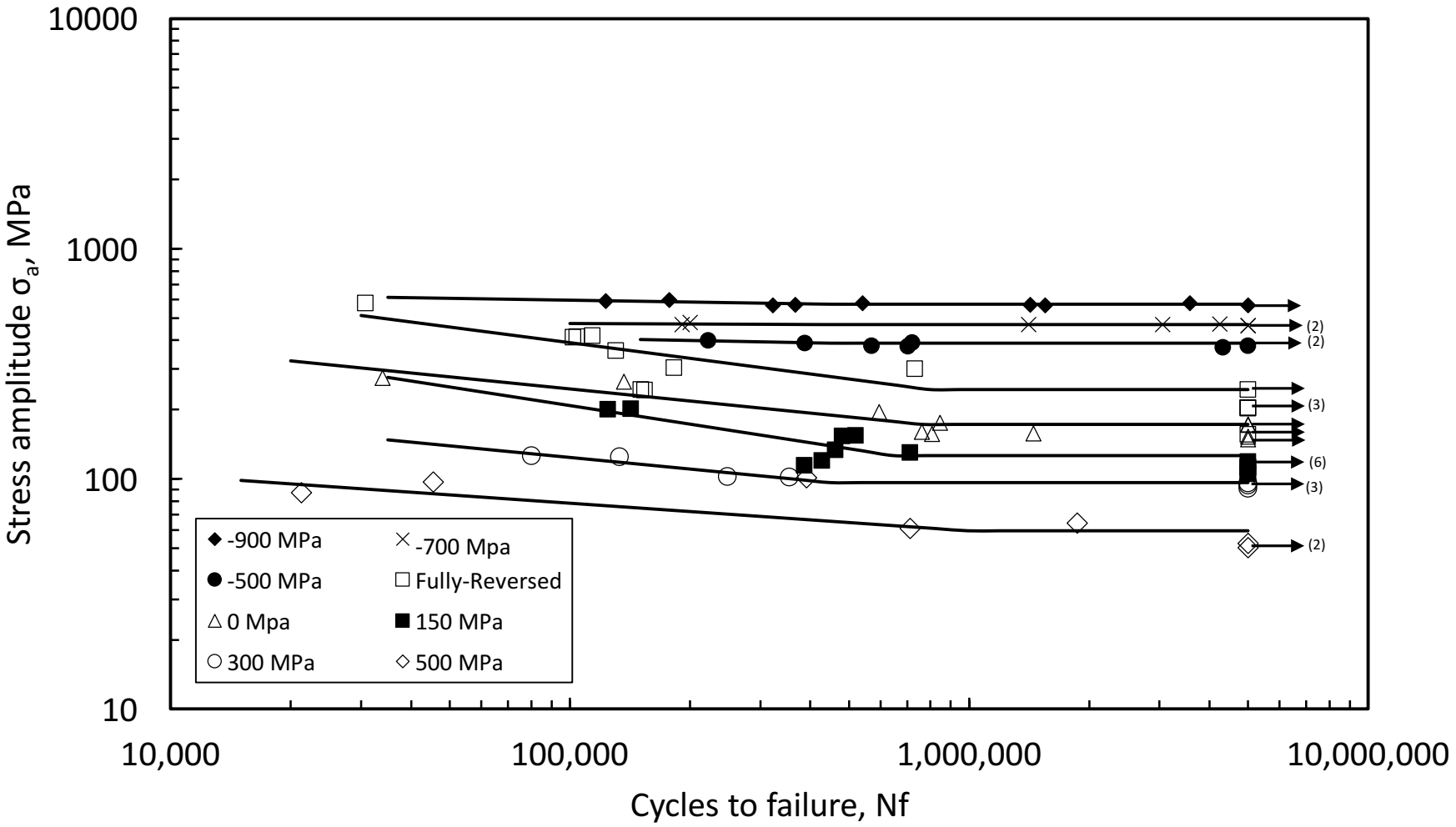

Figure 4.29: Fatigue life of AISI 8620 for different mean stresses

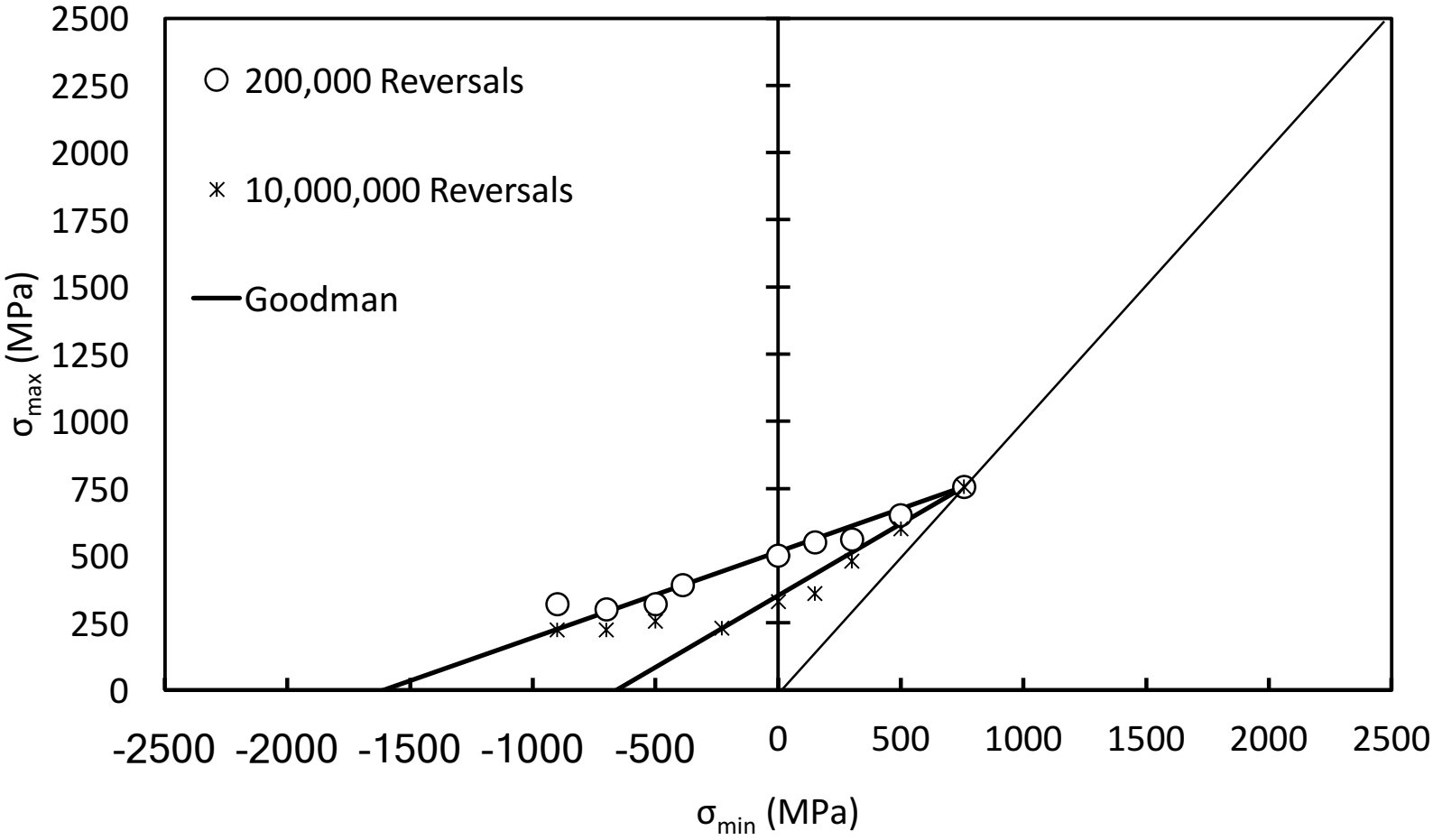

Figure 4.30: Max-min stress diagrams comparing the experimental data for AISI 8620 with the prediction of the Goodman mean stress correction model for 200,000 and 10,000,000 reversals

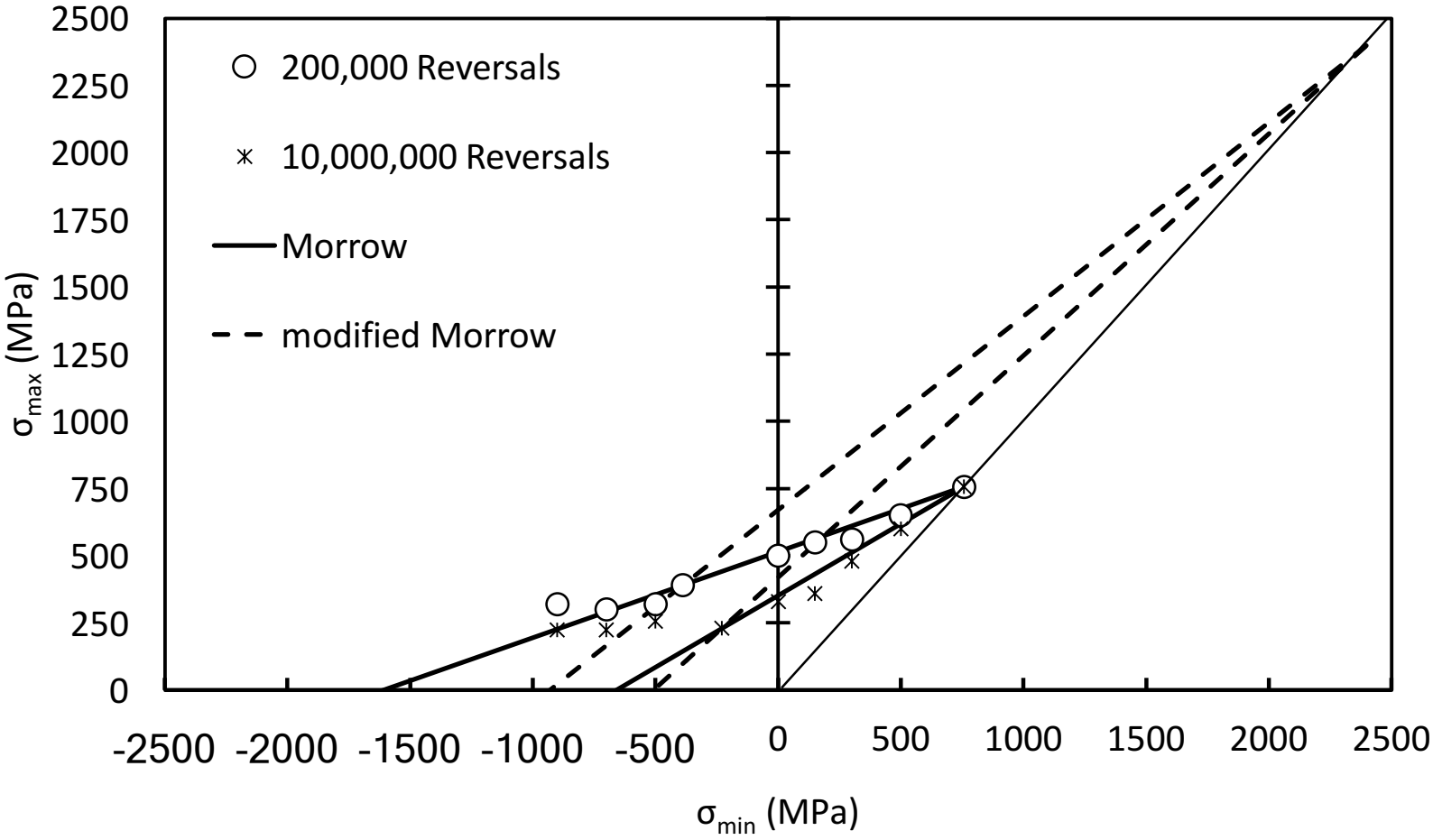

Figure 4.31: Max-min stress diagrams comparing the experimental data for AISI 8620 with the prediction of the Morrow and modified-Morrow mean stress correction models for 200,000 and 10,000,000 reversals

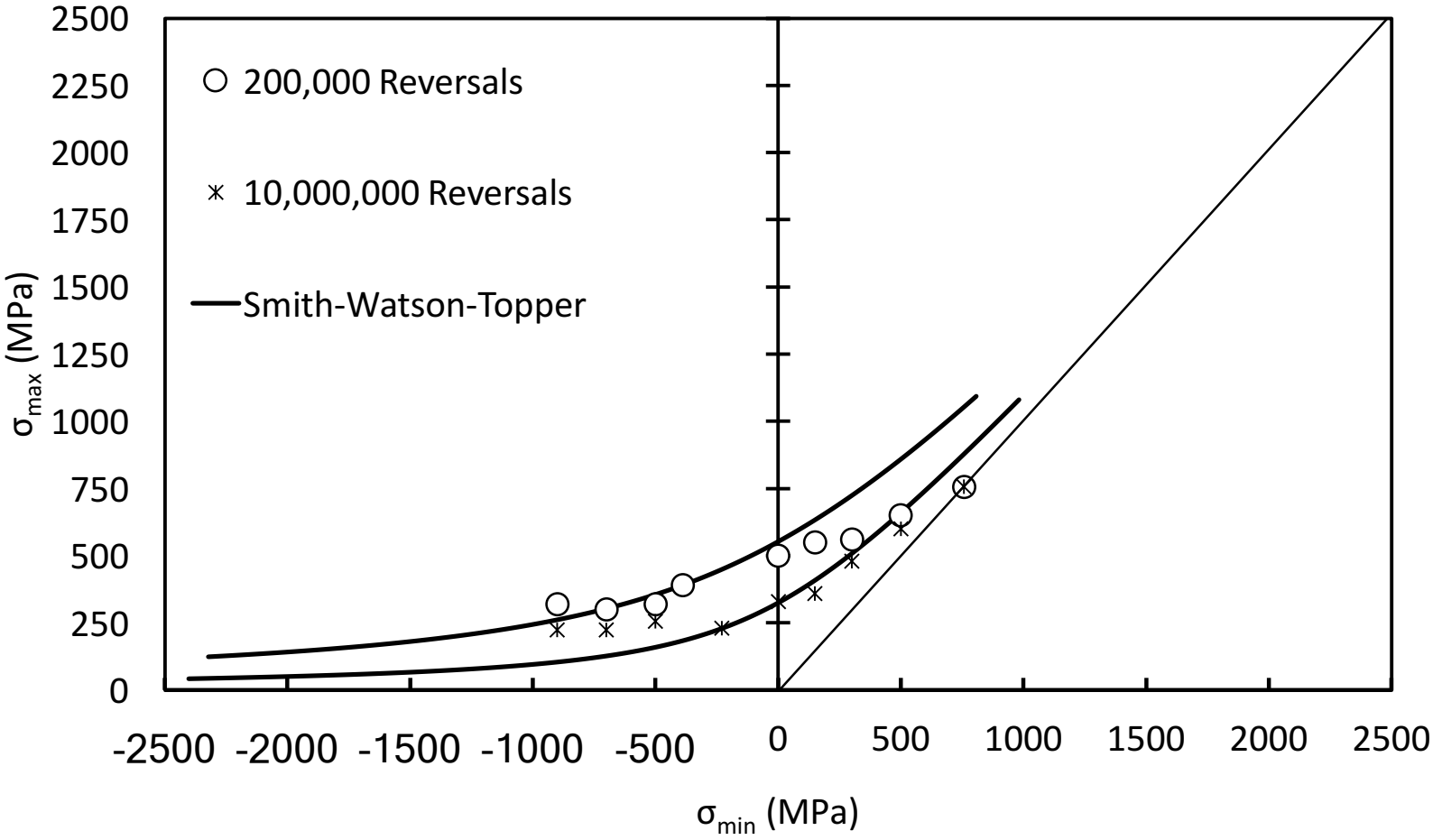

Figure 4.32: Max-min stress diagrams comparing the experimental data for AISI 8620 with the prediction of the Smith-Watson-Topper mean stress correction model for 200,000 and 10,000,000 reversals

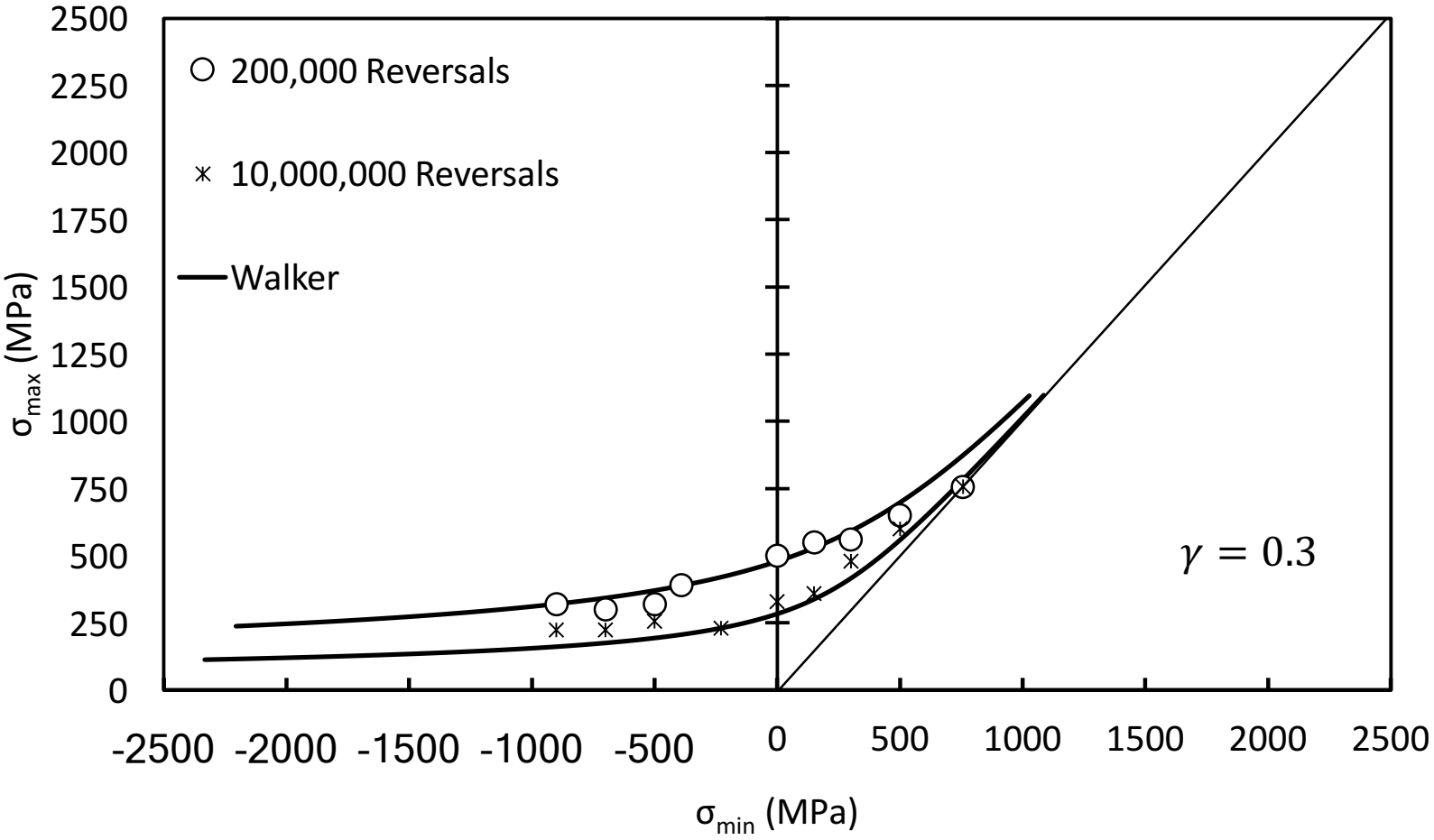

Figure 4.33: Max-min stress diagrams comparing the experimental data for AISI 8620 with the prediction of the Walker mean stress correction model for 200,000 and 10,000,000 reversals

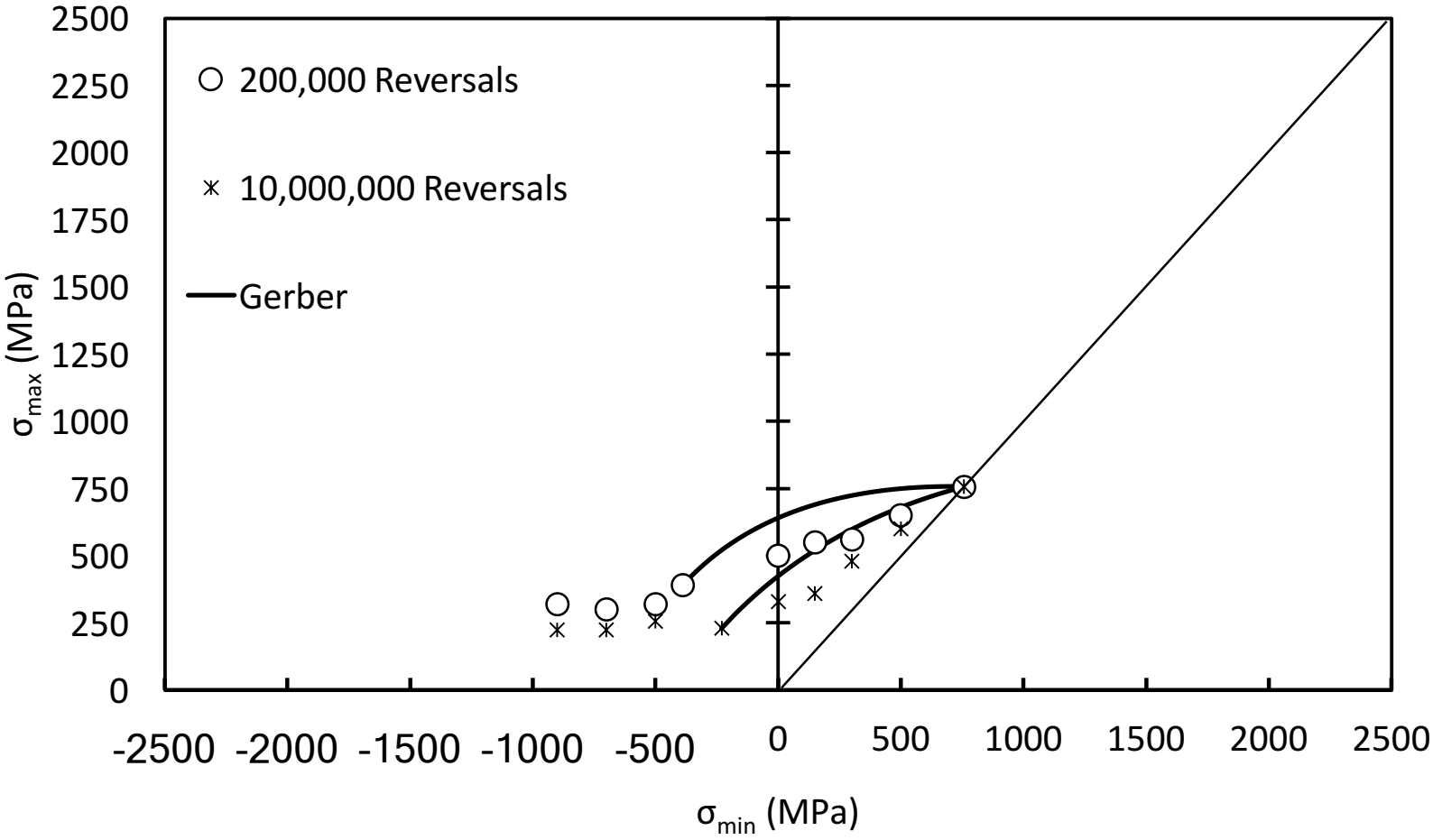

Figure 4.34: Max-min stress diagrams comparing the experimental data for AISI 8620 with the prediction of the Gerber mean stress correction model for 200,000 and 10,000,000 reversals

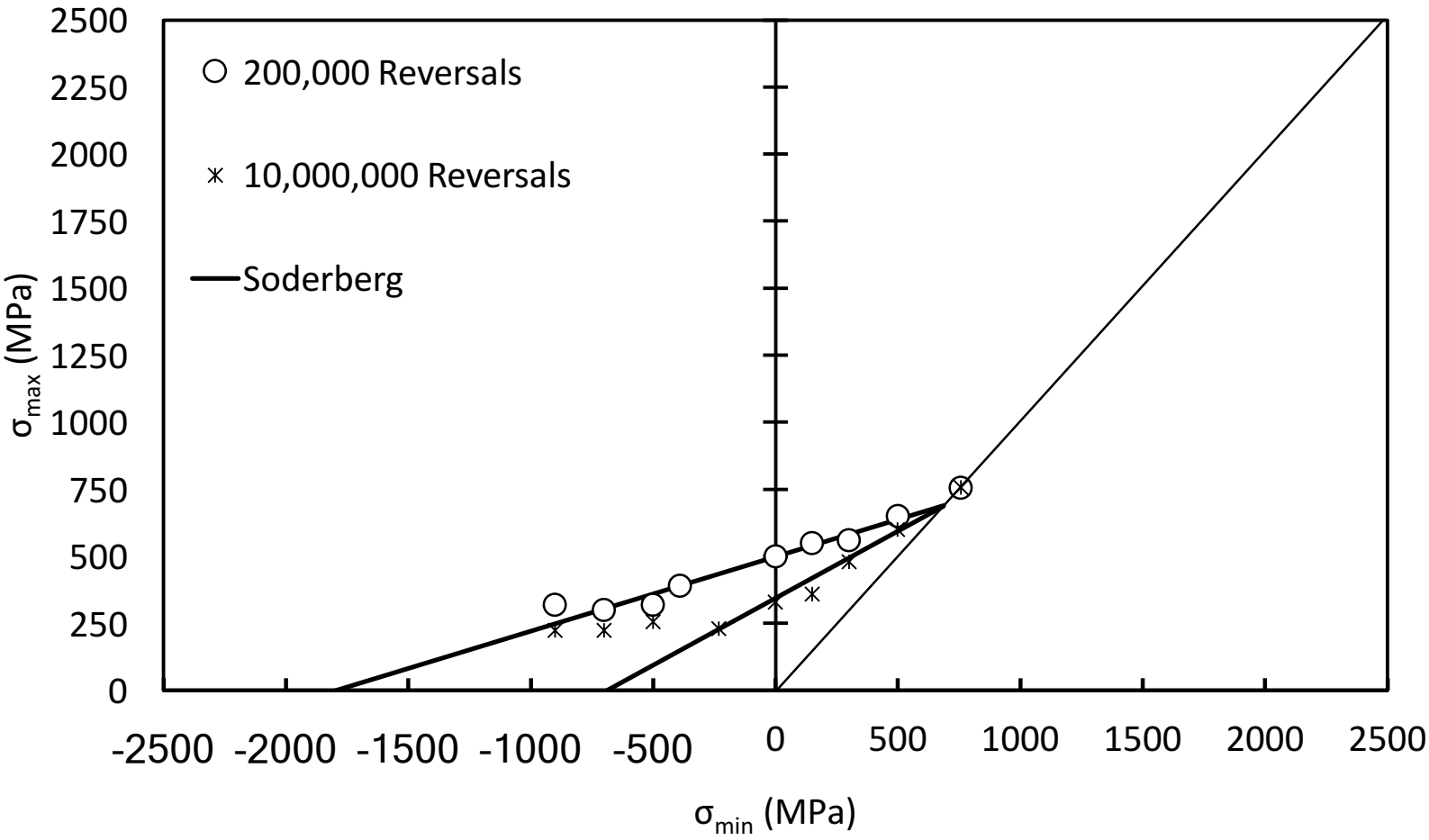

Figure 4.35: Max-min stress diagrams comparing the experimental data for AISI 8620 with the prediction of the Soderberg mean stress correction model for 200,000 and 10,000,000 reversals

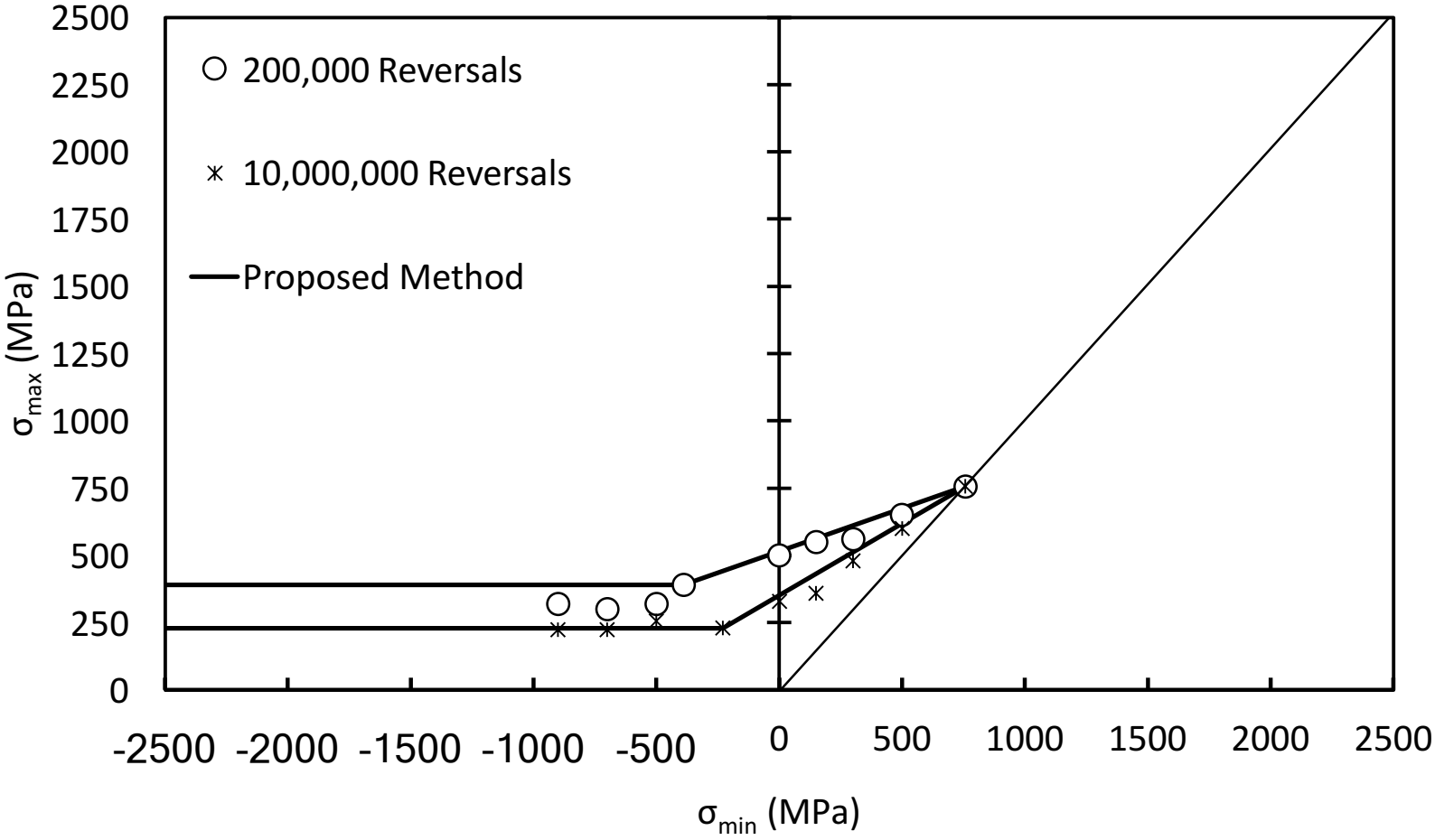

Figure 4.36: Max-min stress diagrams comparing the experimental data for AISI 8620 with the prediction of the proposed mean stress correction model for 200,000 and 10,000,000 reversals

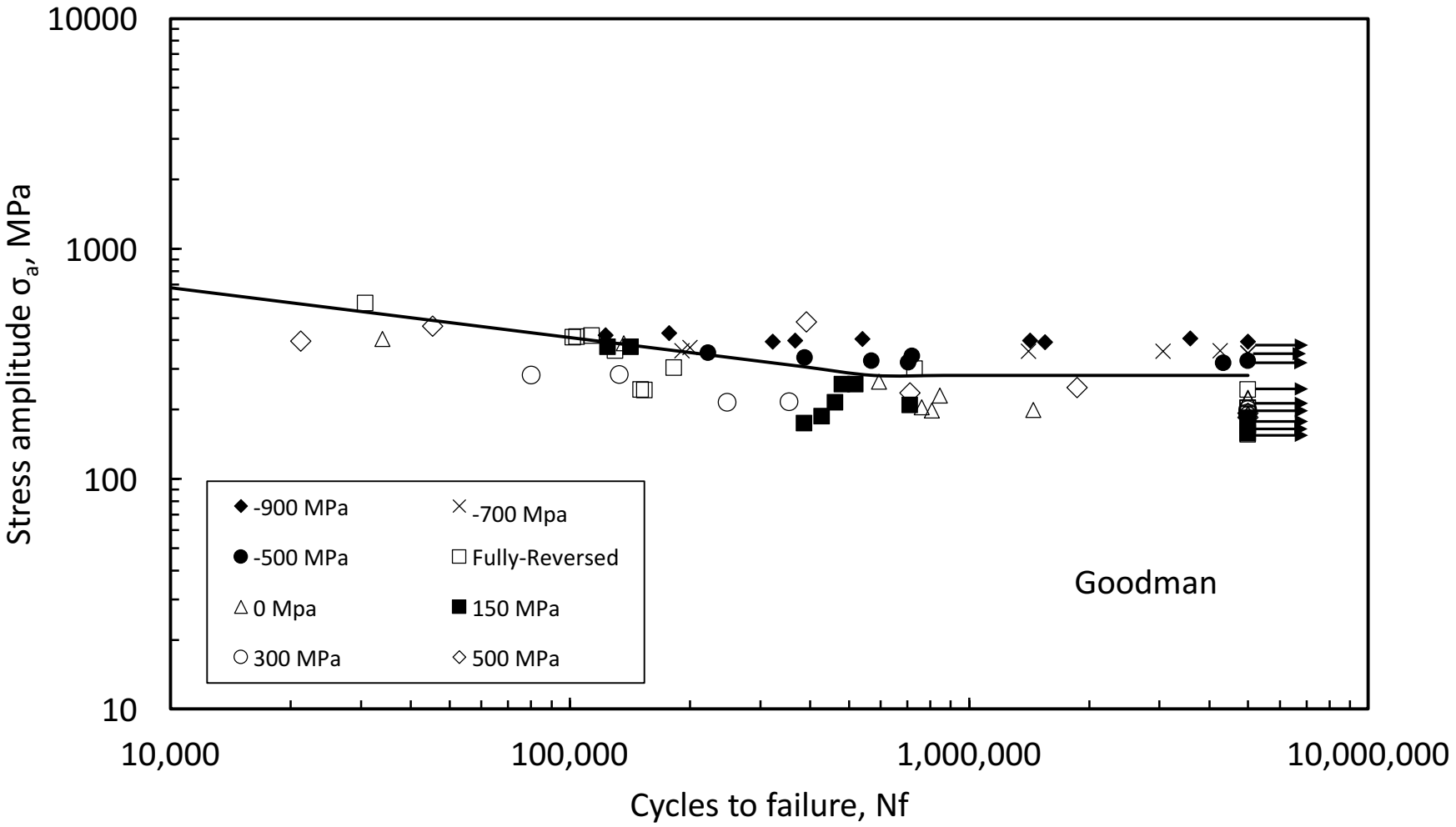

Figure 4.37: Stress-life diagram showing the equivalent stress amplitude for different mean stress levels as corrected by Goodman (AISI 8620)

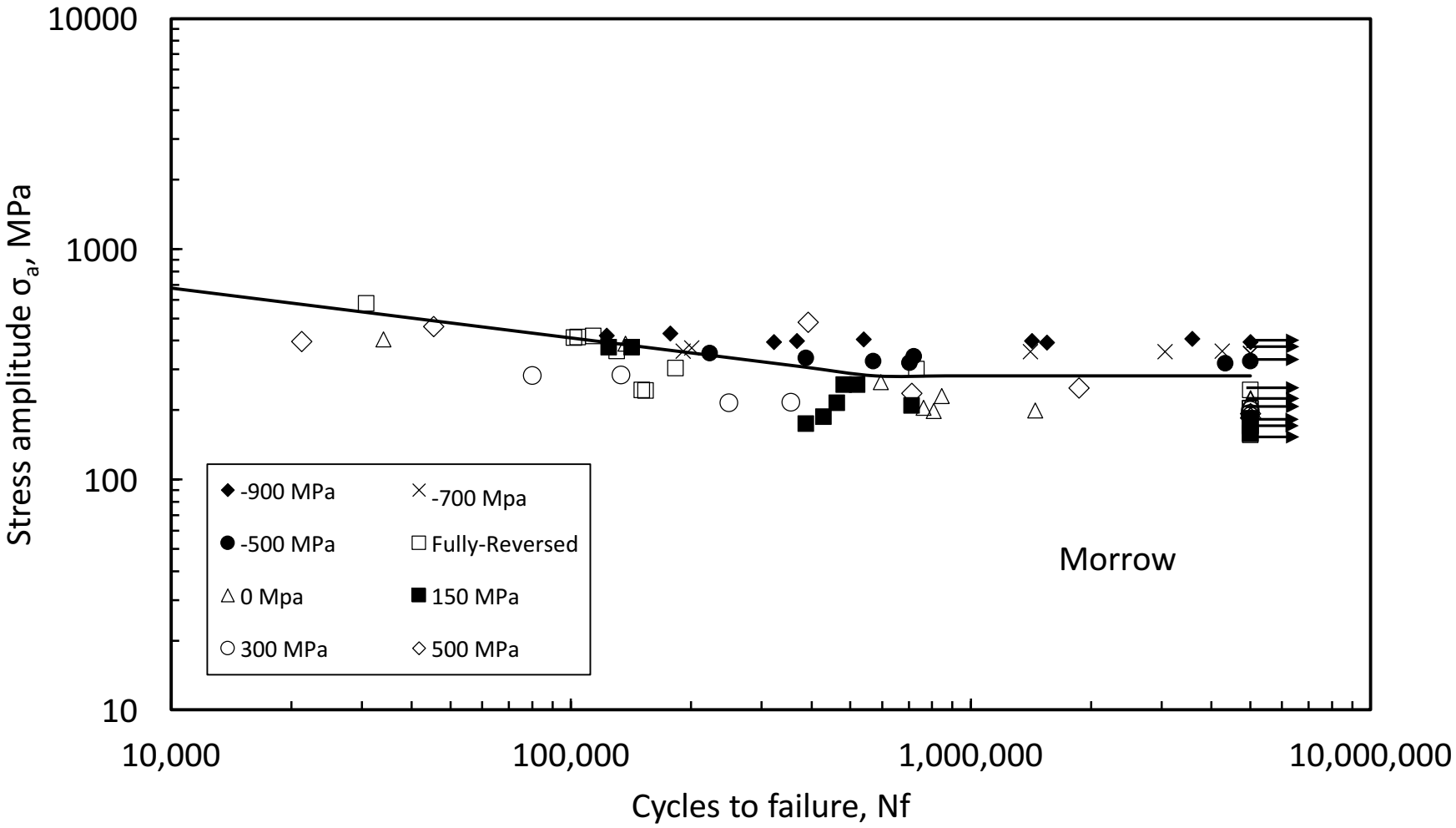

Figure 4.38: Stress-life diagram showing the equivalent stress amplitude for different mean stress levels as corrected by Morrow (AISI 8620)

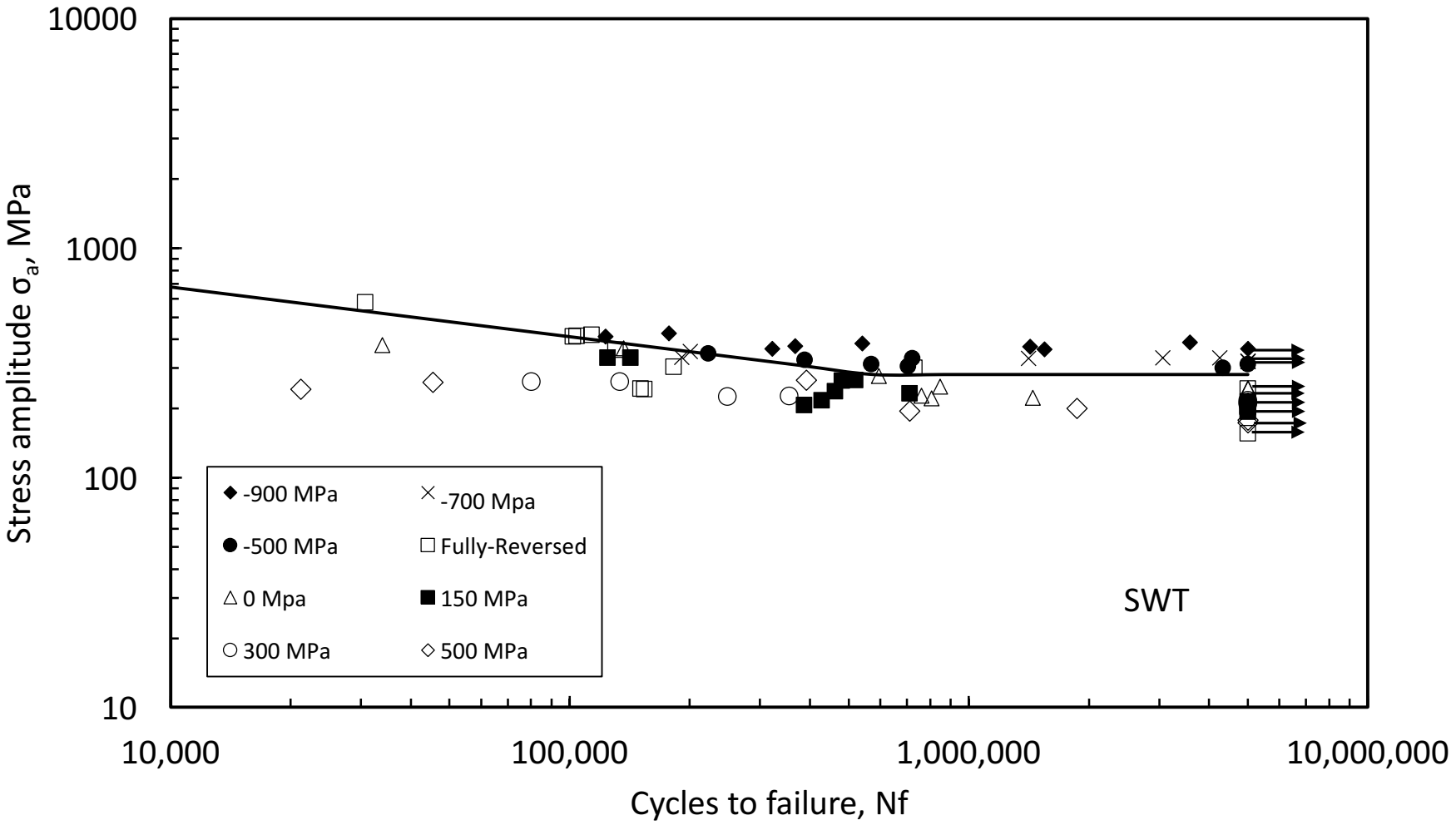

Figure 4.39: Stress-life diagram showing the equivalent stress amplitude for different mean stress levels as corrected by Smith-Watson-Topper (AISI 8620)

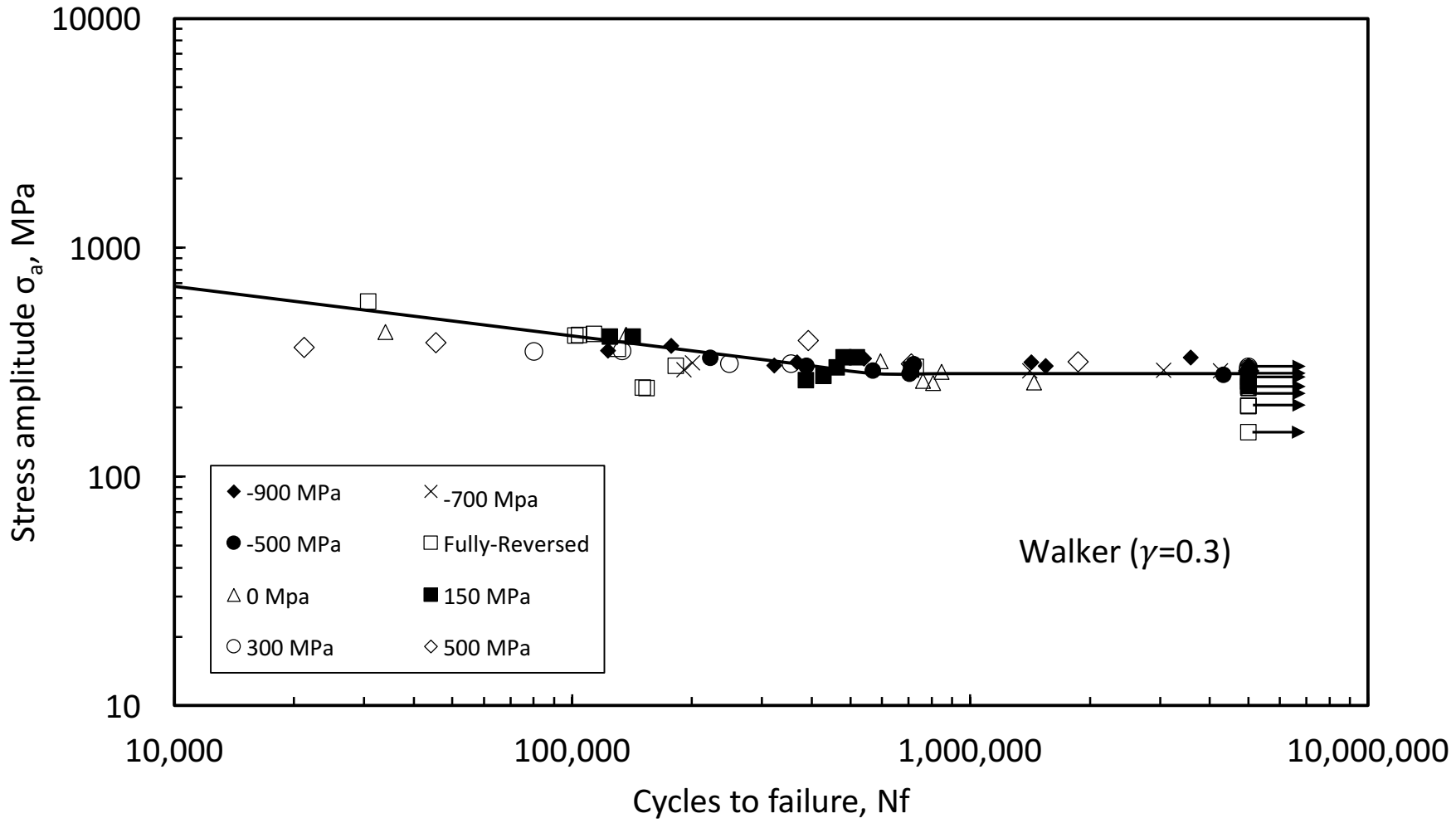

Figure 4.40: Stress-life diagram showing the equivalent stress amplitude for different mean stress levels as corrected by Walker (AISI 8620)

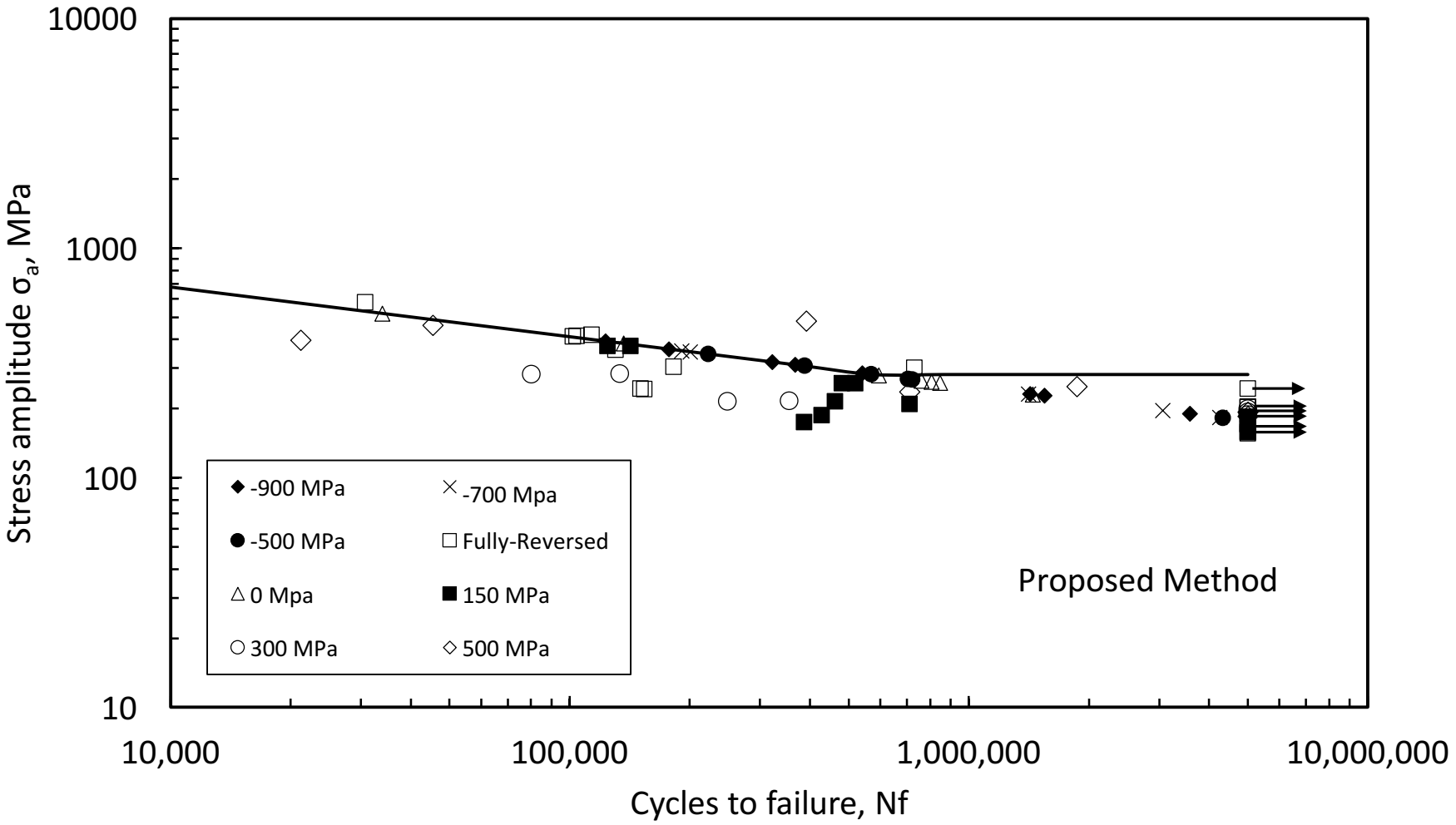

Figure 4.41: Stress-life diagram showing the equivalent stress amplitude for different mean stress levels as corrected by the proposed mean stress method (AISI 8620)

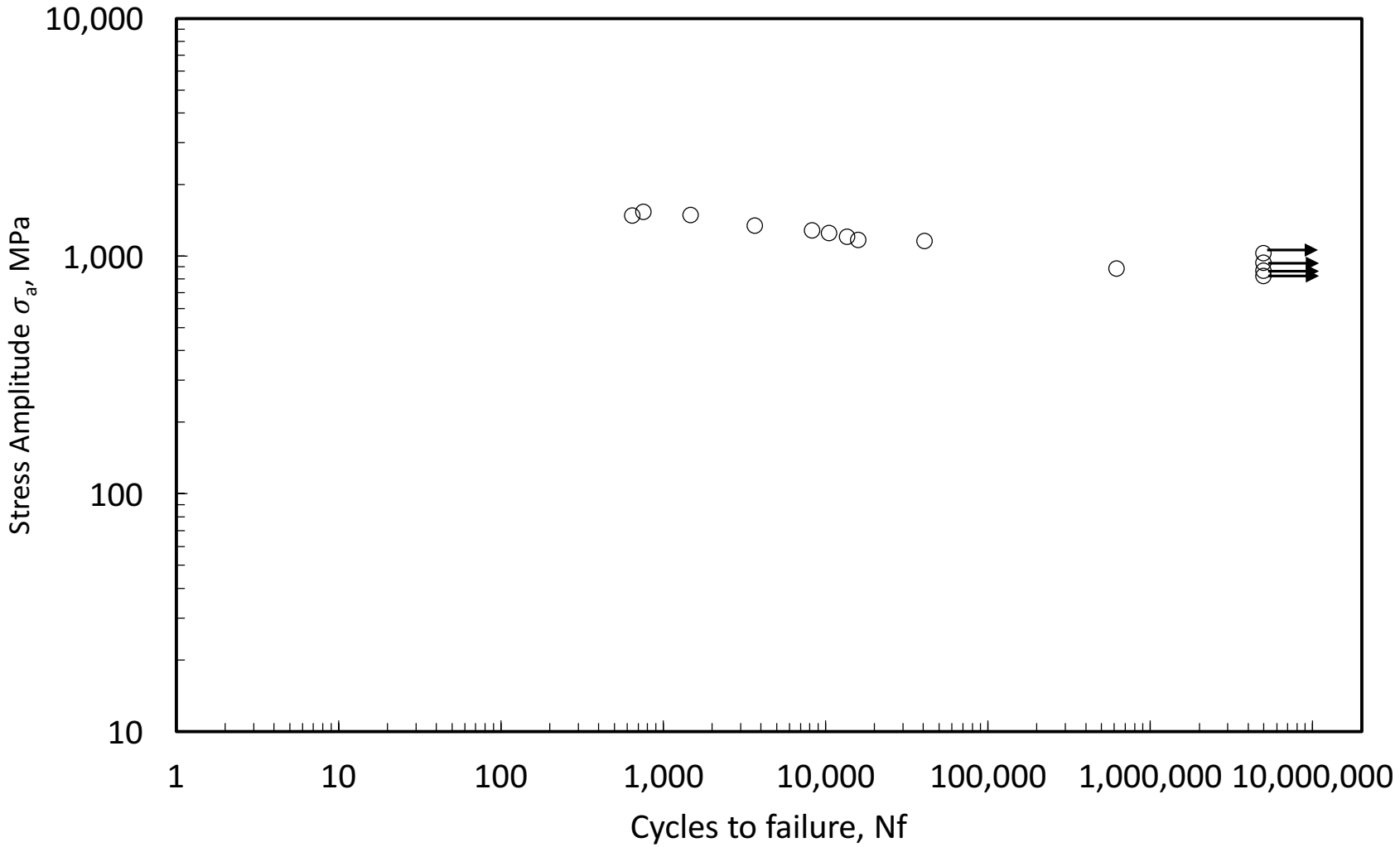

Figure 4.42: Stress-life fatigue curve for pre-stressing wire

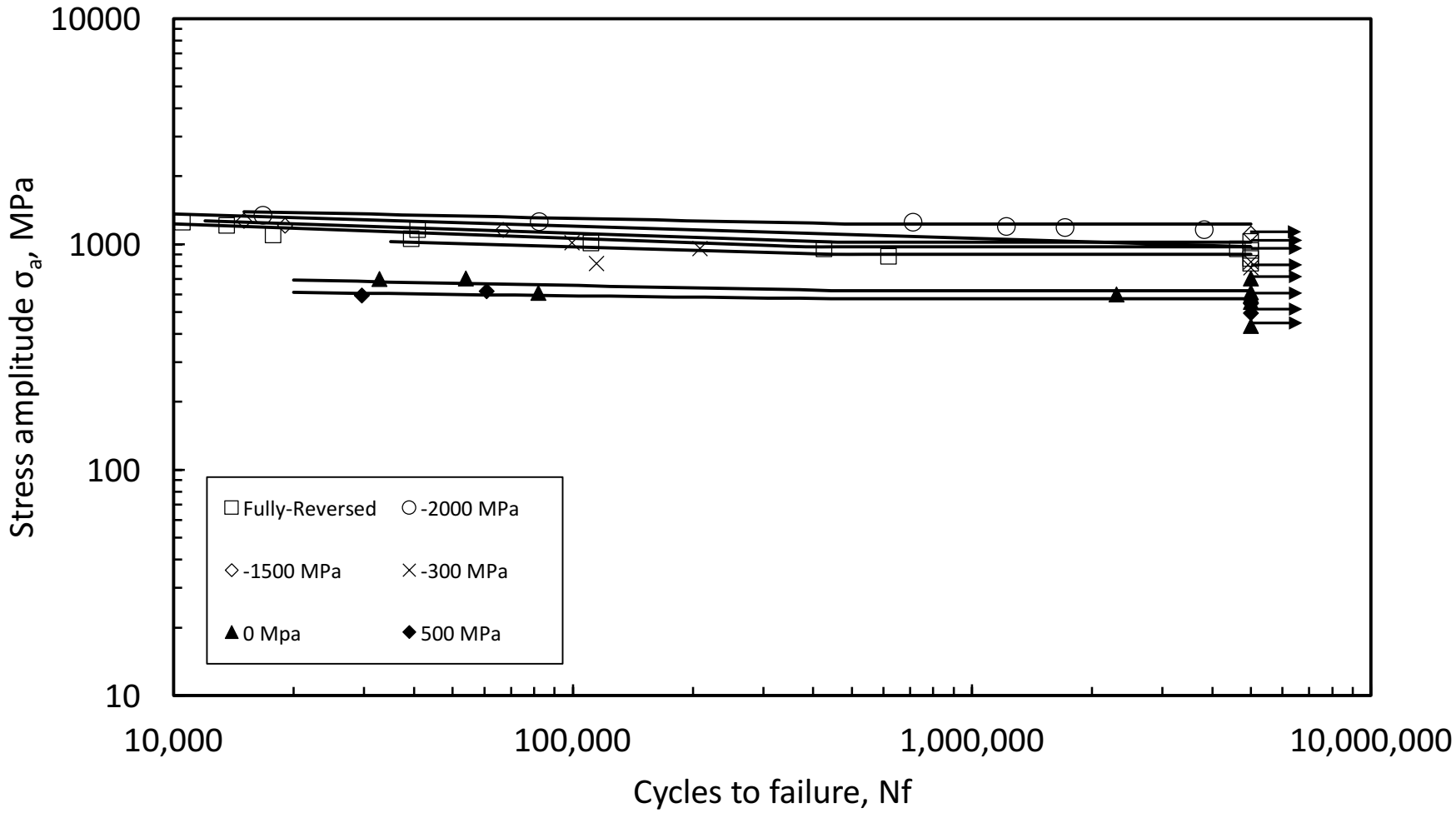

Figure 4.43: Fatigue life of pre-stressing wire for different mean stresses

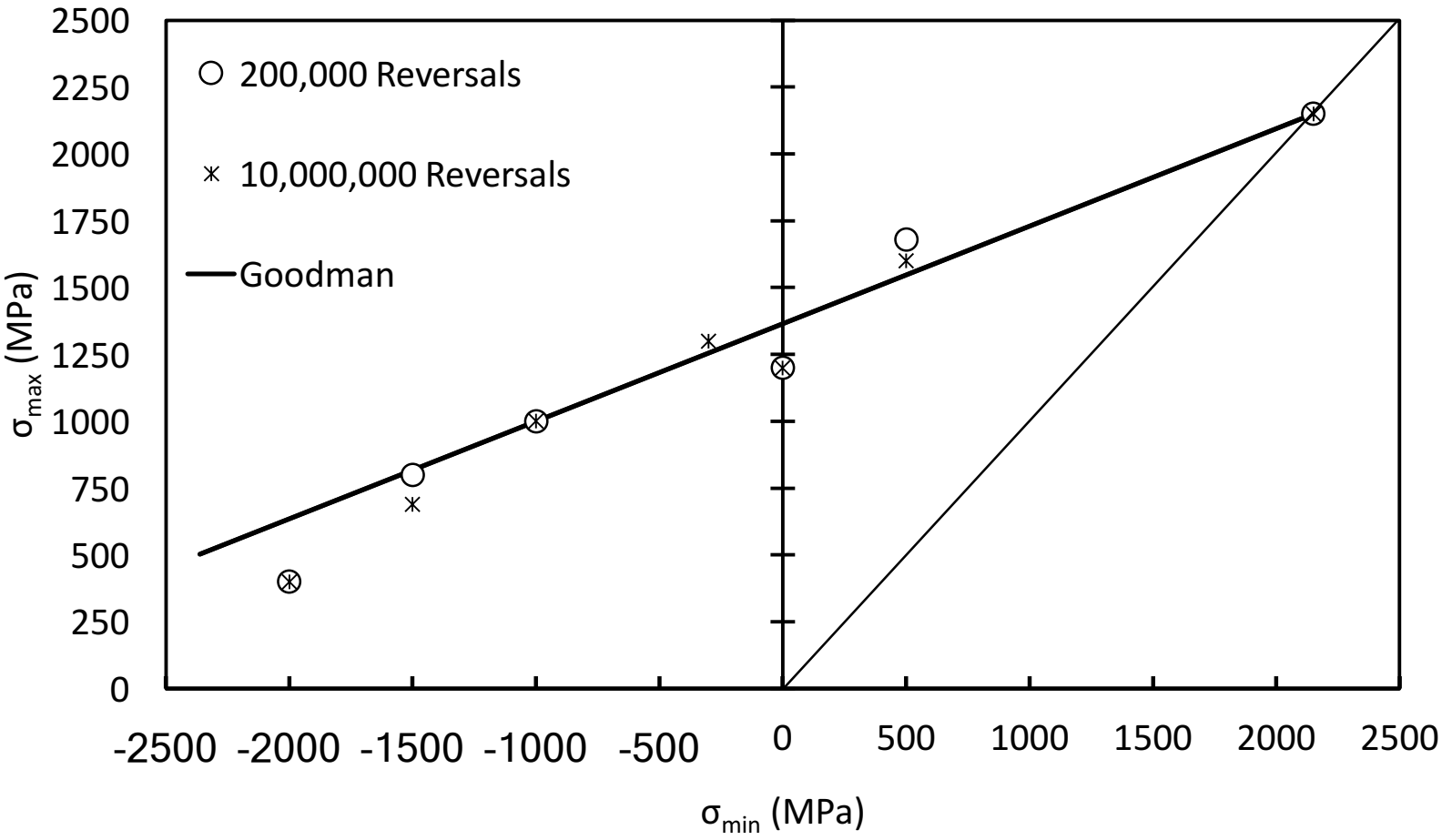

Figure 4.44: Max-min stress diagrams comparing the experimental data for pre-stressing wire with the prediction of the Goodman mean stress correction models for 200,000 and 10,000,000 reversals

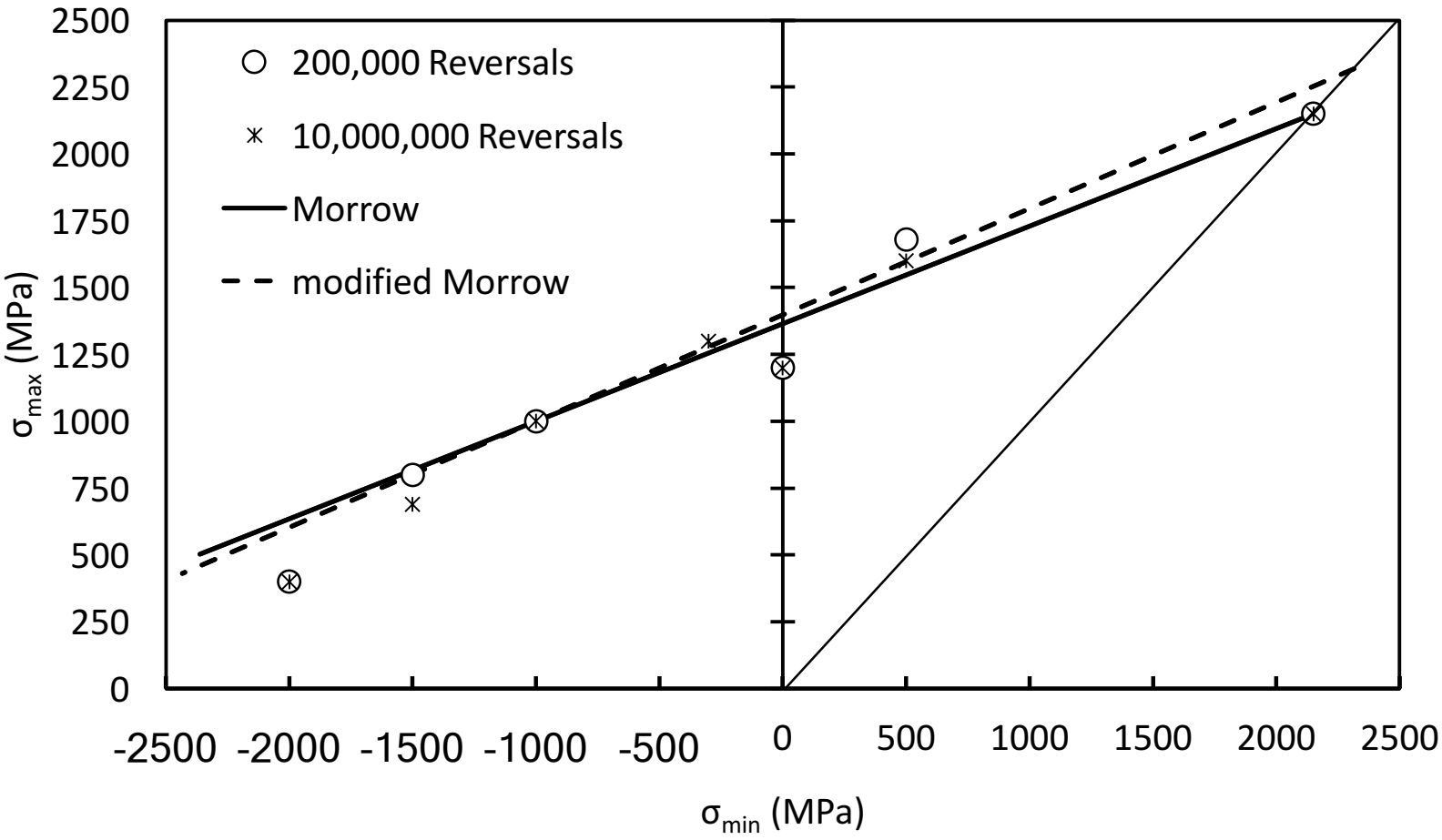

Figure 4.45: Max-min stress diagrams comparing the experimental data for pre-stressing wire with the prediction of the Morrow and modified-Morrow mean stress correction models for 200,000 and 10,000,000 reversals

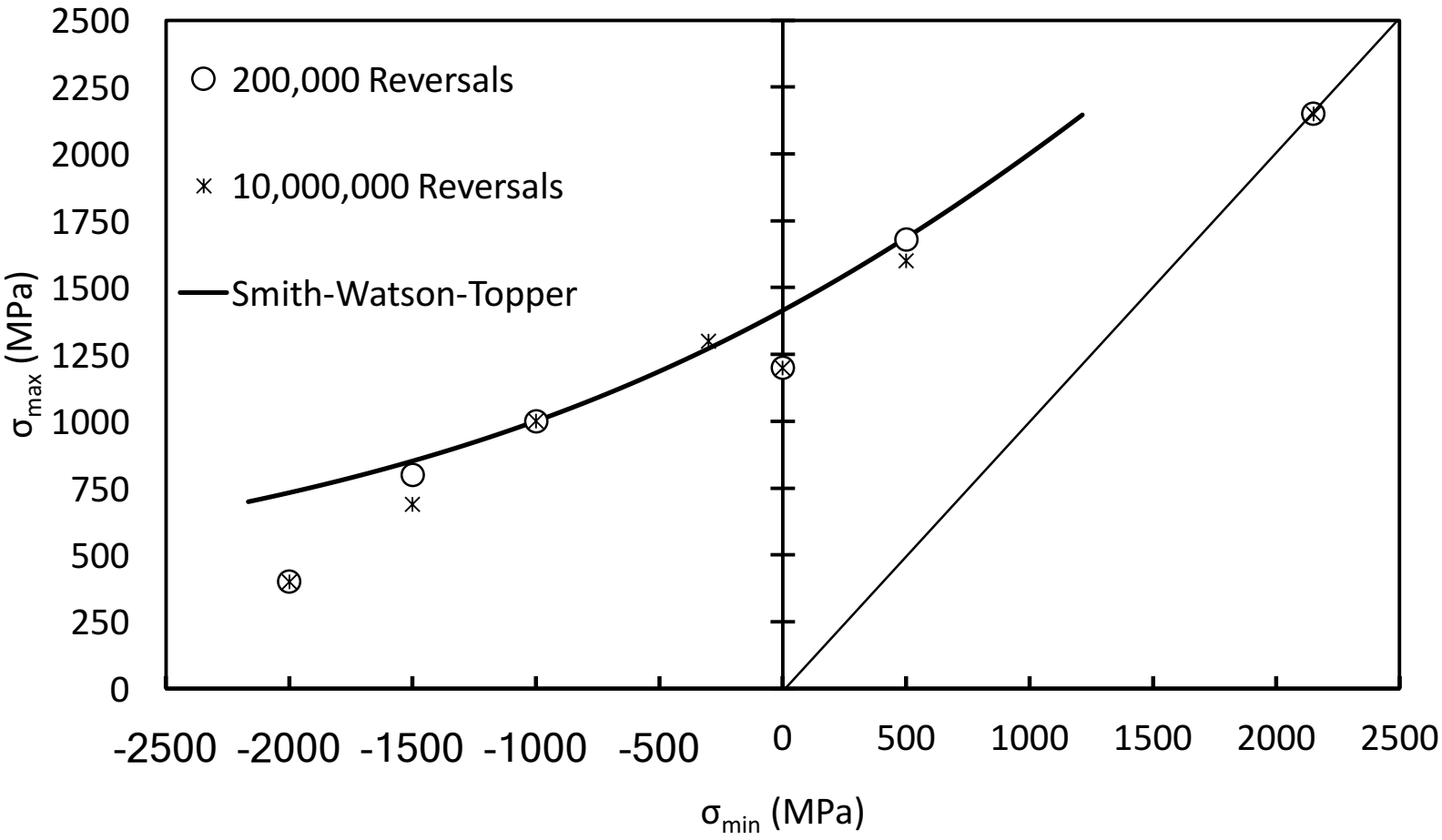

Figure 4.46: Max-min stress diagrams comparing the experimental data for pre-stressing wire with the prediction of the Smith-Watson-Topper mean stress correction models for 200,000 and 10,000,000 reversals

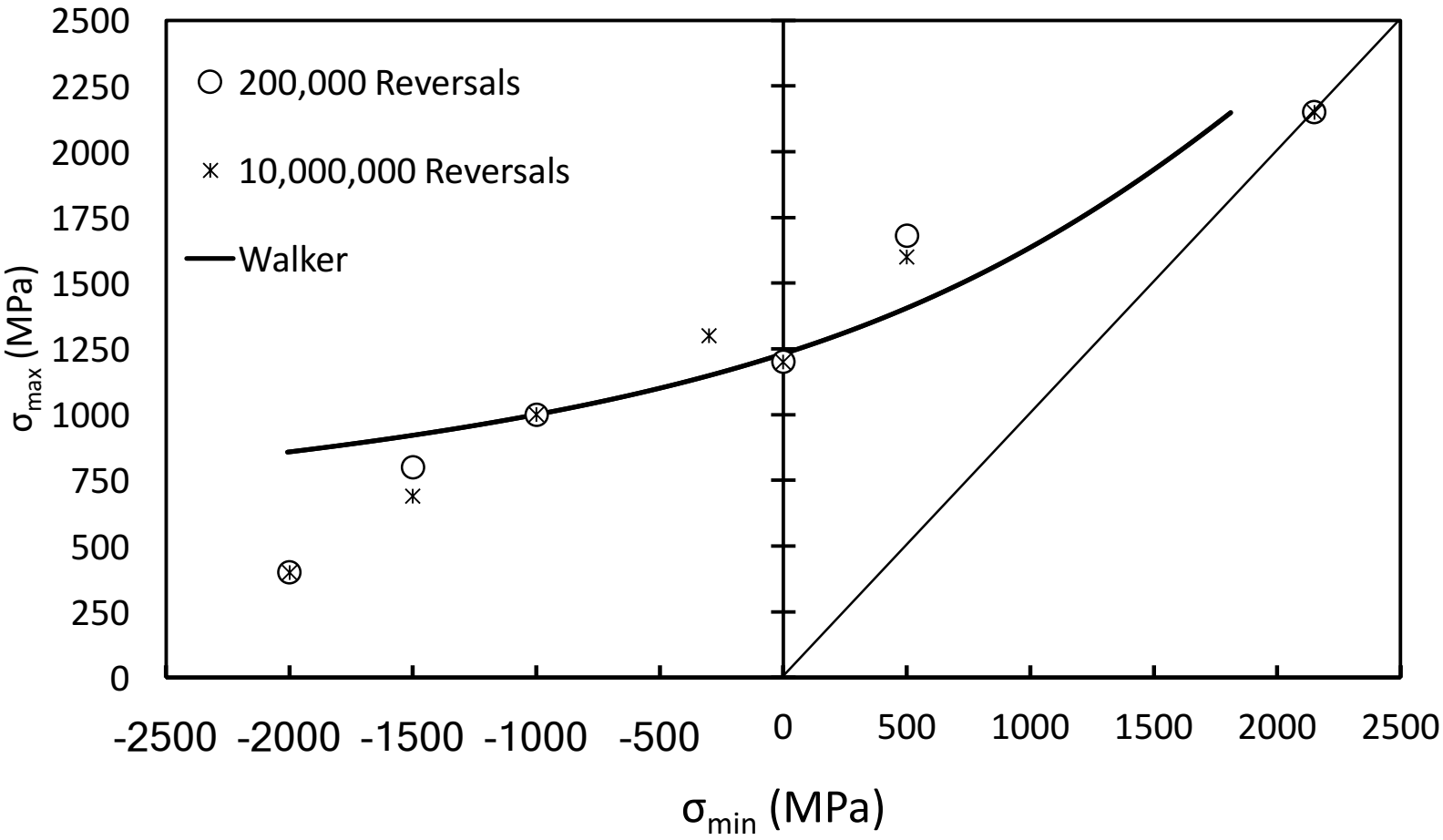

Figure 4.47: Max-min stress diagrams comparing the experimental data for pre-stressing wire with the prediction of the Walker mean stress correction models for 200,000 and 10,000,000 reversals

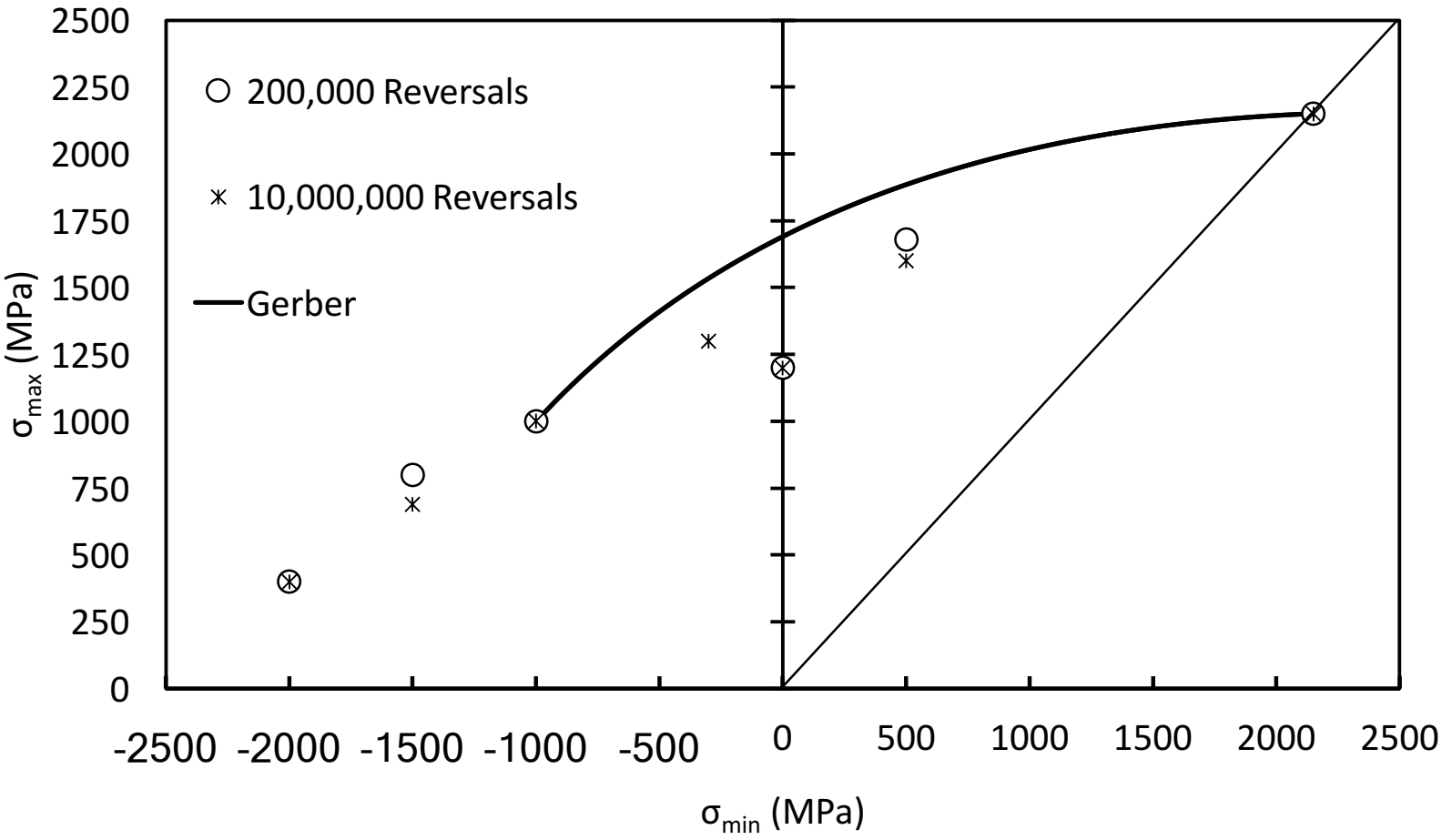

Figure 4.48: Max-min stress diagrams comparing the experimental data for pre-stressing wire with the prediction of the Gerber mean stress correction models for 200,000 and 10,000,000 reversals

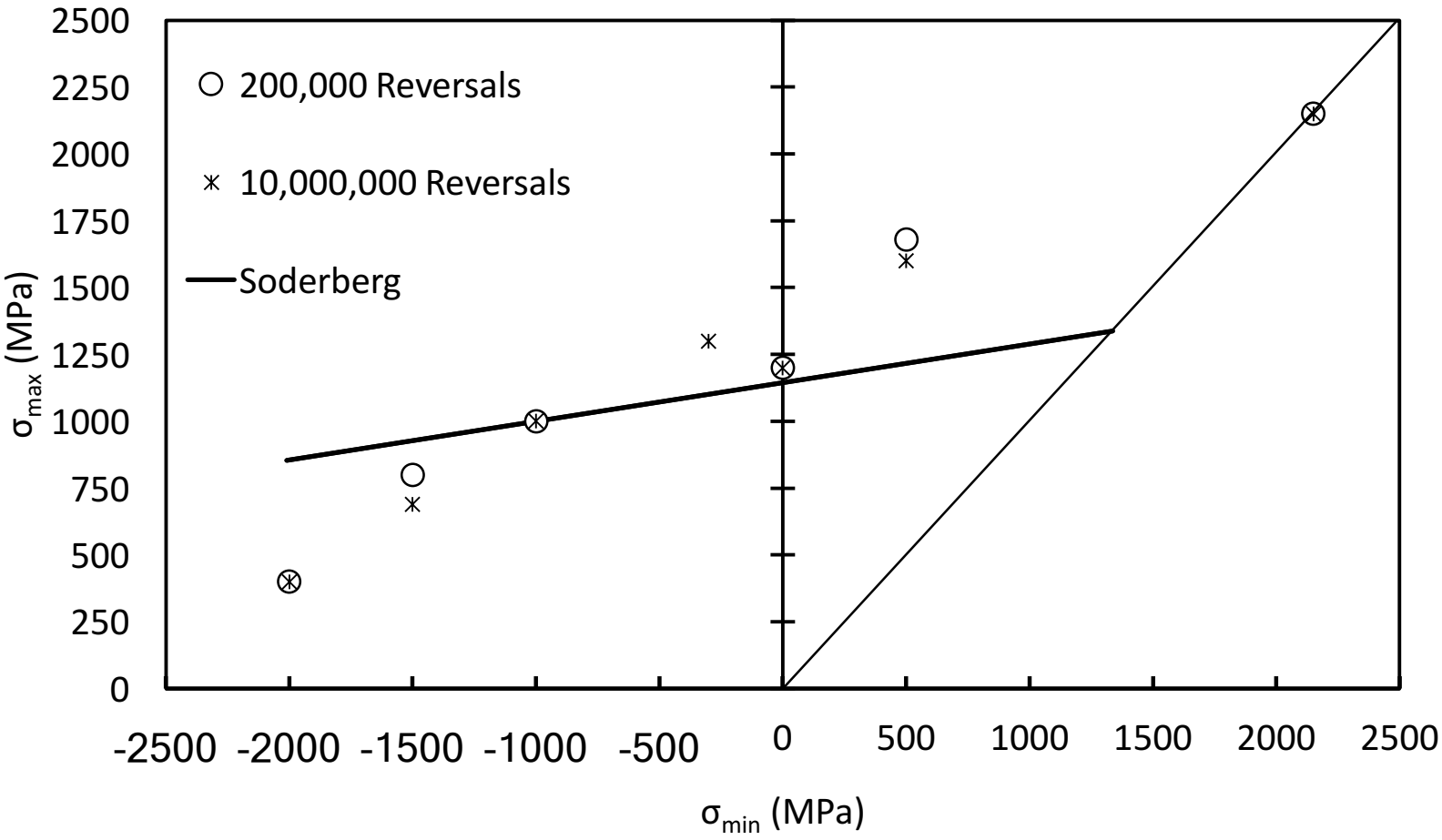

Figure 4.49: Max-min stress diagrams comparing the experimental data for pre-stressing wire with the prediction of the Soderberg mean stress correction models for 200,000 and 10,000,000 reversals

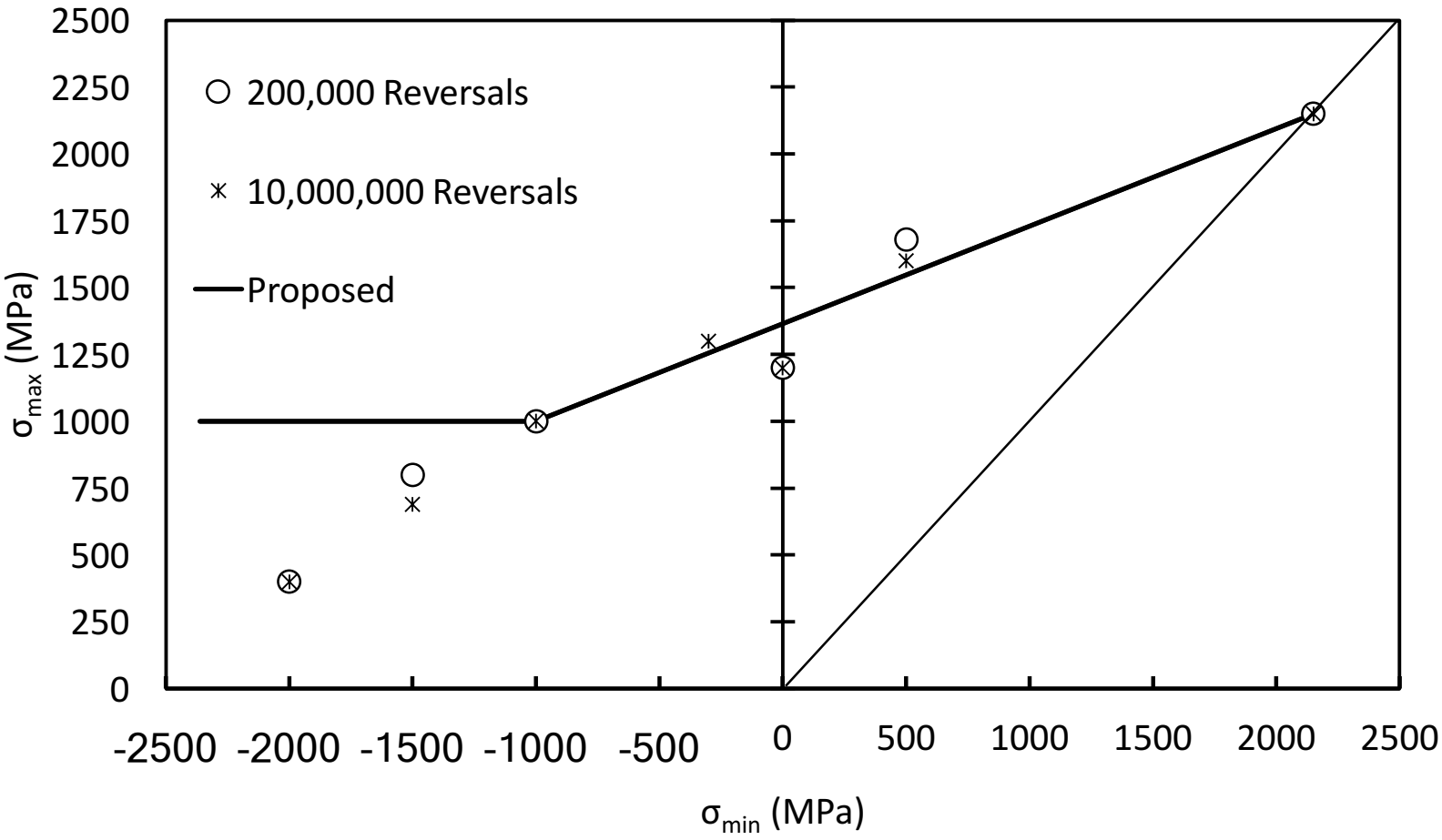

Figure 4.50: Max-min stress diagrams comparing the experimental data for pre-stressing wire with the prediction of the proposed mean stress correction models for 200,000 and 10,000,000 reversals

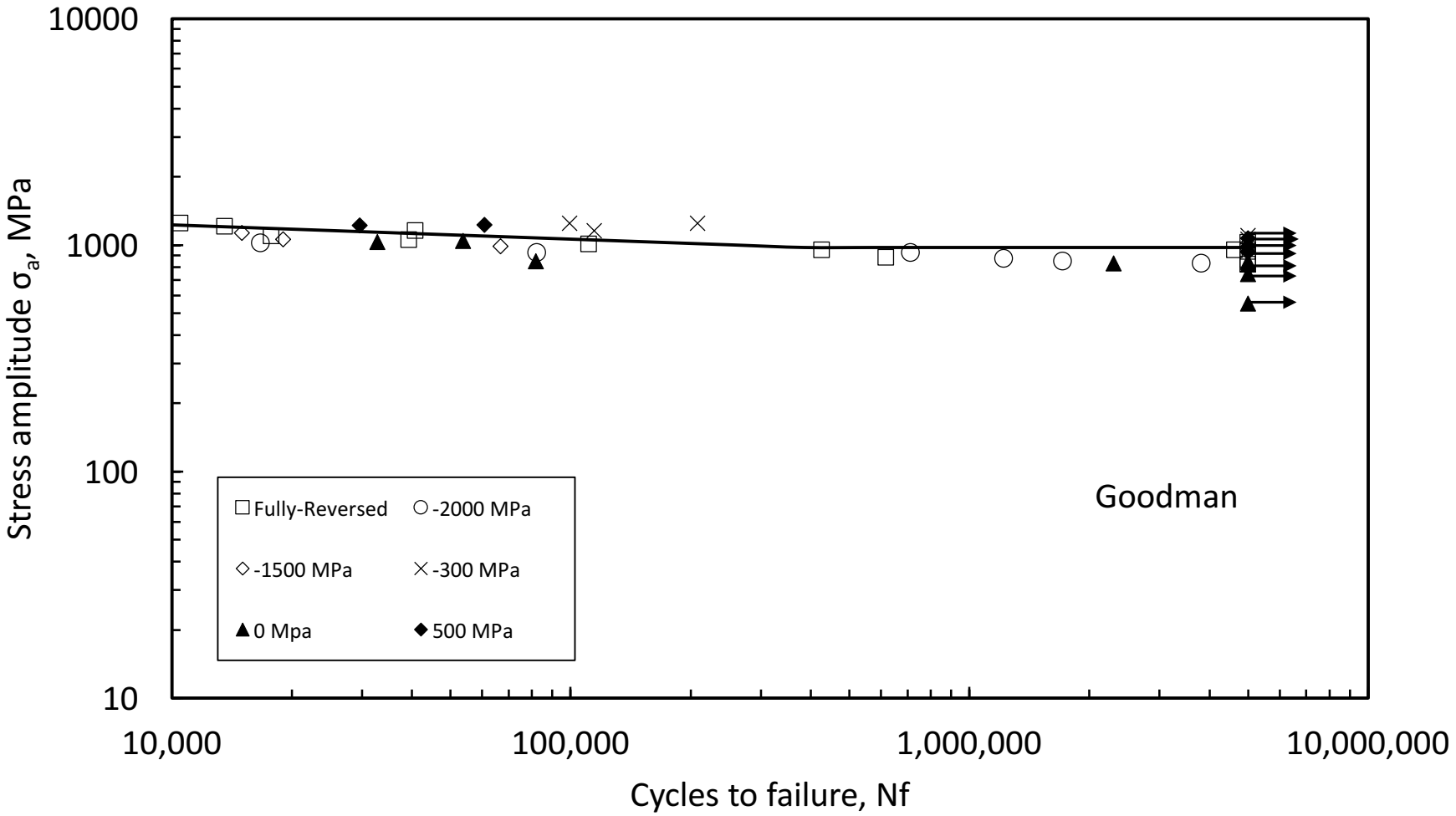

Figure 4.51: Stress-life diagram showing the equivalent stress amplitude for different mean stress levels as corrected by the Goodman method (pre-stressing wire)

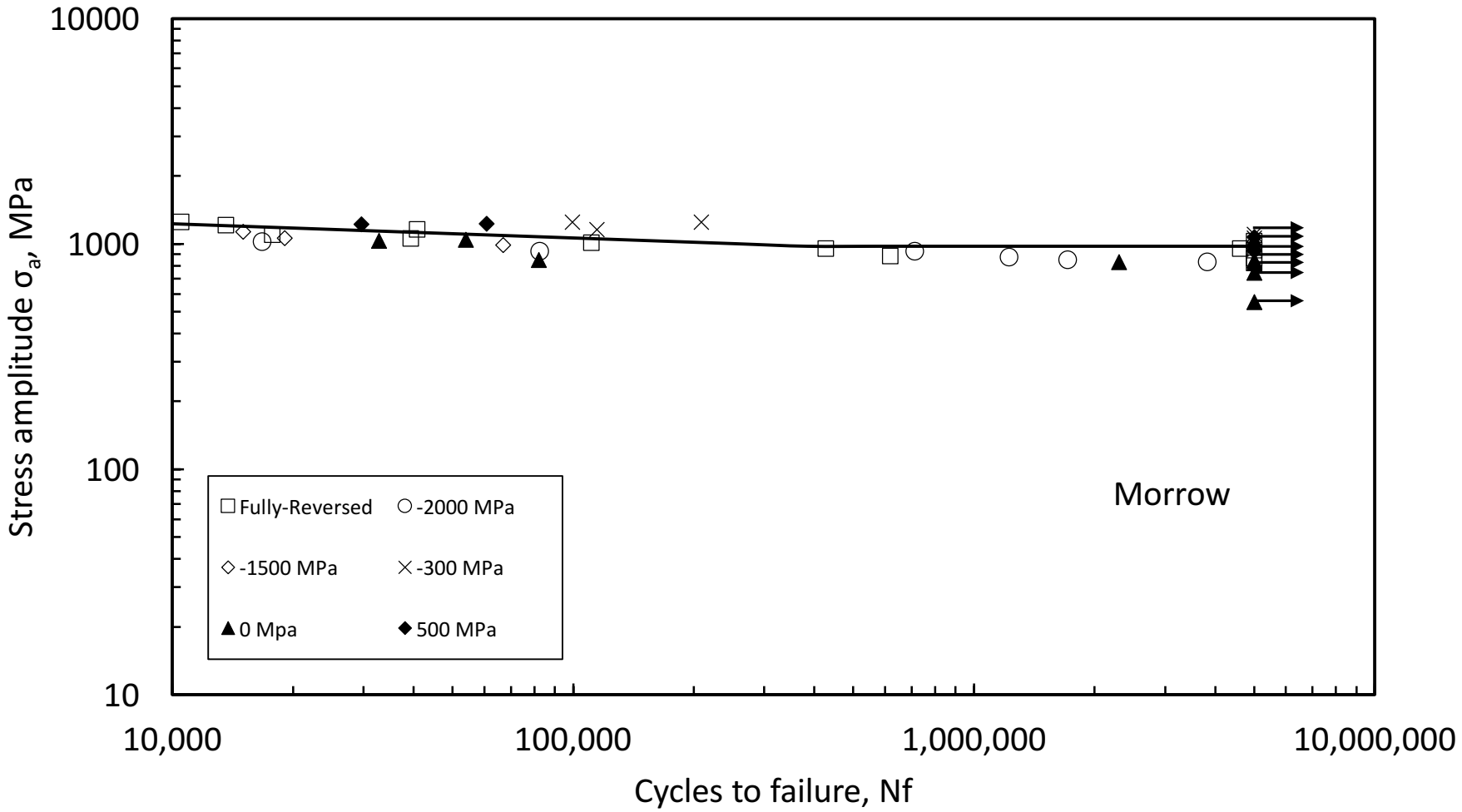

Figure 4.52: Stress-life diagram showing the equivalent stress amplitude for different mean stress levels as corrected by the Morrow method (pre-stressing wire)

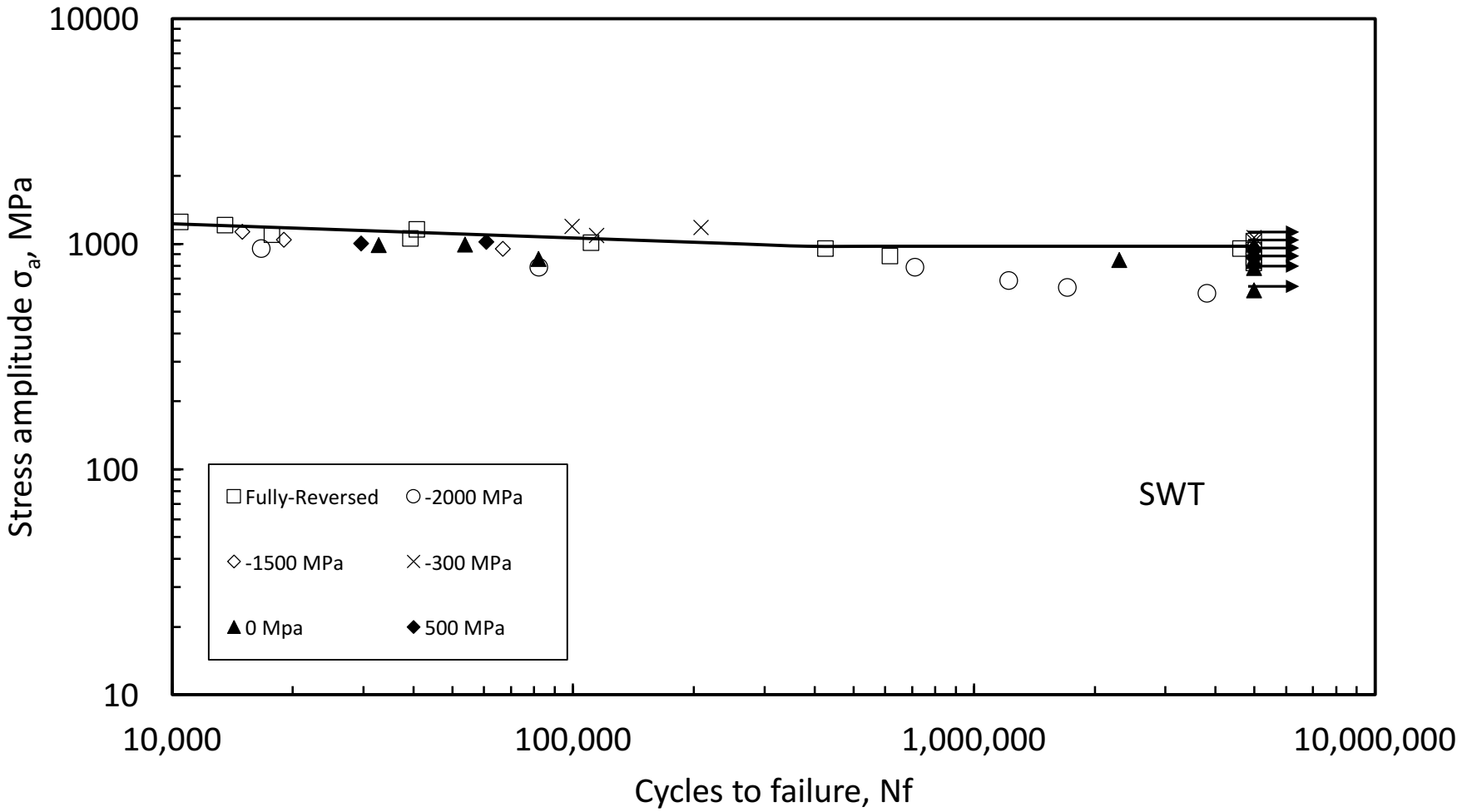

Figure 4.53: Stress-life diagram showing the equivalent stress amplitude for different mean stress levels as corrected by the Smith-Watson-Topper method (pre-stressing wire)

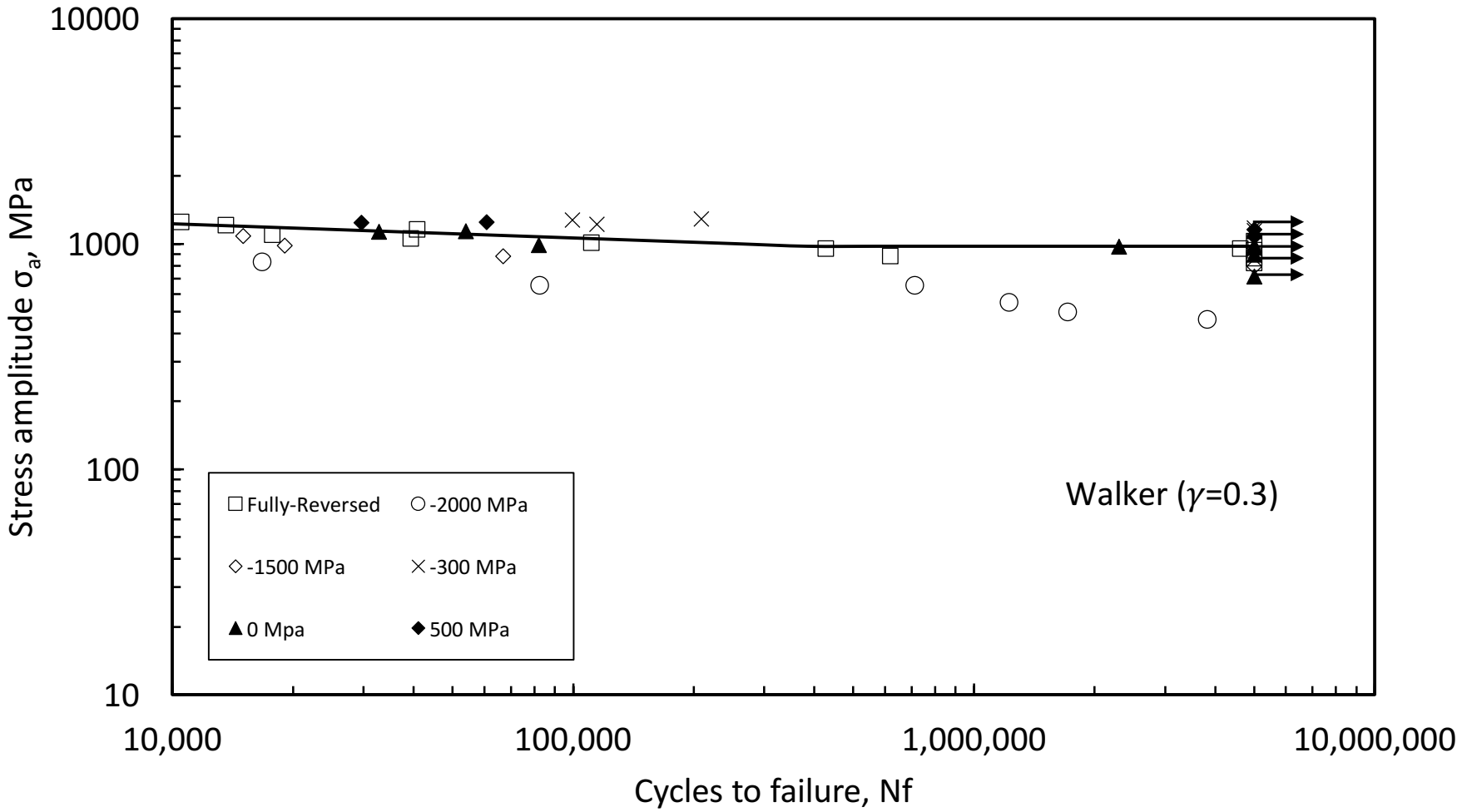

Figure 4.54: Stress-life diagram showing the equivalent stress amplitude for different mean stress levels as corrected by the Walker method (pre-stressing wire)

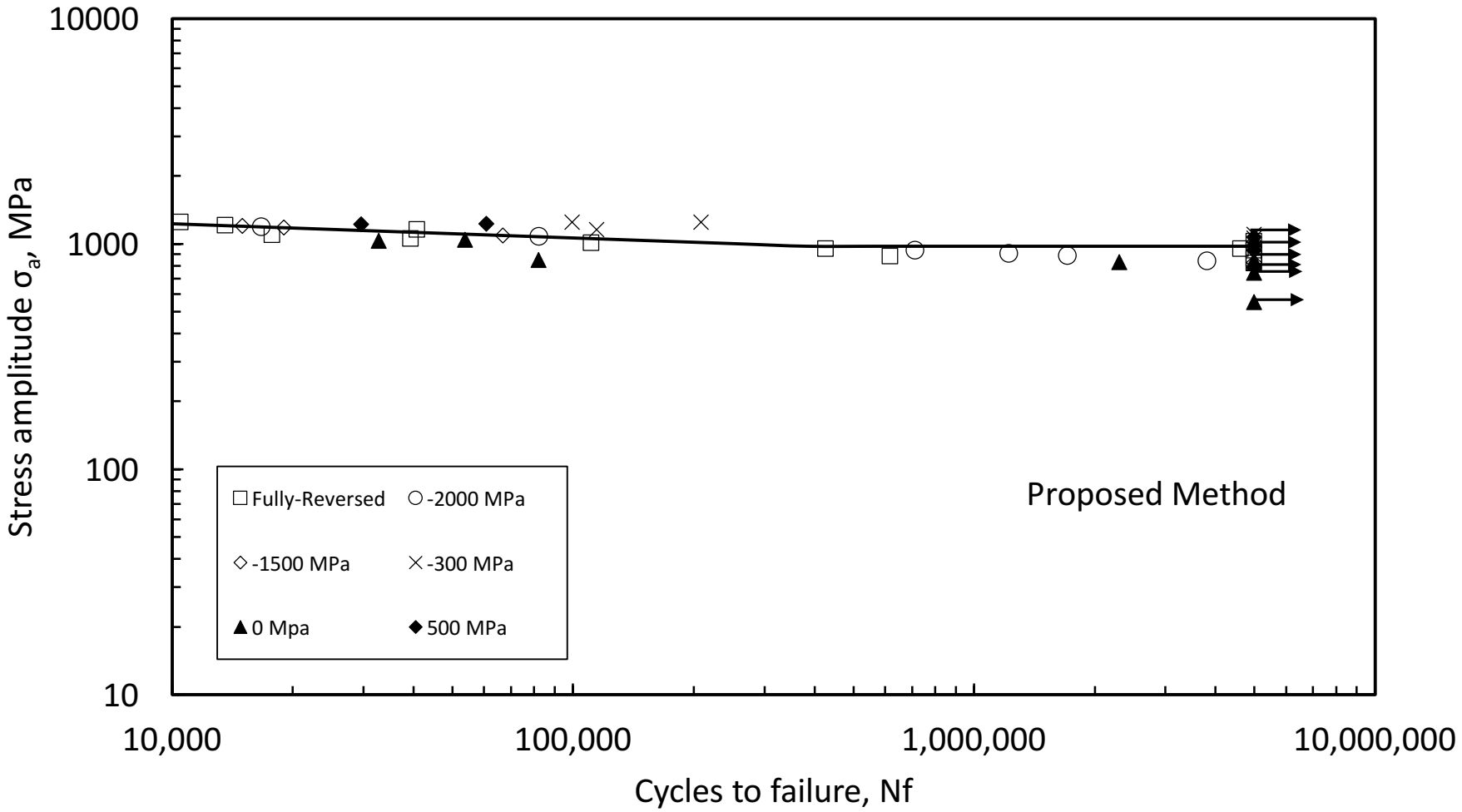

Figure 4.55: Stress-life diagram showing the equivalent stress amplitude for different mean stress levels as corrected by the proposed mean stress method (pre-stressing wire)

CHAPTER 5

ANALYSIS AND DISCUSSION

One of the goals of this investigation was to evaluate the effectiveness of different mean stress correction criteria when applied to very hard steels. The predictions of some of the most commonly used methods were compared for four different steels of varying hardness levels achieved by two hardening methods. Table 5.1 summarizes the mechanical (monotonic and cyclic) properties of the four metals as obtained in this investigation.

Table 5.1: Summary of Mechanical properties of the four steels used in this investigation

Mechanical Properties	Units	AISI 8822	AISI 9310	AISI 8620	Pre-stressing
Elastic Modulus, E	GPa	209	199	203	
Yield Strength, S_y	MPa	-	764	690	
Ultimate Tensile Strength, S_u	MPa	1480	1019	757	2150
% Elongation	%	0.87	0.94	0.5	
% Reduction of area	%	-	0.37	0.24	
True Fracture Strain,	%	0.87	0.94	0.5	
True Fracture Stress, σ_f	MPa	1480	1019	757	
Monotonic Tensile Strength Coefficient, K	MPa	-	4312	2710	
Monotonic Tensile Strain Hardening Exponent, n	-	-	0.273	0.214	
Hardness, Rockwell C (HRC)	-	60	58-60	60-63	53
Cyclic Yield Strength, (0.2% offset) = K' (0.002)n'	MPa	-	1959	3590	1338.5
Cyclic Strength Coefficient, K'	MPa	-	15793	72987	2415.6
Cyclic Strain Hardening Exponent, n'	-	-	0.336	0.485	0.095
Cyclic Elastic Modulus, E_c	GPa	-	199	203	196
Fatigue Strength Coefficient, σ'_f	MPa	2234	4851	2404	2319
Fatigue Strength Exponent, b	-	-0.159	-0.183	-0.159	-0.061
Fatigue Ductility Coefficient, ε'_f	-	0.0006	0.083	0.0006	1.09
Fatigue Ductility Exponent, c	-	-0.295	-0.67	-0.295	-0.707

5.1 Mean stress prediction models

It is important to remember that in order to correctly interpret the maximum versus minimum stress graphs, we should remember that if the curve is below the data points it

means that the method predicts failure at a lower stress level than the results show. That means that the method is conservative, i.e., it overestimates the effect of mean stress. Conversely, if the curve is above the data point, it means that the method underestimates the effect of mean stress, i.e., it is non-conservative.

5.1.1 Goodman

This criterion offers a very good prediction of the effect of mean stress for tensile mean stresses at the fatigue limit (10,000,000 reversals) for all four metals. It is non-conservative, however, for AISI 9310 and AISI 8620 at 200,000 reversals in the positive mean stress region, and data was not available for AISI 8822 at this life level. The predictions were highly conservative in the compressive mean stress region for all carburized steels, while it provided a reasonably good fit for the cold-worked steel.

5.1.2 Morrow

The results for this method were similar to the Goodman criterion because the ultimate strength and fracture strength of the materials investigated are very close due to their low ductility.

5.1.3 Modified-Morrow

The Modified-Morrow method uses the fitting constant σ_f' instead of the fracture strength. This constant is obtained by taking the intercept of the stress-life curve at 0.5 cycles. The predictions of this method did not represent the experimental results for the carburized steels since the stress-life curves were shifted because of the retained austenite effect described in Chapter 3, yielding fitting constants several times greater than the fracture strength for the same material.

This behaviour is not observed in the cold-worked steel and this method provides a slightly better fit to the data than the former Morrow criterion.

5.1.4 Smith-Watson-Topper

The SWT method presents better predictions for the compressive mean stress region for the carburized steels when compared to the previous methods.

It provides a good fit for the AISI 8822 data, but it overestimates the effect of positive mean stresses for AISI 9310 and AISI 8620.

For the pre-stressing wire material, it offers good predictions for most data points, but it overestimates the effect of highly compressive mean stresses.

5.1.5 Walker

An average value of 0.3 for the Walker exponent was found to best fit most of the experimental results.

This method provides the overall best fit of the traditional methods for the AISI 9310 and AISI 8620 data. However, it is conservative in predicting the mean stress effect for AISI 8822. It also fails to fit the data for the cold-worked steel.

Although offering a better fit than other traditional methods, in practice this method is not economically viable since it requires an extensive amount of testing to determine the Walker exponent while the other methods only require the fully-reversed data and one monotonic test constant both of which are usually available.

5.1.6 Gerber

This criterion highly overestimates the effect of mean stress for all four materials. Also, it is not able to predict the effect of compressive mean stresses. Therefore, the use of this method in the prediction of mean stress effect for very hard steels is not recommended.

5.1.7 Soderberg

The Soderberg method is more suited for ductile than hard materials and as expected does not perform well in predicting the results for these hard metals. However, it fits most of the data for AISI 8620 at the fatigue limit and the tensile mean stress data at 200,000 reversals.

It was not possible to evaluate this method for AISI 8822 because the yield limit was not measurable for this material.

5.1.8 Proposed mean stress prediction method

The mean stress correction method proposed in this study is a modification of the Goodman or Morrow criteria. As previously described, the only modification is in the compressive

mean stress region. Therefore, that is the region where improvement was observed. As seen in Figures 4.8, 4.22 and 4.36, this method provides a better fit to the data than the Walker and other methods, but with the simplicity of the Goodman and Morrow methods.

Although it offers very good results for the carburized steels, it does not perform well on the cold-worked steel, since this material shows a behavior more similar to ductile metals. Even though it lost a considerable amount of ductility during the cold-working process, it still presents 42% true strain at fracture, which is considerably more than what was observed for the carburized steels.

5.1.9 Summary

The Walker and the proposed methods offer the overall best predictions for the carburized steels, with the later having the advantage of simplicity and in some cases outperforming the Walker criterion. The other traditional criteria do not adequately describe the observed behavior of these metals that are insensitive to compressive mean stresses. Table 5.2 summarizes the results of the carburized steels.

Table 5.2: Summary of mean stress criteria fit for carburized steels

Method	Compressive mean stress region	Tensile mean stress region
Goodman	Conservative	Good fit
Morrow	Conservative	Good fit
SWT	Conservative	Non-conservative
Walker	Good fit	Good fit
Gerber	—	Highly Non-conservative
Soderberg	Conservative	Good fit
Proposed	Good fit	Good fit

The cold-worked steel shows the sensitivity to compressive mean stresses, usually found in ductile materials. Therefore, the traditional methods provide good predictions for the effect of mean stress in this material. Overall the Goodman and Morrow methods offer the best fit for this material, while Soderberg criterion is the least accurate. Table 5.3 summarizes the results for the cold-worked steel.

Table 5.3: Summary of mean stress criteria fit for cold-worked steel

Method	Compressive mean stress region	Tensile mean stress region
Goodman	Non-conservative	Good fit
Morrow	Non-conservative	Good fit
SWT	Non-conservative	Good fit
Walker	Highly Non-conservative	Conservative
Gerber	—	Highly Non-conservative
Soderberg	Highly Non-conservative	Highly Conservative
Proposed	Highly Non-conservative	Good fit

CHAPTER 6

CONCLUSIONS

This study presented an investigation of the most common mean stress correction methods present in the literature, and examined their effectiveness when applied to hard steels.

6.1 Summary

The study was comprised of an extensive experimental program and analysis. The experimental program consisted of two phases; a material testing phase, and a mean stress fatigue life testing phase. In the material testing phase, samples were tested to identify the material's monotonic and fatigue properties. In the mean stress fatigue life phase, samples were tested to determine their fatigue life when subjected to various mean stress levels.

In this chapter the findings of the study are presented followed by recommendations for future work.

6.2 Conclusions

This work has presented the results of an extensive experimental work on the effects of mean stress on very hard steels. This study's primary contribution is presenting an understanding of the fatigue behaviour of hard steels (53-63 HRC) under different mean stresses, in particular highly compressive mean stresses. Also, included are the proposal and evaluation of an alternate method to describe the results where traditional methods are inaccurate.

Carburized steels, with hardness above 58 HRC and low ductility (below 1%), show a low sensitivity to compressive mean stresses. Traditional mean stress correction models show good accuracy in the tensile mean stress region, as extensively discussed in the literature, but are conservative in the compressive region. The Walker criterion is the only current method that shows consistent predictions for the entire mean stress spectrum for these materials, but has the drawback of requiring extensive testing to determine the value of its fitting constant.

The proposed mean stress correction model improves the effectiveness of the traditional methods in the negative mean stress region while maintaining simplicity.

The other material tested in this study, a steel hardened through cold-work (53 HRC), presents a behaviour more characteristic of ductile metals. The results for this metal are well predicted by the traditional Morrow criterion, without the proposed modification.

6.3 Recommendations for Future Work

In this section, recommendations are made for future work that would expand on the findings of this thesis and contribute to a deeper understanding of the fatigue behaviour of hardened steels under mean stresses that were outside the scope of this study:

- An investigation on the effects of mean stress on very hard steels hardened through other methods, such as induction hardening nitriding, and shot peening;
- An investigation of hard quench and tempered martensitic steels.

REFERENCES

[1] Wikipedia. [Online]. http://en.wikipedia.org/wiki/Eschede_train_disaster

[2] Duga, J. J., Fisher, W. H., Buxbaum, R. W., Rosenfield, A. R., Buhr, A. H., Honton, E. J., et al. (1983). *The economic Effects of fracture in the United States - A Report to NBS by Battelle Columbus laboratories* (Final No. NBS SP 647-2) National Bureau of Standards.

[3] Milne, I. "The importance of the management of structural integrity", Engineering Failure Analysis, vol. 1, no. 3, pp. 171-181, 1994.

[4] Mann, J. Y. (1958). "*The Historical Development of Research on the Fatigue of Materials and Structures,*" The Jnl. Of the Australian Inst. of Metals, Nov. 1958, pp. 222-241

[5] Smith, J. O. (1942). "*The Effect of Range of Stress on the Fatigue Strength of Metals,*" Bulletin No. 334, University of Illinois, Engineering Experiment Station, Urbana, IL. See also Bulletin No. 316, Sept. 1939

[6] Graham, J. A., J. F. Millan, and F. J. Appl, eds. (1968). "*Fatigue Design Handbook,*" SAE Pub. No. AE-4, Society of Automotive Engineers, Warrendale, PA.

[7] Landgraf, R. W. (1966). "*Effect of Mean Stress on the Fatigue Behavior of a Hard Steel,*" Report No. 662. Dept. of Theoretical and Applied Mechanics, University of Illinois, Urbana, IL.

[8] Dowling, N., Calhoun, C., and Arcari, A. (2009). "*Mean stress effects in stress-life fatigue and the Walker equation*," Fatigue & Fracture of Engineering Materials & Structures, vol. 32, no. 3, pp. 163-179.

[9] Fatemi, A., Plaseied, A., Khosrovaneh, A. A. and Tanner, D. (2005) "*Application of bi-linear log-log S-N model to strain-controlled fatigue data of aluminum alloys and its effect on life predictions,* " Int. J. Fatigue 27, 1040-1050.

[10] Budinski, K. Engineering materials, 5th ed. Englewood Cliffs: Prentice Hall, 1996.

[11] M.A. Pompetzki, R.A. Saper, and T.H. Topper, "Software for high frequency control for variable amplitude fatigue tests," Canadian Metallurgical Quarterly, vol. 25, pp. 181-194, 1986.

[12] A. El-Menoufy, "Flexural Fatigue Behaviour of Corroded Pretensioned Beams and Their Repair Using Carbon Fibre Reinforced Polymer Sheets", Ph.D., University of Waterloo, 2015.

[13] M. El-Zeghayar, "The Introduction of Crack Opening Stress Modeling into Strain-Life and Small Crack Growth Fatigue Analysis", Ph.D., University of Waterloo, 2010.

[14] Dowling, N. (2004). "Mean Stress Effects in Stress-Life and Strain-Life Fatigue", SAE Technical Paper Series.

[15] Dowling, N. (2009). "Mean stress effects in strain-life fatigue", Fatigue & Fracture of Engineering Materials & Structures, vol. 32, no. 12, pp. 1004-1019.

[16] DuQuesnay, D., Topper, T., Yu, M. and Pompetzki, M. (1992). "The effective stress range as a mean stress parameter", International Journal of Fatigue, vol. 14, no. 1, pp. 45-50.

[17] Hayama, T. and Yoshitake, H. (1971). "Effect of Mean Stress on Fatigue Strength of Carburized Steel", Bulletin of JSME, vol. 14, no. 78, pp. 1272-1280.

[18] Hayama, T. and Yoshitake, H. (1973). "Effect of Mean Stress on Fatigue Strength of a Rapid Heat Treated Steel", Bulletin of JSME, vol. 16, no. 101, pp. 1657-1666.

[19] Smith, K., Watson, P. and Topper, T. (1970). "Stress- strain function for the fatigue of metals", J Mater, vol. 5, no. 4, pp. 767-778.

[20] Wehner, T. and Fatemi, A. (1991)."Effects of mean stress on fatigue behaviour of a hardened carbon steel", International Journal of Fatigue, vol. 13, no. 3, pp. 241-248.

APPENDIX A

Table A.1: Constant amplitude stress-life data for AISI 8620

Sp. Id	Diameter (mm)	True Strain (%)	True Stress (MPa)	Cycles to Failure
53		0.500	1,018	235
52B		0.489	995	90
41		0.486	975	163
56		0.496	975	70
42		0.395	789	505
58		0.391	776	44
57		0.389	773	52
51B		0.294	598	18,380
61		0.288	580	36,318
43		0.291	579	30,776
44		0.276	562	949
45		0.260	529	18,274
46		0.223	468	17,152
59		0.205	419	56,830
60		0.200	414	52,089
47		0.200	411	50,980
48		0.172	361	130,197
49		0.149	304	182,438
106		0.150	300	730,999
54		0.120	244	150,670
55		0.120	244	5,000,000
50		0.120	242	153,763
52		0.100	204	5,000,000
62		0.100	204	5,000,000
105		0.100	203	5,000,000
51		0.077	156	5,000,000

Table A.2: Constant amplitude data for AISI 8620 at different mean stress levels

Specimen ID	Diameter (mm)	Cycles to Failure (N_f)	Stress Max (MPa)	Stress Min (MPa)
0 MPa Minimum Stress				
1	5.11	846,212	354	3
2	5.12	760,514	323	3
3	5.11	5,000,000	300	3
4	5.04	807,348	316	3
5	5.10	1,447,134	317	3
6	5.10	5,000,000	308	3
7	5.00	5,000,000	348	3
8	5.08	5,000,000	346	3
9	5.08	594,761	394	3
10	5.11	136,643	507	-21
150 MPa Minimum Stress				
1	5.06	462,469	420	153
3	5.04	711,226	415	155
5	5.02	428,495	392	151
6	5.08	386,393	376	148
7	5.08	5,000,000	359	148
7B	5.08	481,748	458	152
8	5.03	5,000,000	372	146
9	5.00	5,000,000	372	150
9B	5.00	519,377	459	150
10	5.05	41,691	616	178
12	5.08	5,000,000	359	149
12B	5.08	141,978	552	150
13	5.08	5,000,000	372	148
13B	5.08	124,290	552	152
14	5.10	5,000,000	388	151
300 MPa Minimum Stress				

1	5.06	5,000,000	480	298
2	5.11	80,157	544	293
3	5.11	248,291	497	293
4	5.10	5,000,000	482	294
5	5.06	5,000,000	489	298
5B	5.06	133,375	549	299
6	5.06	354,778	502	298

500 MPa Minimum Stress

1	5.09	21,211	678	504
2	5.04	710,301	623	501
3	5.12	5,000,000	603	498
4	5.09	5,000,000	602	501
5	5.11	1,862,957	626	497
7	5.10	45,401	694	500
8	5.10	391,194	698	496

-700 MPa Minimum Stress

1	5.13	200,104	261	-697
2	5.16	190,789	238	-700
3	5.09	5,000,000	225	-701
4	5.13	5,000,000	222	-703
5	5.07	4,249,277	236	-707
6	5.07	1,408,878	236	-698
7	5.10	3,056,838	237	-698

-900 MPa Minimum Stress

1	5.11	177,287	304	-889
2	5.08	122,783	284	-903
3	5.09	3,578,476	259	-902
4	5.13	540,000	255	-906
5	5.12	367,067	245	-898
6	5.11	5,000,000	234	-901
7	5.13	1,423,360	244	-897
8	5.12	322,132	233	-903
9	5.13	1,548,608	232	-900

-500 MPa Minimum Stress

1	5.10	222,329	303	-493
2	5.12	387,414	274	-501
3	5.06	5,000,000	257	-501
4	5.12	721,080	280	-501
5	5.11	569,191	257	-497
6	5.13	4,330,138	244	-499
7	5.10	703,739	247	-505

Table A.3: Constant amplitude stress-life data for AISI 8822

Sp. Id	Diameter (mm)	True Strain (%)	True Stress (MPa)	Cycles to Failure
1		0.526	1035	111
2		0.529	1093	184
3		0.523	1068	545
4		0.506	1044	355
5		0.474	997	1,177
6		0.473	982	1,414
7		0.474	974	920
8		0.450	900	1,638
9		0.401	809	1,410
10		0.399	809	13,769
11		0.405	808	11,937
12		0.374	790	4,060
13		0.349	706	7,674
14		0.349	704	12,923
15		0.352	693	32,805
16		0.298	602	127,564
17		0.299	613	1,402,945
18		0.300	613	5,000,000
19		0.273	577	84,153
20		0.276	562	5,000,000
21		0.276	556	63,279
22		0.250	489	5,000,000
23		0.248	511	5,000,000
24		0.250	508	5,000,000

Table A.4: Constant amplitude data for AISI 8822 at different mean stress levels

Specimen ID	Diameter (mm)	Cycles to Failure (N_f)	Stress Max (MPa)	Stress Min (MPa)
160 MPa Minimum Stress				
2B		10,000,000	586	22
2		242,109	1,104	168
7		3,006,200	905	196
12		5,018,453	990	184
6		17,602	1,069	171
1		3,336	1,186	222
315 MPa Minimum Stress				
4		93,603	1,456	289
16		6,530	1,393	293
14		263,100	1,104	326
15		10,000,000	927	339
5		1,609,000	1,003	318
		5,000,000	1,000	315
		5,000,000	1,050	315
		5,000,000	1,103	315
		457,137	1,158	315
650 MPa Minimum Stress				
3		21,184	1,457	662
13		135,058	1,344	642
17		17,926	1,268	645
9		99,185	1,239	653
		171,523	1,220	645
		10,000,000	1,207	650
		10,000,000	1,218	650
		169,003	1,218	638
		143,228	1,184	650
		5,000,000	1,125	650

-1200 MPa Minimum Stress			
1	1,497,635	640	-1,206
2	3,239	585	-1,224
3	2,753,000	579	-1,280
4	5,500,000	579	-1,280
5	1,741,153	560	-1,200
6	5,000,000	532	-1,200
-250 MPa Minimum Stress			
1	5,000,000	801	-250
2	5,000,000	841	-250
3	5,000,000	883	-250
4	1,100,028	927	-250
-900 MPa Minimum Stress			
1	5,000,000	500	-900
2	5,000,000	525	-900
3	5,000,000	551	-900
4	2,049,917	579	-900
850 MPa Minimum Stress			
1	965,007	1,300	850
2	5,000,000	1,173	850
3	5,000,000	1,232	850
4			

Table A.5: Constant amplitude stress-life data for AISI 9310

Sp. Id	Diameter (mm)	True Strain (%)	True Stress (MPa)	Cycles to Failure
1	5.24	0.536	982	6,387
2	5.08	0.652	1195	1,786
3	5.14	0.809	1494	600
4	5.05	0.397	752	57,241
6	5.16	0.284	547	21,326

7	5.12	0.255	499	31,198
8	5.1	0.283	555	18,200
9	5.08	0.284	558	31,620
11	5.11	0.200	411	5,000,000
13	5.21	0.785	1397	113
14	5.12	0.520	994	1,770
15	5.16	0.339	655	9,029
16	5.18	0.531	1014	5,250
17	5.03	0.343	672	10,785
18	5.06	0.340	684	18,117
26	5.08	0.230	478	137,704
27	5.04	0.210	446	221,690
31	5.07	0.200	423	5,000,000
33	5.1	0.474	915	4,367
34	5.09	0.590	1117	1,014
35	5.14	0.200	400	5,000,000
37	5.07	0.210	450	5,184,628
38	5.15	0.598	1134	2,066

Table A.6: Constant amplitude data for AISI 9310 at different mean stress levels

Specimen ID	Diameter (mm)	Cycles to Failure (N_f)	Stress Max (MPa)	Stress Min (MPa)
0 MPa Minimum Stress				
1	5.11	13,011	807	0
2	5.08	39,736	699	0
3	5.08	301,722	568	-6
4	5.02	5,000,000	506	0
5	5.06	613,241	549	3
6	5.11	5,000,000	538	0
7	5.08	445,044	539	3
8	5.13	5,000,000	520	6
9	5.06	274,307	519	3

10	5.05	744,757	497	3
11	5.06	5,000,000	477	0

-900 MPa Minimum Stress

1	5.11	38,239	600	-900
2	5.06	3,745,819	503	-918
3	5.08	116,675	488	-911
4	5.11	79,312	472	-890
5	5.09	5,000,000	448	-891
6	5.06	4,887,113	454	-896
7	5.09	267,906	432	-907
8	5.08	473,017	401	-900

300 MPa Minimum Stress

1	5.06	44,373	800	298
2	5.1	104,134	749	300
3	5.1	135,872	699	300
4	5.12	221,973	647	291
5	5.13	526,832	598	293
6	5.11	5,000,000	541	298
7	5.12	459,701	580	291
8	5.11	676,690	559	300
9	5.1	5,000,000	552	300
10	5.01	995,181	548	304
11	5.1	5,000,000	535	301

500 MPa Minimum Stress

1	5.11	48,102	852	493
2	5.09	111,068	799	497
3	5.13	140,464	755	481
4	5.12	501,472	699	491
5	5.12	5,000,000	651	496
6	5.06	5,000,000	683	497
7	5.12	2,001,068	681	494
8	5.11	1,351,076	670	498
9	5.08	3,966,051	678	504

-1200 MPa Minimum Stress

1	5.09	460,301	486	-1161
2	5.11	426,739	461	-1200
3	5.1	1,491,675	441	-1205
4	5	4,365,340	437	-1198
5	5.12	161,227	438	-1206
6	5.13	231,039	430	-1208
7	5.11	212,928	433	-1200
8	5.1	67,118	417	-1198
9	5.03	254,628	423	-1196
10	5.06	98,637	406	-1205
11	5.08	3,061,507	409	-1196
12	5.1	127,877	399	-1198
13	5.06	293,383	388	-1193
14	5.11	491,989	380	-1194
15	5.1	143,278	364	-1198
16	5.14	240,814	359	-1203
17	5.09	4,331,414	342	-1203
18	5.09	3,781,860	342	-1203
19	5.09	2,209,348	330	-1203
20	5.04	440,734	325	-1191
21	5.12	5,000,000	297	-1201
22	5.13	5,000,000	302	-1196

-650 MPa Minimum Stress

1	5.09	169,628	442	-646
2	5.12	539,340	434	-641
3	5.11	209,715	410	-644
4	5.12	297,938	399	-647
5	5.11	525,767	401	-647
6	5.04	904,696	379	-650
7	5.08	5,000,000	358	-648
8	5.06	318,636	379	-647
9	5.08	1,180,903	358	-651
10	5.11	2,353,974	339	-647

11	5.04	5,000,000	337	-650
12	5.06	5,000,000	334	-644
		-1400 MPa Minimum Stress		
1	5.03	954,189	387	-1394
2	5.02	1,583,701	378	-1399
4	5.04	2,757,105	364	-1416
5	5.1	5,000,000	339	-1393
6	5.05	5,000,000	362	-1410
7	5.08	5,000,000	358	-1404
7B	5.08	75,248	445	-1394
8	5	5,000,000	369	-1405

Table A.7: Constant amplitude data for pre-stressing wire at different mean stress levels

Sp. Id	Diameter (mm)	True Strain (%)	True Stress (MPa)	Cycles to Failure
1	2.01	1.263	1532	755
2	1.97	0.861	1339	3,673
3	2.00	0.411	821	5,000,000
4	1.95	0.432	864	5,000,000
5	1.93	0.441	882	619,021
6	2.02	0.468	936	5,000,000
7	2.05	0.577	1154	40,882
8	2.01	0.727	1276	8,263
9	2.01	0.757	1248	10,517
10	2.03	0.602	1205	13,597
13	2.04	0.514	1028	5,000,000
14	2.04	1.172	1487	1,480
2	2.00	0	1167	9,251
3	2.05	0	1098	17,764
4	2.00	0	1055	39,386
5	2.02	0	1006	111,185
6	2.03	0	949	4,627,406
7	2.00	0	949	426,973

Table A.8: Constant amplitude data for pre-stressing wire at different mean stress levels

Specimen ID	Diameter (mm)	Cycles to Failure (N_f)	Stress Max (MPa)	Stress Min (MPa)
0 MPa Minimum Stress				
1	5.11	13,011	807	0
2	5.08	39,736	699	0
3	5.08	301,722	568	-6
4	5.02	5,000,000	506	0
5	5.06	613,241	549	3
6	5.11	5,000,000	538	0
7	5.08	445,044	539	3
8	5.13	5,000,000	520	6
9	5.06	274,307	519	3
10	5.05	744,757	497	3
11	5.06	5,000,000	477	0
-900 MPa Minimum Stress				
1	5.11	38,239	600	-900
2	5.06	3,745,819	503	-918
3	5.08	116,675	488	-911
4	5.11	79,312	472	-890
5	5.09	5,000,000	448	-891
6	5.06	4,887,113	454	-896
7	5.09	267,906	432	-907
8	5.08	473,017	401	-900
300 MPa Minimum Stress				
1	5.06	44,373	800	298
2	5.1	104,134	749	300
3	5.1	135,872	699	300
4	5.12	221,973	647	291
5	5.13	526,832	598	293

6	5.11	5,000,000	541	298
7	5.12	459,701	580	291
8	5.11	676,690	559	300
9	5.1	5,000,000	552	300
10	5.01	995,181	548	304
11	5.1	5,000,000	535	301

500 MPa Minimum Stress

1	5.11	48,102	852	493
2	5.09	111,068	799	497
3	5.13	140,464	755	481
4	5.12	501,472	699	491
5	5.12	5,000,000	651	496
6	5.06	5,000,000	683	497
7	5.12	2,001,068	681	494
8	5.11	1,351,076	670	498
9	5.08	3,966,051	678	504

-1200 MPa Minimum Stress

1	5.09	460,301	486	-1161
2	5.11	426,739	461	-1200
3	5.1	1,491,675	441	-1205
4	5	4,365,340	437	-1198
5	5.12	161,227	438	-1206
6	5.13	231,039	430	-1208
7	5.11	212,928	433	-1200
8	5.1	67,118	417	-1198
9	5.03	254,628	423	-1196
10	5.06	98,637	406	-1205
11	5.08	3,061,507	409	-1196
12	5.1	127,877	399	-1198
13	5.06	293,383	388	-1193
14	5.11	491,989	380	-1194
15	5.1	143,278	364	-1198
16	5.14	240,814	359	-1203
17	5.09	4,331,414	342	-1203

18	5.09	3,781,860	342	-1203
19	5.09	2,209,348	330	-1203
20	5.04	440,734	325	-1191
21	5.12	5,000,000	297	-1201
22	5.13	5,000,000	302	-1196

-650 MPa Minimum Stress

1	5.09	169,628	442	-646
2	5.12	539,340	434	-641
3	5.11	209,715	410	-644
4	5.12	297,938	399	-647
5	5.11	525,767	401	-647
6	5.04	904,696	379	-650
7	5.08	5,000,000	358	-648
8	5.06	318,636	379	-647
9	5.08	1,180,903	358	-651
10	5.11	2,353,974	339	-647
11	5.04	5,000,000	337	-650
12	5.06	5,000,000	334	-644

-1400 MPa Minimum Stress

1	5.03	954,189	387	-1394
2	5.02	1,583,701	378	-1399
4	5.04	2,757,105	364	-1416
5	5.1	5,000,000	339	-1393
6	5.05	5,000,000	362	-1410
7	5.08	5,000,000	358	-1404
7B	5.08	75,248	445	-1394
8	5	5,000,000	369	-1405